MIXED CONVECTIVE TRANSPORT IN A POROUS MEDIUM SATURATED WITH POWER-LAW FLUID

A THESIS SUBMITTED TO
NATIONAL INSTITUTE OF TECHNOLOGY WARANGAL, INDIA
FOR THE AWARD OF THE DEGREE OF

DOCTOR OF PHILOSOPHY

IN

MATHEMATICS

BY

GONTLA VENKATA SUMAN

(Roll No. 701440)

UNDER THE SUPERVISION OF

Dr. J. PRANITHA

DEPARTMENT OF MATHEMATICS
NATIONAL INSTITUTE OF TECHNOLOGY
WARANGAL-506004, INDIA

JULY 2018

C E R T I F I C A T E

This is to certify that the thesis entitled " **Mixed Convective Transport in a Porous Medium Saturated with Power-law Fluid** " submitted to National Institute of Technology Warangal, for the award of the degree of **Doctor of Philosophy**, is bonafide research work carried out by **Mr. GONTLA VENKATA SUMAN** under my supervision. To the best of my knowledge, the contents of this thesis have not been submitted elsewhere for the award of any degree or diploma.

Dr. J. Pranitha
Assistant Professor
Department of Mathematics
National Institute of Technology Warangal
Telangana State, INDIA

.

DECLARATION

This is to certify that the work presented in the thesis entitled **"Mixed Convective Transport in a Porous Medium Saturated with Power-law Fluid"**, is a bonafide work done by me under the supervision of **Dr. J. PRANITHA** and has not been submitted elsewhere for the award of any degree.

I declare that this written submission represents my ideas in my own words and where others' ideas or words have been included, I have adequately cited and referenced the original sources. I also declare that I have adhered to all principles of academic honesty and integrity and have not misrepresented or fabricated or falsified any idea / data / fact /source in my submission. I understand that any violation of the above will be a cause for disciplinary action by the Institute and can also evoke penal action from the sources which have thus not been properly cited or from whom proper permission has not been taken when needed.

Gontla Venkata Suman

Roll No. 701440

Date:_____

Dedicated to

My Parents, Wife

&
Sri Venkateshwara Swamy

ACKNOWLEDGEMENTS

I am most grateful to God for giving me his grace to achieve all I have so far. It is a rare privilege and boon that I could associate myself for pursuing my research work with Dr. J. Pranitha, Assistant Professor of Mathematics, National Institute of Technology Warangal, India. I sincerely record my gratitude for her invaluable guidance and constant encouragement throughout the preparation of this thesis and her involvement and meticulous supervision while my work was in progress. With her inimitable qualities as a good teacher, she chiseled my path towards perfection. Ever since I met her, she has been a perpetual source of motivation, inspiration, encouragement and enlightenment. She is responsible for making the period of my research work as an educative and enjoyable learning experience. The thesis would not have seen the light of the day without her unrelenting support and cooperation. I deem it a privilege to have worked under her amiable guidance. My vocabulary is inadequate to express my gratitude.

I am greatly indebted to the dynamic personality Prof. D. Srinivasacharya, Head, Department of Mathematics for his affectionate support, encouragement and for sparing his valuable time in bringing a proper form for presentation of the results in the thesis. It is not an exaggeration to state that without his assistance and suggestions, this thesis would not have taken this form.

I am extremely thankful to Prof. D.A.S Rees, Department of Mechanical Engineering, University of Bath, U.K for sharing his valuable time, during my Newton Bhabha PhD internship program (4 months), especially for his help in my research work.

I am grateful to Prof. T.K.V. Iyengar (Late), Prof. G. Radhakrishnamacharya (Retd.), Prof. Y. N. Reddy and Prof. K.N.S. Kasi Viswanadham, Department of Mathematics for their help and support throughout my research period. Also, I thank the office non-teaching staff.

I thank the members of the Doctoral Scrutiny Committee, Prof. J. V. Ramana Murthy, Prof. D. Srinivasacharya, Department of Mathematics and Prof. V. Suresh Babu, Department of Mechanical Engineering for their valuable suggestions, moral support and encouragement while my work was in progress.

I place on record my gratitude to Dr. Ch. Ramreddy and all other faculty members of the Department of Mathematics, for their constant encouragement. Also, I thank the office non-teaching staff.

I express my sincere thanks to Department of Science & Technology, New Delhi, INDIA, for providing financial support to enable conducting this research work under inspire fellowship program.

I express my sincere thanks to British council and Department of Science & Technology, New Delhi, INDIA, for provided financial support for four months Internship program, U.K under Newton Bhabha PhD placement program.

I express my sincere thanks to Prof. N.V. Ramana Rao, Director, National Institute of Technology, Warangal for his kind support and encouragement at every stage of this endeavor.

I owe my special thanks to Dr. K. Kaladhar, Dr. M. Krishna Prasad, Dr. M. Upendar, Dr. O. Surender, Dr. P. Vijay kumar, Dr. G. Madhava Rao for their support. I thank Mr. Ch. Venkata Rao, Mr. P. Naveen, Dr. N. Vijay kumar, Dr. Jaipal, Dr. T. Pradeepa, Dr. K. Hima Bindu, Dr. Md. Shafeeurrahaman, Dr. P. Jagadeeshwar, Mr. I. Sreenath, Mr. Om prakash, Dr. M. Varun Kumar, Dr. G. Nithish Kumar and all other research colleagues in the Department of mathematics and my friends, who helped me during my Ph.D cooperatively and also making my stay at NITW campus fruitfully and cherishable every moment.

My deepest gratitude to my parents, G. Sreeramulu and G. Subbarathnamma, my in-laws V. Raja Guru and V. Rukmini, my brother G. Sudheer my sister G. Supraja and other family members for their continuous support and constant encouragement over the years. All of their love and affection have been motivating force behind what I am today.

Finally, and most importantly, I would like to thank my better half, Mrs. Girija Rani for her support, patience and understanding. Without her help and encouragement, I would not have achieved this mile-stone in my life.

. Gontla Venkata Suman

A B S T R A C T

Modeling and analysis of the dynamics of a power-law fluid continue to be an area of intensive research activity. This stems from the evident that these types of fluids have a large variety of engineering and industrial applications. Moreover, the theoretical analysis of power-law fluids in a Darcy/non-Darcy porous medium has been attracting attention for several decades because of its great importance in practical applications of engineering and industrial problems. Industrial fluids like molten plastics, glues, pulp, slurries, etc., do not obey the linear relationship between shear stress and shear rate, and are described as non-Newtonian in their flow attributes. The main aim of the thesis is to investigate the mixed convective flow in a power-law fluid saturated porous medium in the presence of variable properties, double dispersion, thermophoresis, Soret, MHD, thermal radiation and local thermal equilibrium.

The thesis consists of FOUR parts and NINE chapters. *Part-I* consists of a single chapter (Chapter - 1), which provides an introduction to the concepts in power-law fluid, porous medium, stability analysis and a review of the pertinent literature. *Part-II* contains four chapters (i.e., Chapters 2, 3, 4, and 5) and deals with the similarity solution for mixed convective flow along a vertical plate in a Darcy porous medium saturated with power-law fluid. Chapters-2 deal with the mixed convective flow over a vertical plate embedded in a power-law fluid saturated porous medium in the presence of double dispersion and variable viscosity effects, whereas Chapter-3 explore the effects of variable properties and thermophoresis on mixed convective flow of a power-law fluid saturated porous medium. Chapters-4 examines the influence of thermal radiation, Soret and variable properties on mixed convective flow in a porous medium saturated by power-law fluid. Chapter-5 investigates the linear stability of the vertical throughflow in a horizontal porous layer saturated with power-law fluid. The linearized disturbance equations are reduced to a eigenvalue problem in ordinary differential by assuming a periodic train of convection cells. This eigenvalue problem is solved using finite differences and a matrix-based method. *Part-III* consists of three chapters (Chapters 6, 7 and 8) and deal with the similarity solution for a power-law fluid flow along a vertical plate in a non-Darcy porous medium. Chapter-6 is an extension of Chapter-2 in which MHD and non-Darcy porous medium are considered. Chapter-7 is an extension of Chapter-3 in which MHD and non-Darcy porous medium are taken into consideration. Mixed convection in a power-law fluid saturated non-Darcy porous medium with the effects of MHD, thermal radiation and variable properties, is discussed in Chapter-8. The final *Part-IV* consists of only one chapter (Chapter-9) which gives a summary, overall conclusions and scope for future work.

NOMENCLATURE

B	Buoyancy ratio
B_0	Magnetic filed strength
C	Dimensionless concentration
$\overline{C}$	Concentration
C_w	Wall concentration
C_∞	Ambient concentration
d^*	Pore diameter
D	Mass diffusivity
G	Non-Darcy parameter
g	Gravitational acceleration
K	Permeability constant
H	Non-dimensional inter phase heat transfer coefficient
k	Wavenumber
L	Characteristic length
Le	Lewis number
M	Magnetic parameter
n	Power-law index
$Nu_{\overline{x}}$	Local Nusselt number
Pe	Péclet number
R	Radiation parameter
Sr	Soret parameter
Ra	Rayleigh number
Pe_γ	Thermal Dispersion parameter
Pe_ζ	Solutal Dispersion parameter
Sc	Schmidt number
P	Pressure gradient
τ	Thermophoretic parameter
Ra_c	Critical Rayleigh number
$Sh_{\overline{x}}$	Local Sherwood number
$\overline{T}$	Temperature
q_w	Surface heat flux
q_m	Regular mass flux
T	Dimensionless Temperature
T_∞	Ambient temperature
T_w	Wall temperature
u_∞	Free stream velocity
$\overline{u}, \overline{v}$	Velocity components in the $\overline{x}$ and $\overline{y}$ directions respectively
$\overline{x}, \overline{y}$	Cartesian coordinates along the plate and normal to the plate
x, y	Dimensionless coordinates along and normal to the plate

Greek Symbols

α	Thermal conductivity
α_0	Thermal diffusivity
β	Thermal conductivity parameter
β_T^*	Coefficient of thermal expansion
β_c^*	Coefficient of concentration expansion
η	Similarity variable
k^*	Rosseland mean absorption coefficient
λ	Mixed convection parameter
σ	Electrical conductivity of the fluid
τ	Thermophoresis parameter
δ	Thermal property of the fluid
σ^*	Stefan-Boltzmann constant
θ_e	Variable viscosity
θ^*	Consistency factor
μ_∞	Thermal conductivity of the fluid
Ω	Porosity-modified conductivity ratio
γ	Mechanical thermal dispersion
ζ	Mechanical solutal dispersion
μ_e	Magnetic permeability
ν	Kinematic viscosity
ν_∞	Kinematic viscosity constant
ρ_∞	Density of the fluid
ψ	Stream function

Subscripts

w	Wall condition.
∞	Ambient condition.

Superscript

$\prime$	Differentiation with respect to η.

Contents

[1] Published in "**Procedia Engineering**" 127 (2015) 362–369

[2] Accepted in "**Computational Thermal Sciences: An International Journal**"

[3] Published in "**Frontiers in Heat and Mass Transfer**"9, 39 (2017)

[4]Communicated to "**Transport in porous media**"

[5]Published in "**Special Topics & Reviews in Porous Media-An International Journal**" 8(3), 177-195 (2017)

[6]Published in "**International Journal of Pure and Applied Mathematics**", Vol.113, no.12, pp.160-168, 2017.

[7] Communicated to "**Journal of Nanofluid**"

Part I

INTRODUCTION

Chapter 1

Preliminaries and Review

1.1 Introduction

Fluid mechanics is the study of behavior of fluids that are, either at rest or in motion. It is one of the primary engineering sciences that has important applications in many engineering disciplines. For example, aeronautical and aerospace engineers use fluid mechanical principles to study the flight of aeroplane and to design propulsion systems. Civil engineers use this subject to design drainage channels, water networks, sewer systems and water-resisting structures such as dams and levees. Fluid mechanics is used by mechanical engineers to design pumps, compressors, turbines, process control systems, heating and air conditioning equipment. Chemical engineers use the concept of this subject to design equipment used for filtering, pumping and mixing fluids (Batchelor [11], Russell [87], Yuan [110]).

This subject is proven to be a highly exciting and challenging subject of modern sciences in view of its applications in every aspect of our daily life. The quest for deeper understanding of the subject has not just enlivened the development of the subject itself but has additionally proposed the progress in the supporting areas, such as applied mathematics,

numerical computing, and experimental techniques. A large number of problems in fluid dynamics have claimed the attention of mathematicians, physicists, and engineers for many years. As a result, an enormous body of established results has accumulated steadily but remains scattered in the literature.

The mechanism of heat transfer is the passage of thermal energy from a hot to a cold body. It occurs through conduction, convection, radiation or any combination of these. The molecular transport of heat in bodies or between bodies in the thermo dynamical system is referred to as conduction. Convection is concerned with the fluid medium and/or the fluid in the medium. The heat transfer due to the movement of fluid from one region to the other region in the medium is called convection. Radiation heat transfer is a mechanism in which the internal energy of a substance is converted into radiant energy. The transport of heat by convection together with conduction is known as convective heat transfer. Further, the free, forced and mixed convection are three classifications of the convective flows.

The transport of a component in a mixture, from a region of high concentration to a region of low concentration, is called mass transfer. The involvement and applications of mass transfer process have gained much attention, and it goes to a greater length in multiple fields such as the industrial, biological, physical and chemical engineering processes. Mass transfer is divided into two modes: Diffusive mass transfer and Convective mass transfer. The convective mass transfer is analogous to the convective heat transfer, it occurs between a moving mixture of fluid species and an exposed solid surface. Coupled heat and mass transport constitute a significant area of research in modern fluid dynamics such as an electronic cooling, drying processes, manufacture of electric cable insulations, curing of plastics, solar energy system, purification processes, etc.

A Newtonian fluid is a fluid that exhibits a viscosity that remains constant regardless of any external stress that is placed upon it, such as mixing or a sudden application of force. One example is water, since it flows the same way, in spite of of whether it is left alone or agitated vigorously. Another way to describe these fluids is that they have a linear relationship between viscosity and shear stress. Regardless of the shear stress applied to these fluids, the coefficient of viscosity will not change. Further, Newtonian fluids are those that

obey Newtons law relating shear stress and shear rate with a simple material property (the viscosity) dependent on basic thermodynamic variables such as temperature, concentration and pressure, but independent of flow parameters such as shear rate and time. This can be contrasted with non-Newtonian fluids, which can become thicker or thinner when stress is applied.

1.2 Porous Medium

The analysis of porous media plays an essential role in many fields of science and engineering, for instance, petroleum engineering, groundwater hydrology, agricultural engineering and soil mechanics. To study the motion of fluids through porous media, one must have sufficient under-standing of the governing equations for the fluid flow through porous medium. Owing to the intricate structure of the porous medium, several models have been proposed to explain mathematical and physical aspects of porous media. Among these, the Darcy model and a series of its modifications have attained much acceptance. Further, the boundary layer assumptions have been successfully applied to these models and much work over the last few decades has been done on them for a wide variety of geometries.

The study of convective heat and mass transport through porous media has been a fascinating and prominent research area for the past few decades, because of its wide range of industrial and engineering applications such as ground water contamination, thermal insulation, extraction of crude oil, chemical catalytic reactors, etc. Previous studies indicate that the Darcy model is applicable only for slow flows through porous media with low permeability (see Darcy [23]). At higher flow rates, modifications to the Darcy model are suggested, in view of nonlinear drag due to the solid matrix (see Forccheimer [30]) and viscous stresses by the solid boundary (see Brinkman [14]). A detailed review of convective heat and mass transport in Darcian and non-Darcian porous medium can be found in the book by Nield and Bejan [69].

The governing equation for fluid motion in a vertical porous column was first given by

Darcy [23] in 1856. It represents a balance of gravitational force, viscous force and pressure gradient. In mathematical form, it is given as

$$V = -\frac{K}{\mu}(\nabla \mathrm{P} - \rho_\infty \, g) \tag{1.1}$$

where V represents the space averaged velocity or Darcian velocity, μ represents the coefficient of viscosity, K represents the permeability of the medium, P represents the pressure, and g represents the body force per unit volume, ρ_∞ represents the density of the fluid. For one-dimensional flow and low porosity system, the above law appears to provide good agreement with experimental results. As this model does not take inertial effects into consideration, it is valid for seepage flows only i.e., for flows with low Reynolds number $(O(Re) < 1)$.

It is assumption that the flow through anisotropic porous medium with high permeability must reduce to the viscous flow in limit. In viewing this, Brinkman felt the need to account for the viscous force exerted by a flowing fluid on a dense swarm of spherical particles embedded in a porous mass and added the term $\mu' \nabla^2 V$ to balance the pressure gradient. Here μ' represents the effective viscosity given by $\mu' = \mu \, [1 - 2.5(1 - \epsilon)]$. The validity of the Brinkman model is restricted to the high porosity medium (as confirmed by the experiments). Its governing equation can be written as

$$-\left[\nabla P - \rho_\infty g\right] = \frac{\mu}{K} V - \mu' \nabla^2 V \tag{1.2}$$

In 1901, Forchheimer conducted experiments and proposed that the inertial effects can be accounted for through the addition of square of velocity in the momentum equation. At higher velocities one gets separation effects and wake effects both of which arise due to the nonlinearity of the Navier-Stokes equations, but which, in an averaged sense. Causes a mild quadratic effect to be added to Darcys law. So the pressure gradient is rendered less effective than it would be if everything satisfied a linear equation. The modification to the Darcy's

equation can be written as follows

$$\left[1 + \frac{\rho_\infty C_F \sqrt{K}}{\mu}|V|\right] V = -\frac{K}{\mu}\left[\nabla P - \rho_\infty g\right] \tag{1.3}$$

where C_F represents the dimensionless form drag coefficient. The coefficients of Darcy and Forchheimer terms contain both fluid properties and the microstructure of the porous medium. Some other models are also found in the literature related to porous media, and the validity and limitations of these models are well discussed in Nield and Bejan [69].

1.3 Power-law Fluid

It is well known that most of the fluids which are encountered in chemical and allied processing applications do not adhere to the classical Newtonian viscosity postulate and are accordingly known as non-Newtonian fluids. One particular class of fluids which are of considerable practical importance is that in which the viscosity depends on the shear stress or on the flow rate. Due to important applications of non-Newtonian fluids for the design of equipment and in the industrial processing, considerable efforts have been directed towards the analysis and understanding of such fluids. In modeling with the complexities of non-Newtonian fluid flows, methods that allow the description, interpretation and correlation of fluids properties are required. A number of mathematical models have been proposed in the literature to describe the rheological behavior of such fluids. Among these, a model which has been most widely used for non-Newtonian fluids and frequently encountered in chemical engineering processes, is the empirical Ostwald-deWaele model, or so-called power-law model. In this model, the relation between shear stress and viscosity is given by

$$\tau_{xy} = \mu^* \left|\frac{\partial u}{\partial y}\right|^{n-1} \frac{\partial u}{\partial y} \tag{1.4}$$

where μ^* is the consistency coefficient and n is the power-law index. The dimension of μ^* depends on the value of n and n being non-dimensional. When $n = 1$, the equation represents

a Newtonian fluid with a dynamic coefficient of viscosity μ^*. Therefore, deviation of n from a unity indicates the degree of deviation from Newtonian behavior. One may interpret the physical behavior of the fluid by appealing to an effective viscosity. For $n > 1$, the fluid is dilatant i.e, the effective viscosity increases from zero as the rate of strain increases from zero, which means that the fluid is easily moved by applying small forces. For $n < 1$, the fluid is pseudo-plastic i.e, the effective viscosity decreases from infinity as the rate of strain increases from zero, and therefore the fluid becomes runnier but it's very highly viscous at low strain rates. Shenoy [91] explained that numerous applications of convective heat transport in a porous medium saturated by a non-Newtonian power-law fluid. Chahtour *et al.* [15] investigated the effect of magnetic field on thermal instabilities of a power-law fluid saturated porous medium. Chamkha and Al-Humoud [17] presented the mixed convection for a non-Newtonian power-law fluid from a permeable vertical plate embedded in a fluid saturated porous medium with heat generation or absorption effects.

1.4 Fundamental Equation

The modified Darcy Law for the Power-law fluids is given by Kumari and Murthy [50]

$$\frac{\mu^*}{K}|V|^{n-1}V = -\nabla P - \rho_\infty g \tag{1.5}$$

where μ^* is the effective consistency factor, K is the permeability, n is power law index, ρ is the fluid density at the reference temperature and P is the dynamic pressure. The expression for the modified permeability K for flows of non-Newtonian power-law are given by

$$K = \begin{cases} \frac{6}{25}\left(\frac{n\epsilon}{3n+1}\right)^n \left(\frac{\epsilon d}{3(1-\epsilon)}\right)^{n+1}, \text{(Christopher and Middleman [20])} \\ \frac{2}{\epsilon}\left(\frac{d\epsilon^2}{8(1-\epsilon)}\right)^{n+1}\left(\frac{6n+1}{10n-3}\right)\left(\frac{16}{75}\right)^{\frac{3(10n-3)}{10n+1}}, \text{(Dharmadhikari and Kale [24])} \end{cases} \tag{1.6}$$

It is noted that the vertical plate embedded in a porous medium is saturated with power-

law fluid. The fluid and the saturated porous medium are locally thermodynamic equilibrium and the properties of the porous medium are homogeneous and isotropic. Since the porous medium is to be closely packed, Darcy's law is moderate and adequate. For thermal and concentration convection to occur, the fluid density is to be a function of the temperature and concentration and hence it is necessary to consider an equation of state which couples the equation of mass, momentum and energy.

$$\rho_\infty = \rho\left(1 - \beta_T(T - T_\infty) - \beta_C(C - C_\infty)\right) \tag{1.7}$$

Subsequently, we employ the Boussinesq approximation, which is valid and provided that density variation along with temperature gradient and concentration gradient of the medium(Solid and fluid).

Using the above approximations and employing the boundary layer assumptions, we get the following simplified equations for continuity equation, modified Darcy law, conservation of energy and conservation of concentration

$$\frac{\partial u}{\partial x} + \frac{\partial v}{\partial y} = 0 \tag{1.8}$$

$$u^n = \frac{K}{\mu}\left(\frac{\partial p}{\partial x} + g\rho\left(\beta_T(T - T_\infty) + \beta_C(C - C_\infty)\right)\right) \tag{1.9}$$

$$u\frac{\partial T}{\partial x} + v\frac{\partial T}{\partial y} = \frac{\partial}{\partial y}\left[\alpha\frac{\partial T}{\partial y}\right] \tag{1.10}$$

$$u\frac{\partial C}{\partial x} + v\frac{\partial C}{\partial y} = D\frac{\partial}{\partial y}\left[\frac{\partial C}{\partial y}\right] \tag{1.11}$$

where T_∞ is the free stream temperature, C is the species concentration, C_∞ is the concentration, g is the acceleration due to gravity, ρ is the reference density, K is the permeability, β_T and β_C are the thermal and concentration expansion coefficients respectively. Here, n is the index in the power-law variation of viscosity, $n < 1$ for the pseudo-plastic fluids, $n > 1$ for the dilatant fluids and $n = 1$ for the Newtonian fluids.

1.5 Local thermal non-equilibrium model

In most cases studied in the literature it has been assumed that the porous matrix and the fluid flowing through it are in local thermal equilibrium (LTE). At the microscopic level, the temperature and the rate of heat flux at the interface between solid and fluid phases must be identical, but the average value over a representative elementary volume should not yield locally equal temperatures for the two phases. In this case the two phases are in local thermal non-equilibrium (LTNE). Rees and Pop [86] explained that LTNE is not necessarily an unsteady phenomenon, but it can also arise in steady flows. A recent review by Rees and Pop [86] summarises much of the present knowledge, including the various models used for LTNE and their application to free, mixed and forced convective flows and to stability analyses. Following Banu and Rees [6] and Barletta [7] the simplest way to model the LTNE in an isotropic porous medium is to use two thermal balance equations, one for the fluid phase and one for the solid matrix, namely

$$\epsilon(\rho_c)_f \frac{\partial T_f}{\partial \bar{t}} + (\rho_c)_f \, \underline{\bar{u}}.\nabla T_f = \epsilon k_f \nabla^2 T_f + h(T_s - T_f), \tag{1.12}$$

$$(1-\epsilon)(\rho_c)_s \frac{\partial T_s}{\partial \bar{t}} = (1-\epsilon) k_s \nabla^2 T_s + h(T_f - T_s), \tag{1.13}$$

where T_f is the fluid temperature, T_s is the solid temperature, ϵ is the porosity of the porous medium and h is the interphase heat transfer coefficient, respectively. Most papers which deals with convective flows in porous media assume that LTE holds. However, important cases where LTE cannot be invoked may exist. First introduced by Schumann [88], Eqs. 1.12 and 1.13 use simple linear source/sink terms to model the local (i.e. microscopic) heat transfer between the phases at the pore level.

When $T_s > T_f$ the final term in Eq. 1.12 acts as a source of thermal energy into the fluid phase, while the final term in Eq. 1.13 is a thermal sink for the solid phase. Equation 1.12 also shows us that, when a medium is of low porosity ($\epsilon \ll 1$) and the solid and fluid phases exhibit the temperature difference, ΔT, then the rate of change of the fluid temperature is $O(h\Delta T/\epsilon\rho_c)_f$. As this is inversely proportional to ϵ, there is a rapid change in the fluid

temperature towards that of the solid phase to establish LTE.

1.6 Stability

The study of hydrodynamic stability aims to determine conditions under which a given flow is stable, i.e. realizable in practice, or unstable. This is undertaken by adding disturbances to a known flow, often called the basic state, and the fate of such disturbances is found using either analytical or numerical methods. For a convective flow the disturbances may be to either the velocity or temperature field or both, and may also arise because of imperfections in the overall system such as rough bounding surfaces. There are two main ways of approaching such flow instability problems. One is the use of a linear stability theory where the disturbances have a sufficiently small magnitude that nonlinear terms may be neglected, and therefore their exponential growth rate may be computed. The other is a nonlinear stability analysis which may take a variety of forms such as a weakly nonlinear analysis or energy/integral methods.

Linear Stability

The method of linear stability analysis consists of introducing infinitesimal perturbations to an initial state of the flow whose stability is to be examined. The procedure to find the condition on stability is described in this section.To examine the stability of a physical system, let Ψ be a steady state (initial state) solution. Then we add a perturbation $\Psi\, x$ to the steady state solution Ψ, and substitute ($\Psi = \Psi_b + \psi$) into the flow governing equations. From the resulting equations, we subtract away the basic terms which Ψ satisfies identically. We remain with the perturbation equations. Then, we have to linearize the perturbation equations by assuming small (infinitesimal) perturbations, and by neglecting the product of perturbations. The linearized perturbation equations can be simplified by assuming a form for the perturbations. These linearized perturbation equations should be homogeneous with homogeneous boundary conditions. From this system of equations, eigenvalue problem can

be obtained. These eigenvalues determine the condition on the stability. In this analysis, the problem is linearized by neglecting the product of perturbations. And therefore, this method examines the initial behavior of the perturbations.

When a physical system is perturbed, either the amplitude of perturbation gradually decays; or grows with time in such a way that the system progressively departs from its initial state and never comes back to it. In the first case, the system is stable with respect to that particular perturbation; in the second case, it is unstable. We say that the system is stable if it is stable with respect to all possible perturbations. However, the system is unstable even if it is unstable with respect to only one perturbation.

As explained above, to check the stability of the system one needs to check the stability of all possible perturbations. In practice, we take an arbitrary perturbation in terms of normal modes. In illustration of how one does this, consider a system which is confined between two parallel planes and in which the physical variable in the steady state are functions only of z normal to the plane. In this case, the time dependent periodic perturbations in horizontal plane can be written in the form

$$\Psi = f(z)e^{\lambda t}\cos kx; \quad \Theta = g(z)e^{\lambda t}\sin kx; \quad \Phi = h(z)e^{\lambda t}\sin kx \tag{1.14}$$

where λ is the exponential growth rate and k is the wavenumber of the disturbance.

1.7 Numerical methods

The governing equations of convective heat and mass transfer in Newtonian and/or non-Newtonian fluids are essentially coupled and non-linear partial differential equations. Generally, these non-linear partial differential equations cannot be solved analytically, so recourse must be made to a numerical approach. Various numerical methods, including the finite element methods, finite difference methods, finite volume methods, spectral methods, boundary element methods, homotopy analysis method, cubic spline collocation method, etc., have

been used by several researches to solve the system of nonlinear differential equations. Here, we have used two numerical methods namely, shooting method and matrix-based method. Shooting method used to solve the boundary value problems, and matrix-based method used to solve the eigenvalue problems obtained in hydrodynamic stability.

Shooting Method

Shooting method is very simple and it is particularly easy to modify from problem to problem, basically it requires to change in only one subroutine that contains the first order differential equations. Moreover, it is easy to implement different boundary conditions in shooting method. The basic idea of shooting method for solving boundary value problem is to try to find an appropriate initial condition for which the computed solution "hit the target" so that the boundary conditions at other points are satisfied. The major steps for applying shooting method are as follows

- The higher order non-linear differential equations are converted into simultaneous non-linear differential equations of first order.
- Assume some values for variables which are not specified at the initial point
- Integrate the first order equations using the 4^{th} order Runge-Kutta method with assumed initial values from initial point to terminal point
- Check the accuracy of the assumed initial values by comparing the calculated terminal values with the given values
- This process is continued until the agreement between the calculated and the given condition at terminal point is within the specified degree of accuracy.

Matrix-based Method

In shooting method, we have considered the Péclet number range from 0.1 to 2.0. When we increased the range of Péclet number for certain parameters they are not converging, Hence to over come these difficulties, we have resort to a numerical method called matrix-based method. These matrix methods play an important role, and offer useful alternative to the shooting method. The main advantages of matrix-based method are the achievement of a global solution, faster convergence and produce as many eigenvalues and the corresponding functions as one desired. This method is easy to extend to higher order systems. More importantly, finite difference method is particularly suitable for eigenvalue problems, in which the differential equations contain a singular form.

Therefore the equations for both the eigenvalue problem and the basic state were solved by approximating the derivatives in the above-quoted equations by second order central differences and the resulting algebraic written in matrix/vector form. A uniform grid of points of length, δ, was used where the numerical values of f at $z = z_i = i\delta$ are denoted by f_i. When there are N internal points, then $(N+1)\delta = 1$ and we denote the vector of f-values by $\underline{\mathrm{f}} = (f_1, f_2, \cdots, f_{N-1}, f_N)$. In the following, we shall illustrate the method by taking $N \times N$ when N intervals are used in range, $0 \leq z \leq 1$.

1.8 Literature Review

The study of free and mixed convection due to a heated or cooled vertical surface provides one of the most basic scenarios for heat and mass transfer theory and thus is of considerable theoretical and practical interest. Free convection of heat and mass transfer occurs simultaneously in the fields of design of chemical processing equipment, distributions of temperature, formation and dispersion of fog, groves of fruit trees and moisture over agricultural fields. It also occurs in the context of damage to crops due to freezing and pollution of the environment. The phenomenon of mixed convection occurs in many technical and industrial problems such as solar collectors, nuclear reactors cooled during an emergency shutdown,

electronic devices cooled by fans, a heat exchanger placed in a low-velocity environment and so on.

Convective flow along a vertical surface embedded in a porous medium, is one of the fundamental and classical problems in the heat and mass transfer theory. It has attracted a great deal of interest from many investigators owing to the broad applications such as geothermal systems, energy-storage units, heat insulation, heat exchangers, drying technology, catalytic reactors, nuclear waste repositories, etc. The literature relevant to the convective flows over different surface geometries in Darcy and non-Darcy porous media has been reported by Ingham and Pop [40], Nield and Bejan [69], Vafai [106] (see the citations therein).

In wide range, most of the researchers considered the effects of buoyancy force by assuming that the temperature and density vary linearly (it is known as linear Boussinesq approximation or simply Boussinesq approximation). However, there are several reasons for the density-temperature relationship to become non-linear, for instance when the temperature difference between the surface of the body and the ambient fluid becomes significantly large. In this case, non-linear density and temperature variations in the buoyancy force term may exert a strong influence on the flow field and heat transfer characteristics (for details see Barrow and Rao [10]). This physical concept has a unavoidable applications in geothermal and engineering process such as pore water convection near salt domes, cooling of electric equipment, and the residual warm water discharged from a geothermal power plant. In view of the above said applications, Partha [75] developed a mathematical model on non-Darcy porous medium with a temperature-concentration dependent density relation, in which they observed that an increase in nonlinear temperature and concentration parameters, the heat and mass transfer varies extensively depending on Darcy and non-Darcy porous medium. Prasad *et al.* [77] scrutinized the natural convection flow along a vertical at plate in a non-Darcy porous medium with the nonlinear density-temperature variation under prescribed constant surface temperature. The convective flow of nonlinear density-temperature relationship over an impulsive stretching sheet has been examined by Motsa *et al.* [61] (and also see the citations therein).

In flow problems the thermo physical properties of fluid were assumed to be constant.

However, it is known that these properties, especially for fluid viscosity and fluid thermal conductivity, may change with temperature. To predict the heat transfer rate accurately, it is necessary to take into account the variation of viscosity and thermal conductivity. In recent years, the effect of variable viscosity and thermal conductivity on the convective heat and mass transfer has gained much importance in production of paper, plastic film's drawing, hot rolling glass fiber, glass fiber production, etc. Ling and Dybbs [53] found theoretically that the viscosity of water decreases by about 240% when the temperature increases from $10^{\circ}C(\mu = 0.0131g/cms)$ to $50^{\circ}C(\mu = 0.00548g/cms)$. Hossain *et al.* [37] discussed the free convective boundary layer flow along a vertical plate in the presence of variable viscosity. The effect of variable viscosity, thermal radiation and velocity slip on the flow of a power-law fluid over a non-linearly stretching surface has been examined by Megahed [59]. Noghrehabadi *et al.* [70] investigated the effect of variable viscosity and thermal conductivity on the natural convection heat transfer along a vertical plate in a porous medium saturated by nanofluid. Mahanti and Gaur [54], studied the effects of variable viscosity and thermal conductivity on free convective flow of a viscous incompressible fluid along an isothermal vertical plate in the presence of heat sink. Umavathi [105] discussed the influence of variable viscosity and thermal conductivity on free convective flow, heat and mass transfer in a vertical channel filled with porous medium. Recently, The two dimensional stagnation point flow of a viscous incompressible electrically conducting fluid over a linearly stretching sheet in porous media with variable viscosity and thermal conductivity, has been presented by Rao *et al.* [80].

The influence of thermal and solutal dispersion in a porous medium are essential due to the existence of inertial effects (see Nield and Bejan [69]). The heat and mass transport due to the hydrodynamic mixing is called thermal and solutal dispersions, respectively. The interest in the above studies is motivated by numerous engineering applications such as thermal insulation systems, geothermal engineering, packed bed reactors, petroleum recovery, ceramic processing, sensible heat storage beds, groundwater pollution, etc. In view of the above said applications, Telles and Trevisan [100] presented the hydrodynamic dispersion effect on free convective heat and mass transfer near to the vertical surface in a porous medium. The effects of thermal and solutal dispersion in a non-Darcy porous medium have

been discussed by Murthy [63]. The effects of double dispersion and variable viscosity on free convective flow of a non-Newtonian fluid over the vertical cone embedded in a non-Darcy porous medium have been explored by Kairi [43]. Afify and Elgazery [1] presented the effects of double dispersion, melting and thermal radiation on mixed convective heat and mass transfer flow over a vertical surface in a non-Darcy porous medium. Narayana and Sibanda [67] analyzed the double dispersion effects on MHD mixed convective flow along a vertical flat plate embedded in a non-Darcy porous medium. Murthy and Singh [65] investigated the thermal dispersion effect on the mixed convective flow over the isothermal vertical cone embedded in a non-Darcy porous medium.

The effect of thermal radiation in different fluid flows, is very useful in the nuclear plants, gas turbines, various propulsion devices for aircraft, missiles, satellites, space vehicles, etc. At high temperature, the thermal radiation can significantly affect the heat transfer rate and the temperature distribution within the boundary layer flow of a participating fluid. Also, the thermal radiation may play an essential role in controlling the heat transfer in industries where the quality of final product depends on the heat controlling factors to some extent. Because of these applications, Hossain and Takhar [38] considered the mixed convective boundary layer flow along a heated vertical plate in the presence of thermal radiation. Grosan and Pop [31] discussed numerically the influence of radiation free convective flow over a vertical surface in a power-law fluid. Hayat *et al.* [34] focused on two dimensional mixed convection stagnation-point flow of power-law fluids towards a stretching sheet with the effect of MHD and thermal radiation. Umamaheswar *et al.* [104] studied the free convection flow of a non-Newtonian fluid past an impulsively started vertical plate in the influence of MHD, thermal radiation, thermal diffusion, chemical reaction and heat absorption.

In recent years, several boundary layer flow problems have received attention more attention in context of magneto-hydrodynamics (MHD). Several investigators have extended many of the available boundary layer solutions to include the effects of magnetic fields for those cases when the fluid is electrically conducting. The study of magnetohydrodynamic flow for an electrically conducting fluid past a heated surface has important applications in many engineering problems such as plasma studies, petroleum industries, MHD power gen-

erators, cooling of nuclear reactors, the boundary layer control in aerodynamics, and crystal growth. Aldoss *et al.* [3] have considered the magnetohydrodynamic mixed convection from a vertical plate embedded in a porus medium. Makinde and Aziz [57] numerically investigated the influence of convective boundary condition on MHD mixed convective heat and mass transfer along a vertical plate embedded in a porous medium.

The occurrence of diffusive flux due to temperature gradient is known as the thermal diffusion or Soret effect. In most of the studies, Soret effect is neglected on the basis that it is of a smaller order of magnitude than the effects described by Fourier's and Fick's laws. This Soret effect plays an important role in many natural activities, viz., in the underlying physics of the solar ponds, the demographics of an ocean and also convection in stars (see Ingham and Pop [40]). Also, it has been utilized for isotope separation and in a mixture between gases with very light weight molecular (H_2, He) and of medium weight molecular (N_2, air) [26]. Due to its significant applications, several authors analyzed the Soret effect on Newtonian and non-Newtonian fluids through different geometries. Dursunkaya and Worek [25] studied the cross-diffusion effects on natural convective flow along a vertical surface. Kafoussias and Williams [42] discussed the mixed convective flow along a vertical plate under the influence of Dufour and Soret effects.

In the recent past, many researchers focused on different procedures for obtaining the similarity solution of the convective transport phenomena problems arising in fluid dynamics, plasma physics, aerodynamics, meteorology and some branches of engineering. One such procedure is Lie group analysis. The concept of Lie group analysis, initiated by Sophus Lie, is also known as symmetry analysis. It determine point transformations which map a given differential equation to itself and it combines almost all known exact integration techniques (Ref. [73], [72], [13]). It provides a potent, sophisticated and systematic tool for generating the invariant solutions of the system of nonlinear partial differential equations (PDEs) with relevant initial or boundary conditions. A special form of Lie group transformations, known as the scaling group of transformation, has been suggested by various researchers to study convection flows of different flow phenomena with some unavoidable limitations (see Tapanidis *et al.* [99], Hassanien and Hamad [33], Kandasamy *et al.* [45], Mutlag *et al.* [66],

Ramreddy *et al.* [79] etc. are worth observing).

The flow and heat transfer in an electrically conducting fluid in the presence of a magnetic field has attracted several researchers in view of its applications in engineering, technology and science. Makinde and Aziz [57] numerically investigated the influence of convective boundary condition on MHD mixed convective flow along a vertical plate embedded in a porous medium. Mahmoud [56] investigated the effect of thermal radiation, viscous dissipation and variable viscosity on the problem of unsteady MHD flow on natural convection flow over a vertical plate. Khidir *et al.* [47] analyzed the MHD convective flow due to a porous rotating disk under the influence of variable properties, viscous dissipation, Ohmic heating, Hall current, and thermal radiation. Mukhopadhyay and Mandal [62] studied the effects of velocity slip and thermal slip on magnetohydrodynamic boundary layer mixed convection flow heat transfer over a vertical porous plate in the presence of suction/blowing.

The infinitesimal convection occurring in a horizontal fluid saturated porous medium heated from below was extensively studied since the first papers by Horton and Rogers [36] and Lapwood [52] (motivated from the works of Rayleigh [83]). This work was generally known as *Horton-Rogers-Lapwood* problem or *Darcy-Bénard* problem. In this study, they investigated on the convection in a homogeneous and isotropic porous layer with uniform thickness. The flow in their studies was governed by the Darcy-law, and the Oberbeck-Boussinesq approximation was employed; and also fluid and solid phases were in local thermal equilibrium condition. These works showed as to how the porous layer becomes unstable when the temperature difference exceeds certain critical value. This critical value is determined by the coefficient of thermal conductivity, thermal expansion coefficient, kinematic viscosity, length of porous layer and boundary conditions. Sutton [97] found the critical Rayleigh number for the convective flow in a porous channel.

The above works were based on convective instability in a porous layer due to vertical temperature difference alone. The stability of convection in a horizontal porous layer with horizontal as well as vertical temperature gradients was studied in Weber [107]. In this work, temperature was varied linearly along the boundaries, where as the vertical temperature difference was kept constant. This work was limited to small horizontal temperature

gradients. The analysis of this problem showed that the critical Rayleigh number for this problem is always larger than the critical Rayleigh number for the Darcy-Bénard problem. In the standard Darcy-Bénard problem, the instability is driven by density variations caused by temperature difference between upper and lower boundaries. Convective instability of the Darcy-Bénard problem with throughflow in a porous layer saturated by a power-law fluid (see Kumari and Murthy [50], Alves and Barletta [4]).

Local thermal non-equilibrium (LTNE) arises under various circumstances when considering heat transfer in porous media. Given that the temperature field is an average over a Representative Elementary Volume, one which is small compared with any macroscopic length scale of interest, but one which is large compared with the microstructure of the medium, it is quite possible for the respective fluid and solid temperatures which are associated with a given point to be different. Examples of such circumstances include the rapid heating of one of the phases or the sudden and rapid infiltration of a fluid with a different temperature from that of the previous equilibrium. In such cases, two Fourier's equations are used, one for each phase, and these are coupled by source/sink terms which allow for microscopic heat transfer between the phases. Detailed correlations for a wide variety of possible porous structure were given in Rees (Ref. [85], [84]). Within context of the Darcy-Bénard problem, a comprehensive analysis of the effect of LTNE was given by Banu and Rees [6]. These found that LTNE serves to increase both the critical wavenumber and Darcy-Rayleigh number from the classical values quoted above. In some circumstances, (namely where $hd^2/\epsilon k_f \gg 1$ but where $hd^2/(1-\epsilon)k_s = O(1)$, where ϵ is the porosity and k represents the conductivity of the fluid and solid phases,) the critical wavenumber can become extremely large.

Due to the important applications of power-law fluid saturated Darcy/non-Darcy porous medium, the usefulness of convective flows over the vertical plate has been analyzed in this thesis. In addition, a problem of linear stability of the Darcy-Bénard convection on a power-law fluid has been studied. The problems considered in this thesis are outlined in the next section. Although the literature mentioned above is small, we will provide a good amount of literature in the subsequent chapter which motivated us to study these problem.

1.9 Aim and Scope

The objective of the present thesis is to obtain the numerical solutions for the convective heat and mass transport in a power-law fluid saturated porous medium. The study focusses on the attributes of various effects such as MHD, variable properties, double dispersion, Soret, thermophoresis and thermal radiation in Darcy and/or non-Darcy porous medium saturated with a power-law fluid. The problems considered in this thesis deal with boundary layer flow, and/or linear stability analysis for the Darcy-Bénard convection.

1.10 Outline of the Thesis

This thesis is arranged in FOUR Parts with a total of NINE Chapters.

Part-I consists of a single **Chapter 1** which is introductory in nature. In this chapter we present the governing equations of fluid flow, heat and mass transfers of power-law fluid along with a brief review of the basic terminology related to the thesis and the existing literature.

Part II presents the similarity solution for mixed convective flow along a vertical plate in a Darcy porous medium saturated with power-law fluid. This part consists of four Chapters (i,e., Chapters 2-5). In Chapters 2-4, Lie scaling group of transformations are applied to get the similarity representation to the governing equations and then the resulting systems of ordinary differential equations are solved using the shooting method. The obtained results are compared with previously published work and are found to be in good agreement. In chapter-5, a linear stability analysis for the Darcy-Bénard convection is studied. The linearized disturbance equations are reduced to a eigenvalue problem in ordinary differential by assuming a periodic train of convection cells. Then the critical Rayleigh number is found as the eigenvalue of that system. The details of these chapters are given below.

The effects of variable properties and double dispersion on mixed convective flow over a vertical plate embedded in a power-law fluid saturated porous medium, are studied in

Chapter-2. The variable viscosity is assumed to vary as a inverse linear function of temperature and thermal conductivity as a linear function of temperature. The numerical results for the non-dimensional velocity, temperature and concentration are displayed graphically for different values of variable viscosity, thermal conductivity, thermal dispersion and solutal dispersion.

Chapter-3 deals with the mixed convective heat and mass transport along a vertical plate in a power-law fluid saturated Darcy porous medium. The influence of variable viscosity, thermal conductivity and thermophoresis parameters on the non-dimensional velocity, temperature and concentration profiles are displayed graphically for pseudo-plastic, Newtonian and dilatant fluid. Further, the dimensionless heat and mass transfer rates are displayed in a tabular form.

Chapter-4 an analysis is made for the influence of thermal radiation, Soret and variable properties on mixed convective flow, heat and mass transfer from a vertical plate in a Darcy porous medium saturated by a power-law fluid. The numerical results for dimensionless velocity, temperature and concentration profiles for pseudo-plastic, Newtonian and dilatant fluids are presented graphically for different values of Soret, thermal radiation, variable viscosity and thermal conductivity parameters. The non-dimensional Nusselt and Sherwood numbers are presented in tabular form. The present numerical results are compared with previously published work and the results are found to be in excellent agreement.

In **Chapter-5**, a horizontal porous layer which is heated from below is subjected to a vertical throughflow which eventually confines the temperature field to being near one the bounding surfaces when the throughflow is sufficiently strong. The saturating fluid is taken to be of power-law form, and the solid and fluid phases of the porous medium are assumed not to be in local thermal equilibrium; thus there are separate heat transport equations for the fluid and solid phases. The basic state, whose stability characteristics are to be sought, are solved numerically, because no analytical solution is available. The linear stability analysis is then carried out, by descritizing the tenth-order eigenvalue problem using finite differences then solving it by a matrix-based method. The neutral stability curves and the critical Rayleigh number for the onset of instability are obtained. It is found that the critical wavenumber

and Rayleigh number both increase as the Péclet number increases.

Part III presents the similarity solution for a power-law fluid flow along a vertical plate in a non-Darcy porous medium. This part consists of three Chapters (i,e., Chapters 6-8). In these chapters, Lie scaling group of transformations are applied to get the similarity representation to the system of partial differential equations and then the resulting systems of equations are solved by shooting method. Comparisons with the published works are performed and are found to be in very good agreement. The details of these chapters are given below:

Chapter-6 explores the effects of magnetohydrodynamic, double dispersion and variable properties on mixed convective flow past a vertical surface in a power-law fluid saturated porous medium. The influence of relevant parameters on the non-dimensional velocity, temperature, and concentration for pseudo-plastic fluid, Newtonian and dilatant fluids are discussed and displayed graphically. The behaviors of heat and mass transfer coefficients are shown in tabular form.

The objective of **Chapter-7**, is to analyse the hydromagnetic mixed convective heat and mass transfer over a vertical plate in a power-law fluid saturated non-Darcy porous medium under the influence of thermophoresis, variable viscosity and variable thermal conductivity. The numerical results for the non-dimensional velocity, temperature and concentration are discussed and displayed graphically for various parameters such as magnetic field, thermophoresis, variable viscosity and thermal conductivity.

The analysis of steady mixed convective heat and mass transfer along a permeable vertical plate in a non-Darcy porous medium saturated with power-law fluid, is examined in **Chapter-8**. The effects of thermal radiation, variable properties and MHD parameters on physical quantities of the fluid flow are exhibited graphically.

For solving the problems in chapters (2,3,4,6,7 and 8), shooting technique which uses Runge-Kutta fourth-order method is employed. In chapter-5, the tenth-order eigenvalue problem is solved using finite differences and a matrix-based method.

Finally, **Part IV** consists of single Chapter (i.e., **Chapter-9**) which presents the main conclusions of the thesis and point out various problems which are yet to be solved in this area.

List of references is given at the end of the thesis. The references are arranged in an alphabetical order and according to this order, citations appear in the text.

Considerable part of the work in the thesis is published/accepted for publication in reputed journals. The remaining part is communicated for possible publications. The details are presented below.

List of Papers Published

1. "Effects of Double Dispersion on Mixed Convection in a Power-Law Fluid Saturated Porous Medium With Variable Properties Using Lie Scaling Group Transformations", *Procedia Engineering*, Vol. 127 (2015), pp.362–369.

2. "Influence of Variable Properties and Double Dispersion on Mixed Convection in a Power-Law Fluid-Saturated Non-Darcy Porous Medium", *Special Topics & Reviews in Porous Media: An International Journal*, Vol. 8(3) (2017), pp.177–195.

3. "Scaling Group Transformation for Mixed Convection in a Power-Law Fluid Saturated Porous Medium with Effects of Soret, Radiation and Variable Properties", *Frontiers in Heat and Mass Transfer* , Vol. 9(1), (2017).

4. "Mixed Convection in a Power-law Fluid Saturated Non-Darcy Porous Medium with Influence of Variable Properties, MHD and Thermophoresis", *International Journal of Pure and Applied Mathematics*, Vol. 113(12), (2017), pp.160-168.

List of Papers Accepted

5. "Numerical Study on Mixed Convection in a Power-law Fluid Saturated Porous Medium with Variable properties and Thermophoresis effects via Lie Scaling Group Transformations", Accepted for publication in *Computational Thermal Sciences*.

List of Papers Communicated

6. "Radiation Effect on MHD Mixed Convection Flow of a Power-law Fluid Saturated non-Darcy Porous Medium With Variable Properties", Communicated to *Journal of Nanofluid*.

7. "Linear stability of the Darcy-Bénard convection of a power-law fluid with local thermal non-equilibrium", Communicated to *Transport in Porous Media*.

Part II

SIMILARITY SOLUTION FOR MIXED CONVECTIVE FLOW ALONG A VERTICAL PLATE IN A DARCY POROUS MEDIUM SATURATED WITH POWER-LAW FLUID

Chapter 2

Mixed Convective Flow over a Vertical Plate Embedded in a Power-law Fluid Saturated Porous Medium with Double Dispersion and Variable Properties [1]

2.1 Introduction

In the recent past, the study of fluid flow, heat and mass transfers with the variable thermo physical properties has received much attention. Jayanthi and Kumari [41] analyzed the effect of variable viscosity in a power-law fluid saturated porous medium. Srinivasacharya *et al.* [94] obtained a similarity solution to explore the effects of Soret and Dufour on mixed convective flow along a vertical wavy surface in a porous medium with variable properties. Rao *et al.* [80] investigated the influence of thermal radiation on MHD flow over a linearly stretching sheet in a porous medium in the presence of variable viscosity and thermal

[1] Published in "**Procedia Engineering**" 127 (2015) 362–369

conductivity.

The energy and concentration transport due to the hydrodynamic mixing is called thermal and solutal dispersions, respectively. The effects of thermal and solutal dispersions (double dispersion) in a Darcy porous medium are necessary due to the presence of inertial effects (see Nield and Bejan [69]). The thermal and solutal dispersion effects in a homogeneous and isotropic Darcian porous media have been studied by Dagan [22]. Thermal and solutal dispersions are used in many engineering and industrial applications. The effects of thermal and solutal dispersion on mixed convective flow of a porous medium saturated with power-law fluid have been analysed by Kairi and Murthy [43]. Kameswaran and Sibanda [44] analyzed thermal dispersion on a non-Newtonian power-law nanofluid over an impermeable vertical plate. Srinivasacharya *et al.* [96] investigated the magnetic and double dispersion effects on natural convection in non-Darcy porous media saturated with power-law fluid.

The aim of the present chapter is to study the effects of variable properties and double dispersion on convective transport in a power-law fluid along a vertical plate. This type of mathematical modeling becomes slightly more complicated leading to the complex interactions of the flow, heat and mass transfer mechanism. In spite of this complexity, the similarity representation to the system of non-dimensional equations is obtained using Lie group transformations. The main advantages of these Lie group transformations is to obtain similarity representation for the system of nonlinear partial differential equations. Moreover, the Lie group technique has been applied by many researchers (see Oberlack [71], Kandasamy *et al.* [46], Afify *et al.* [2], Ferdows *et al.* [29] and Uddin *et al.* [103]). The solution of the reduced system of ODE is obtained by the well known shooting method. These numerical results for the non-dimensional velocity, temperature and concentration are illustrated graphically for different values of variable viscosity, thermal conductivity, thermal dispersion and solutal dispersion parameters. In addition, local heat and mass transfer are shown in a tabular form.

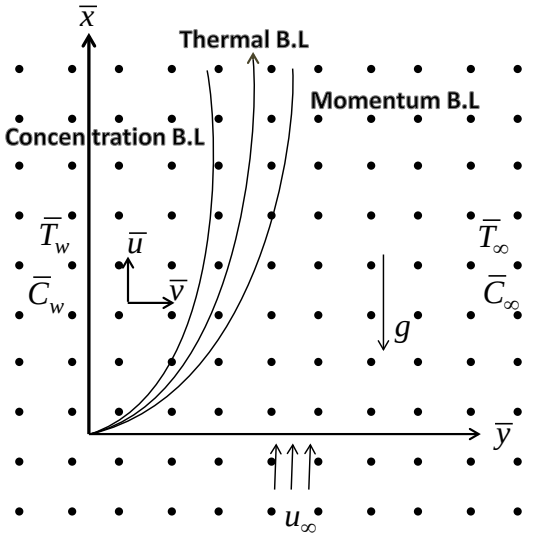

Figure 2.1: Physical model and coordinate system.

2.2 Mathematical Formulation

Consider a steady, laminar, incompressible, mixed convection heat and mass transfer boundary layer flow over a vertical plate in a power-law fluid saturated Darcy porous medium. Choose the two dimensional coordinate system such that the $\overline{x}$-axis is along the vertical plate and $\overline{y}$-axis normal to the plate. The gravitational acceleration g acts in a downward direction. The physical model and coordinate system is shown in Fig. (2.1). The wall is maintained at constant temperature and concentration $\overline{T}_w$ and $\overline{C}_w$, respectively. These values are assumed to be greater than the ambient temperature and concentration $\overline{T}_\infty$ and $\overline{C}_\infty$, respectively.

By using Boussinesq approximation and the boundary layer assumptions, the governing equations, namely, the equations of continuity, momentum, energy and concentration for the power-law fluid (see Shenoy [91]), are given by

$$\frac{\partial \overline{u}}{\partial \overline{x}} + \frac{\partial \overline{v}}{\partial \overline{y}} = 0 \tag{2.1}$$

$$n\overline{u}^{n-1}\frac{\partial \overline{u}}{\partial \overline{y}} = \frac{\partial}{\partial \overline{y}}\left[\frac{gK\rho_\infty}{\mu}\left(\beta_T^*(\overline{T}-\overline{T}_\infty)+\beta_C^*(\overline{C}-\overline{C}_\infty)\right)\right] \tag{2.2}$$

$$\overline{u}\frac{\partial \overline{T}}{\partial \overline{x}} + \overline{v}\frac{\partial \overline{T}}{\partial \overline{y}} = \frac{\partial}{\partial \overline{y}}\left[\alpha_e \frac{\partial \overline{T}}{\partial \overline{y}}\right] \tag{2.3}$$

$$\overline{u}\frac{\partial \overline{C}}{\partial \overline{x}} + \overline{v}\frac{\partial \overline{C}}{\partial \overline{y}} = \frac{\partial}{\partial \overline{y}}\left[D_e \frac{\partial \overline{C}}{\partial \overline{y}}\right] \tag{2.4}$$

where $\overline{x}$ and $\overline{y}$ are the Cartesian coordinates, $\overline{u}$ and $\overline{v}$ are the Darcy velocity components in $\overline{x}$ and $\overline{y}$ directions, respectively. Further, $\overline{T}$ is the temperature, $\overline{C}$ is the concentration, g is the acceleration due to gravity, ρ_∞ is the reference density, K is the permeability, β_T^* and β_C^* are the thermal and concentration expansion coefficients respectively. Here, n is the index in the power-law variation of viscosity, $n < 1$ for the pseudo-plastic fluids (shear-thinning fluid), $n > 1$ for the dilatant fluids (shear-thickening fluids) and $n = 1$ for the Newtonian fluids.

The associated boundary conditions are

$$\left.\begin{aligned} &\overline{v} = 0, \quad \overline{T} = \overline{T}_w, \quad \overline{C} = \overline{C}_w \quad \text{at} \quad \overline{y} = 0 \\ &\overline{u} = u_\infty, \quad \overline{T} = \overline{T}_\infty, \quad \overline{C} = \overline{C}_\infty \quad \text{as} \quad \overline{y} \to \infty \end{aligned}\right\} \tag{2.5}$$

where the subscripts w and ∞ indicate the conditions at the wall and at the outer edge of the boundary layer, respectively.

The fluid properties are assumed to be isotropic and constant except fluid viscosity and thermal conductivity. The viscosity μ of the fluid is assumed to be an inverse linear function of temperature and it can be expressed as (see Lai and Kulacki [51])

$$\frac{1}{\mu} = \frac{1}{\mu_\infty}[1 + \delta^*(\overline{T} - \overline{T}_\infty)] \quad \text{or} \quad \frac{1}{\mu} = b^*(\overline{T} - \overline{T}_e) \tag{2.6}$$

where $b^* = \frac{\delta^*}{\mu_\infty}$, $\overline{T}_e - \overline{T}_\infty = -\frac{1}{\delta^*}$, μ_∞ is the coefficient of the viscosity far away from the plate. Here b^*, $\overline{T}_\infty$ are constants and their values depend on the reference state and the thermal property of the fluid, i.e δ^* in general $b^* > 0$ for liquids and $b^* < 0$ for gases. The variable thermal conductivity α is to vary as a linear function of temperature (see Slattery [92]) such as

$$\alpha = \alpha_0 \left(1 + E(\overline{T} - \overline{T}_\infty)\right) \tag{2.7}$$

where α_0 is the thermal diffusivity, E is a constant depending on the nature of fluid. This can be written in the non-dimensional form as

$$\alpha = \alpha_0(1 + \beta\theta) \tag{2.8}$$

where $\beta = E(\overline{T}_w - \overline{T}_\infty)$ is the thermal conductivity parameter.

Following Telles and Trevisan [100], the expressions for the effective thermal diffusivity and mass diffusivities are taken as

$$\begin{aligned} \alpha_e &= \alpha + \gamma d^* \overline{u} \\ D_e &= D + \zeta d^* \overline{u} \end{aligned} \tag{2.9}$$

where α is the thermal conductivity, D is the molecular diffusivities, γ is the mechanical thermal dispersion, ζ is the mechanical solutal dispersion and d^* is the pore diameter. The above model for thermal dispersion has been used extensively by researchers like (see Nield and Bejan [69], Murthy [63], Srinivasacharya [95]) in studies of convective heat transfer in porous media.

Introducing the following non-dimensional variables

$$\begin{aligned} x = \frac{\overline{x}}{\mathrm{L}}, \quad y = \frac{\overline{y}}{\mathrm{L}}\mathrm{Pe}^{\frac{1}{2}}, \quad u = \frac{\overline{u}\mathrm{L}}{\alpha_0 \mathrm{Pe}}, \quad v = \frac{\overline{v}\mathrm{L}}{\alpha_0 \mathrm{Pe}^{\frac{1}{2}}} \\ \theta(\eta) = \frac{\overline{T} - \overline{T}_\infty}{\overline{T}_w - \overline{T}_\infty}, \quad \phi(\eta) = \frac{\overline{C} - \overline{C}_\infty}{\overline{C}_w - \overline{C}_\infty} \end{aligned} \tag{2.10}$$

where $\mathrm{Pe} = \dfrac{u_\infty \mathrm{L}}{\alpha_0}$ represents the Péclet number and L represents the characteristic length. In view of the continuity equation (2.1), we introduce stream function ψ by

$$u = \frac{\partial \psi}{\partial y}, \quad v = -\frac{\partial \psi}{\partial x}. \tag{2.11}$$

Substituting Eqs.(2.6)-(2.11) into Eqs. (2.2)- (2.4), we get the following equations

$$\Delta_1 = n\left(\frac{\partial\psi}{\partial y}\right)^{n-1}\frac{\partial^2\psi}{\partial y^2} + \frac{\lambda^n}{\theta_e}\left[\theta + \mathrm{B}\phi\right]\frac{\partial\theta}{\partial y} - \lambda^n\left[\frac{\partial\theta}{\partial y} + \mathrm{B}\frac{\partial\phi}{\partial y}\right]\left[1 - \frac{\theta}{\theta_e}\right] \tag{2.12}$$

$$\Delta_2 = \frac{\partial\psi}{\partial y}\frac{\partial\theta}{\partial x} - \frac{\partial\psi}{\partial x}\frac{\partial\theta}{\partial y} - \beta\left(\frac{\partial\theta}{\partial y}\right)^2 - (1+\beta\theta)\frac{\partial^2\theta}{\partial y^2} - Pe_\gamma\left[\frac{\partial\psi}{\partial y}\frac{\partial^2\theta}{\partial y^2} + \frac{\partial^2\psi}{\partial y^2}\frac{\partial\theta}{\partial y}\right] \tag{2.13}$$

$$\Delta_3 = \frac{\partial\psi}{\partial y}\frac{\partial\phi}{\partial x} - \frac{\partial\psi}{\partial x}\frac{\partial\phi}{\partial y} - \frac{1}{\mathrm{Le}}\frac{\partial^2\phi}{\partial y^2} - Pe_\zeta\left[\frac{\partial\psi}{\partial y}\frac{\partial^2\phi}{\partial y^2} + \frac{\partial^2\psi}{\partial y^2}\frac{\partial\phi}{\partial y}\right] \tag{2.14}$$

The corresponding boundary conditions (2.5) becomes

$$\left.\begin{aligned} &\frac{\partial\psi}{\partial x} = 0, \quad \theta = 1, \quad \phi = 1 \quad \text{at} \quad y = 0 \\ &\frac{\partial\psi}{\partial y} = 1, \quad \theta = 0, \quad \phi = 0 \quad \text{as} \quad y \to \infty \end{aligned}\right\} \tag{2.15}$$

where $\mathrm{B} = \dfrac{\beta_c^*(\overline{C}_w - \overline{C}_\infty)}{\beta_T^*(\overline{T}_w - \overline{T}_\infty)}$ is the Buoyancy ratio, $\mathrm{Ra} = \dfrac{\mathrm{L}}{\alpha_0}\left[\dfrac{gK\beta_T^*(\overline{T}_w - \overline{T}_\infty)}{\nu}\right]^{1/n}$ is the generalized Rayleigh number, $\mathrm{Le} = \dfrac{\alpha_0}{D}$ is the Lewis number, $\theta_e = \dfrac{\overline{T}_e - \overline{T}_\infty}{\overline{T}_w - \overline{T}_\infty}$ is the variable viscosity, $Pe_\gamma = \dfrac{\gamma u_\infty d^*}{\alpha_0}$ is the thermal dispersion parameter, $Pe_\zeta = \dfrac{\zeta u_\infty d^*}{\alpha_0}$ is the solutal dispersion parameter and $\lambda = \dfrac{\mathrm{Ra}}{\mathrm{Pe}}$ is the mixed convection parameter.

Similarity equations via Lie scaling group transformations

Finding the similarity solutions of Eqs. (2.12)-(2.14) is equivalent to determining the invariant solutions of these equations under a particular continuous one parameter group (see Seddeek [89]). One of the methods is to search for a transformation group from the elementary set of one parameter scaling transformation, defined by the following group (Γ)

$$\Gamma : x^* = x\,e^{\varepsilon\,a_1}, \quad y^* = y\,e^{\varepsilon\,a_2}, \quad \psi^* = \psi\,e^{\varepsilon\,a_3}, \quad \theta^* = \theta\,e^{\varepsilon\,a_4}, \quad \phi^* = \phi\,e^{\varepsilon\,a_5} \tag{2.16}$$

Here $\varepsilon \neq 0$ is the parameter of the group and a's are arbitrary real numbers whose interrelationship will be determined. Transformation in Eq.(2.16) treated as a point transformation,

transforming the coordinates

$$(x,\, y,\, \psi,\, \theta,\, \phi) = (x^*,\, y^*,\, \psi^*,\, \theta^*,\, \phi^*) \tag{2.17}$$

Investigating the relationship among the exponents a's such that

$$\Delta_j \left[x^*, y^*, u^*, v^*, ..., \frac{\partial^2 \psi^*}{\partial y^{*2}}\right] = H_j \left[x, y, u, v, ..., \frac{\partial^2 \psi^*}{\partial y^{*2}}; a\right] \Delta_j \left[x, y, u, v, ..., \frac{\partial^2 \psi^*}{\partial y^{*2}}\right] (j = 1; 2; 3) \tag{2.18}$$

Since this is the requirement that the differential forms Δ_1, Δ_2 and Δ_3 are conformally invariant under the transformation group Eq.(2.16). Substituting the transformations Eq. (2.16) in Eqs. (2.12)-(2.14), we have

$$\Delta_1 = e^{\varepsilon(na_2 - na_3 + a_2)} n \left(\frac{\partial \psi^*}{\partial y^*}\right)^{n-1} \frac{\partial^2 \psi^*}{\partial y^{*2}} + \frac{\lambda^n}{\theta_e} \left(e^{\varepsilon(a_2 - 2a_4)} \theta^* \frac{\partial \theta^*}{\partial y^*} + \mathrm{B}\, e^{\varepsilon(a_2 - a_4 - a_5)} \phi^* \frac{\partial \theta^*}{\partial y^*}\right) \tag{2.19a}$$

$$-\lambda^n \left(e^{\varepsilon(a_2 - a_4)} \frac{\partial \theta^*}{\partial y^*} + \mathrm{B}\, e^{\varepsilon(a_2 - a_5)} \frac{\partial \phi^*}{\partial y^*}\right) \left(1 - e^{-\varepsilon a_4} \frac{\theta^*}{\theta_e}\right)$$

$$\Delta_2 = e^{\varepsilon(a_1 + a_2 - a_3 - a_4)} \left(\frac{\partial \psi^*}{\partial y^*} \frac{\partial \theta^*}{\partial x^*} - \frac{\partial \psi^*}{\partial x^*} \frac{\partial \theta^*}{\partial y^*}\right) - \beta e^{\varepsilon(2a_2 - 2a_4)} \left(\left(\frac{\partial \theta^*}{\partial y^*}\right)^2 + \theta^* \frac{\partial^2 \theta^*}{\partial y^{*2}}\right) \tag{2.19b}$$

$$-e^{\varepsilon(2a_2 - a_4)} \frac{\partial^2 \theta^*}{\partial y^{*2}} - e^{\varepsilon(2a_2 + a_2 - a_3 - a_4)} Pe_\gamma \left(\frac{\partial \psi^*}{\partial y^*} \frac{\partial^2 \theta^*}{\partial y^{*2}} + \frac{\partial^2 \psi^*}{\partial y^{*2}} \frac{\partial \theta^*}{\partial y^*}\right)$$

$$\Delta_3 = e^{\varepsilon(a_1 + a_2 - a_3 - a_5)} \left(\frac{\partial \psi^*}{\partial y^*} \frac{\partial \phi^*}{\partial x^*} - \frac{\partial \psi^*}{\partial x^*} \frac{\partial \phi^*}{\partial y^*}\right) - \frac{1}{\mathrm{Le}} e^{\varepsilon(2a_2 - a_5)} \frac{\partial^2 \phi^*}{\partial y^{*2}} \tag{2.19c}$$

$$-e^{\varepsilon(2a_2 + a_2 - a_3 - a_5)}\, Pe_\zeta \left(\frac{\partial \psi^*}{\partial y^*} \frac{\partial^2 \phi^*}{\partial y^{*2}} + \frac{\partial^2 \psi^*}{\partial y^{*2}} \frac{\partial \phi^*}{\partial y^*}\right)$$

The boundary conditions (2.15) becomes

$$\left.\begin{array}{l} e^{\varepsilon(a_1 - a_3)} \frac{\partial \psi^*}{\partial x^*} = 0, \quad e^{-\varepsilon a_4} \theta^* = 1, \quad e^{-\varepsilon a_5} \phi^* = 1 \quad \text{at} \quad y^* = 0 \\ e^{\varepsilon(a_2 - a_3)} \frac{\partial \psi^*}{\partial y^*} = 1, \quad e^{-\varepsilon a_4} \theta^* = 0, \quad e^{-\varepsilon a_5} \phi^* = 0 \quad \text{as} \quad y^* \to \infty \end{array}\right\} \tag{2.20}$$

The system remains invariant under the group transformation Γ. Hence the relationship of arbitrary real constants as follows

$$\left.\begin{aligned} &na_2 - na_3 + a_2 = a_2 - a_4 = a_2 - a_5 = a_2 - 2a_4 = a_2 - a_4 - a_5; \\ &a_1 + a_2 - a_3 - a_4 = 2a_2 - 2a_4 = 2a_2 - a_4 = 2a_2 + a_2 - a_3 - a_4; \\ &a_1 + a_2 - a_3 - a_5 = 2a_2 - a_5 = 2a_2 + a_2 - a_3 - a_5; \\ &a_2 - a_3 = 0; \quad a_4 = 0; \quad a_5 = 0. \end{aligned}\right\} \tag{2.21}$$

Solving the linear system Eq. (2.21), we get

$$a_1 = 2a_3, \quad a_2 = a_3, \quad a_4 = a_5 = 0 \tag{2.22}$$

The set of transformation Γ reduces to

$$x^* = xe^{2\varepsilon a_3}, \quad y^* = ye^{\varepsilon a_3}, \quad \psi^* = \psi e^{\varepsilon a_3}, \quad \theta^* = \theta, \quad \phi^* = \phi \tag{2.23}$$

Expanding by the Taylor series in power of ε, keeping the term up to the first degree (neglecting higher power of ε), we get

$$x^* - x = 2\varepsilon a_3 x, \quad y^* - y = \varepsilon a_3 y, \quad \psi^* - \psi = \varepsilon a_3 \psi, \quad \theta^* = \theta, \quad \phi^* = \phi \tag{2.24}$$

The characteristic equations are

$$\frac{dx}{2a_3 x} = \frac{dy}{a_3 y} = \frac{d\psi}{a_3 \psi} = \frac{d\theta}{0} = \frac{d\phi}{0} \tag{2.25}$$

Solving the above characteristic equations, we get the following similarity transformations

$$\eta = yx^{-1/2}, \quad \psi = x^{1/2} f(\eta), \quad \theta = \theta(\eta), \quad \phi = \phi(\eta) \tag{2.26}$$

On the use of Eq.(2.26) in Eqs. (2.12)-(2.14), we get the following similarity equations

$$n(f')^{n-1} f'' = -\lambda^n (\theta + \mathrm{B}\phi) \frac{\theta'}{\theta_e} + \lambda^n (\theta' + \mathrm{B}\phi') \left(1 - \frac{\theta}{\theta_e}\right) \tag{2.27}$$

$$\beta(\theta')^2 + (1+\beta\theta)\,\theta'' + Pe_\gamma\,(f'\theta'' + f''\theta') + \frac{1}{2}f\theta' = 0 \tag{2.28}$$

$$\frac{1}{\mathrm{Le}}\phi'' + Pe_\zeta\,(f'\phi'' + f''\phi') + \frac{1}{2}f\phi' = 0 \tag{2.29}$$

where the primes indicate differentiation with respect to η.

The transformed boundary conditions (2.15) becomes

$$\left.\begin{aligned} &f(0) = 0, \quad \theta(0) = 1, \quad \phi(0) = 1, \\ &f'(\infty) = 1, \quad \theta(\infty) = 0, \quad \phi(\infty) = 0 \end{aligned}\right\} \tag{2.30}$$

Heat and Mass transfer coefficients

The local heat flux at the vertical wall is given by

$$q_w = -k_e\left[\frac{\partial\overline{T}}{\partial\overline{y}}\right]_{\overline{y}=0} \tag{2.31}$$

The local mass flux at the vertical wall is given by

$$q_m = -D_B\left[\frac{\partial\overline{C}}{\partial\overline{y}}\right]_{\overline{y}=0} \tag{2.32}$$

where $k_e = (\widetilde{k} + k_d)$ and $D_B = (D_m + D_d)$ are the effective thermal and solutal conductivities of the porous medium, in which k_d and D_d are the dispersion thermal and solutal conductivities.

The local Nusselt number $Nu_{\overline{x}} = \dfrac{q_w\overline{x}}{\widetilde{k}(\overline{T}_w - \overline{T}_\infty)}$ and local Sherwood number $Sh_{\overline{x}} = \dfrac{q_m\overline{x}}{D_m(\overline{C}_w - \overline{C}_\infty)}$ are given by

$$\frac{Nu_{\overline{x}}}{\mathrm{Pe}_{\overline{x}}^{1/2}} = -\left[1 + \mathrm{Pe}_\gamma f'(0)\right]\theta'(0) \quad \text{and} \quad \frac{Sh_{\overline{x}}}{\mathrm{Pe}_{\overline{x}}^{1/2}} = -\left[1 + \mathrm{Pe}_\zeta f'(0)\right]\phi'(0) \tag{2.33}$$

2.3 Numerical Solution

The system of nonlinear ordinary differential Eqs. (2.27)-(2.29) along with the corresponding boundary conditions (2.30) are solved numerically using the shooting technique, that uses the Runge-Kutta fourth-order and Newton-Raphson method (Murthy and Singh [64]-Srinivasacharya *et al.* [96]).

In this method, the Eqs. (2.27)-(2.29) are converted into the following system of linear differential equation of first order, by assuming $f = X_1$, $\theta = X_3$, $\phi = X_5$, we get

$$f' = X_2,\ \theta' = X_4,\ \phi' = X_6 \tag{2.34}$$

$$X_2' = -\frac{\lambda^n {\theta_e}^{-1}(X_3 + \mathrm{B}\, X_5)X_4 + \lambda^n (X_4 + \mathrm{B}\, X_6)(1 - X_3\, {\theta_e}^{-1})}{n\, {X_2}^{n-1}} \tag{2.35}$$

$$X_4' = \frac{n\, {X_2}^{n-1}(-\frac{1}{2}X_1X_4 - \beta {X_4}^2) + Pe_\gamma\, \lambda^n\, X_4 \left(X_4\, {\theta_e}^{-1}(X_3 + \mathrm{B}\, X_5) - (X_4 + \mathrm{B}\, X_6)(1 - X_3\, {\theta_e}^{-1})\right)}{n\, {X_2}^{n-1}\,(1 + \beta\, X_3 + Pe_\gamma\, X_2)} \tag{2.36}$$

$$X_6' = \frac{n\, {X_2}^{n-1}(-\frac{1}{2}\mathrm{Le}\, X_1X_6) + Pe_\zeta \mathrm{Le}\, \lambda^n\, X_6 \left(X_4\, {\theta_e}^{-1}(X_3 + \mathrm{B}\, X_5) - (X_4 + \mathrm{B}\, X_6)(1 - X_3\, {\theta_e}^{-1})\right)}{n\, {X_2}^{n-1}\,(1 + \mathrm{Le}\, Pe_\gamma\, X_2)} \tag{2.37}$$

The associated boundary conditions are

$$X_1(0) = 0, \quad X_3(0) = 1, \quad X_5(0) = 1 \tag{2.38a}$$

$$X_2(\infty) = 1, \quad X_3(\infty) = 0, \quad X_5(\infty) = 0 \tag{2.38b}$$

As the initial values for $X_2(0), X_4(0), X_6(0)$ are not specified in the boundary conditions. Assume, some suitable values for $X_2(0), X_4(0), X_6(0)$. Then the Eqs. (2.34)-(2.37) are integrated using 4^{th} order Runge-Kutta method from $\eta = 0$ to η_{max} over successive step lengths 0.01. Here η_{max} is the value of η at ∞ and chosen large enough so that the solution shows little further change for η larger than η_{max}. Further ODE45 solver is used in MATLAB to solve these six first ordered coupled differential equations. The accuracy of the assumed values for $X_2(0), X_4(0), X_6(0)$ are then checked by comparing the calculated values of X_2, X_3, X_5 at $\eta = \eta_\infty$ with their given value at $\eta = \eta_{max}$. If a difference exists, another set of initial

values are assumed and the above process is repeated. In principle, a trial and error-method can be used to determine these initial values, but it is tedious. Alternatively, an algorithm is developed to solve coupled non-linear equations, such as Newton-Raphson method. This approach can be scaled up readily to solve the roots of non-linear coupled equations, can be devised to solve the boundary value problem iteratively.

Newtons method for solving nonlinear equations involves an iterative process of iteratively refining x, by a correction h, $z_{i+1} = z_i + h$, where h is calculated by linear extrapolation of the function $X(z)$, to zero

$$0 = X(z_i) + \left(\frac{dX}{dz}\right)_{z_i} h \tag{2.39}$$

This approach can be scaled up readily to find the roots of coupled equations. For this particular example, the equations in matrix form are

$$\begin{bmatrix} X_2(\eta=0)_{i+1} \\ X_4(\eta=0)_{i+1} \\ X_6(\eta=0)_{i+1} \end{bmatrix} = \begin{bmatrix} X_2(\eta=0)_{i} \\ X_4(\eta=0)_{i} \\ X_6(\eta=0)_{i} \end{bmatrix} + \begin{bmatrix} h_1 \\ h_2 \\ h_3 \end{bmatrix}, \tag{2.40}$$

where $(h_1\, h_2\, h_3)^T$ is the solution to the equation.

$$\begin{bmatrix} 0 \\ 0 \\ 0 \end{bmatrix} = \begin{bmatrix} X_2(\eta=10)_{i} \\ X_3(\eta=10)_{i} \\ X_5(\eta=10)_{i} \end{bmatrix} + \begin{bmatrix} \frac{dX_2(\eta=10)}{dX_2(\eta=0)} \mid_{X_4,X_6} & \frac{dX_2(\eta=10)}{dX_4(\eta=0)} \mid_{X_2,X_6} & \frac{dX_2(\eta=10)}{dX_6(\eta=0)} \mid_{X_2,X_4} \\ \frac{dX_3(\eta=10)}{dX_2(\eta=0)} \mid_{X_4,X_6} & \frac{dX_3(\eta=10)}{dX_4(\eta=0)} \mid_{X_2,X_6} & \frac{dX_3(\eta=10)}{dX_6(\eta=0)} \mid_{X_2,X_4} \\ \frac{dX_5(\eta=10)}{dX_2(\eta=0)} \mid_{X_4,X_6} & \frac{dX_5(\eta=10)}{dX_4(\eta=0)} \mid_{X_2,X_6} & \frac{dX_5(\eta=10)}{dX_6(\eta=0)} \mid_{X_2,X_4} \end{bmatrix} \begin{bmatrix} h_1 \\ h_2 \\ h_3 \end{bmatrix} \tag{2.41}$$

These equations are constructed to find the initial values of X_2, X_4 and X_6 (at $\eta = 0$) that satisfy X_2, X_3 and X_5 (at $\eta = 10$). The equations in X_2, X_3, X_5 are expressed in matrix and vector form as $Z_{i+1} = Z_i + H^*$ and $0 = F + J\, H^*$ respectively, and combined to reach an iterative process

$$Z_{i+1} = Z_i - J^{-1}F$$

where J is the Jacobian matrix. The six derivatives involved in J can be approximated by

two-term forward finite divided difference. The first of the six is estimated by the equation

$$\frac{dX_2(\eta=10)}{dX_2(\eta=0)} \mid_{X_4,X_6} = \frac{X_2(\eta=10)_{(X_2+dX_2,X_4,X_6)} - X_2(\eta=10)_{(X_2,X_4,X_6)}}{dX_2} \tag{2.42}$$

To find the approximation values for six derivatives, the ODE's in Eqs.(2.34)-(2.37) are to be solved for four (3-tuple) of initial values (X_2, X_4, X_6), (X_2+dX_2, X_4, X_6), (X_2, X_4+dX_4, X_6) and (X_2, X_4, X_6+dX_6), where dX_2, dX_4 and dX_6 are small.

At first, the differential equations (2.34)-(2.37) are solved in the interval $0 \leq \eta \leq \eta_{max}$ for four 3-tuples of initial values, where $dX_2 = 0.01, dX_4 = 0.01$ and $dX_6 = 0.01$. The calculated values X_2, X_3, X_5 for each 3-tuple of initial conditions are placed into an array (Z_1, Z_2, Z_3, Z_4).

Now, the six derivatives involved in J are evaluated and third new approximations of initial values are evaluated from (2.34)-(2.37). This process is continuous until the magnitude of the both corrections with 10^{-6}. The accuracy of the solution is enhanced by taking dX_2, dX_4 and dX_6 to reduce the converges.

2.4 Results and Discussion

In order to validate the generated code, the results of the present problem have been compared with that of the results obtained by Chaoyang *et al.* [18] as a special case by taking $Pe_\gamma = Pe_\zeta = \beta = \mathrm{B} = 0$, $\mathrm{Le} = 1$, $\theta_e \to \infty$ and found that they are in good agreement, as presented in Table (3.1).

Table 2.1: *Comparison of heat transfer for λ with varying values of pseudo-plastic, Newtonian and dilatant fluids.*

	$n = 0.5$		$n = 1.0$		$n = 1.5$	
λ	Chaoyang [18]	Present	Chaoyang [18]	Present	Chaoyang [18]	Present
0.0	0.5641	0.564190	0.5641	0.564190	0.5641	0.564190
0.5	0.8209	0.821704	0.6473	0.647396	0.6034	0.60339
1.0	0.9303	0.929635	0.7205	0.720585	0.6634	0.663375
4.0	1.3010	1.300685	1.025	1.025796	1.0180	1.017582

Figures 2.2(a)-2.2(c) represents the non-dimensional velocity $f'(\eta)$, temperature $\theta(\eta)$ and concentration $\phi(\eta)$ profiles for different values of the variable viscosity (θ_e) and power-law index (n) for n=0.6 (pseudo-plastic fluid), n=1.0 (Newtonian fluid) and n=1.5 (dilatant fluid). Figure 2.2(a) shows that increase in the value of variable viscosity tends to increase the momentum boundary layer thickness near the plate and decrease far away from the plate. This is due to the fact that for a given fluid, when δ^* is fixed, smaller θ_e implies higher temperature difference between the wall and the ambient fluid. It demonstrates that θ_e is an indicator of the variation of fluid viscosity with temperature, has a strong effect on the velocity profile within the boundary layer. While Fig. 2.2(b) depicts that the non-dimensional temperature $\theta(\eta)$ of the fluid decreases with increase in the value of the variable viscosity. The concentration $\phi(\eta)$ profile for different values of variable viscosity is given by Fig. 2.2(c), which can be seen that the concentration slightly decreases with increase in the variable viscosity.

The behavior of non-dimensional velocity $f'(\eta)$, temperature $\theta(\eta)$ and concentration $\phi(\eta)$ profiles for different values of the thermal conductivity (β) and power-law index (n), is plotted in Figs. 2.3(a)-2.3(c). It is interesting to note that the increase in the thermal conductivity (β) substantially decreases the velocity $f'(\eta)$ near the plate and increases far away from the plate, as shown in Fig. 2.3(a). It is observed from Fig. 2.3(b) that increasing the thermal conductivity tends to enhance the thermal boundary layer. This is attributed to the fact that the non-linear drag is more pronounced when the velocity is larger. However, Fig. 2.3(c) depicts that concentration boundary layer strongly decreases with increasing values of the thermal conductivity.

Figures 2.4(a)-2.4(c) displays the effect of thermal dispersion (Pe_γ) and the power-law index (n) for fixed values of the parameters on the non-dimensional velocity $f'(\eta)$, temperature $\theta(\eta)$ and concentration $\phi(\eta)$ profiles, respectively. Figure 2.4(a) shows that enhancing the thermal dispersion parameter increases the non-dimensional velocity $f'(\eta)$. The presence of thermal dispersion in the energy equation leads to dominate the conduction over the convection. That is, supplementing dispersion effects to the energy equation gives more thermal conduction. From Fig. 2.4(b) can see that increasing the values of thermal dispersion, in-

creases the non-dimensional temperature $\theta(\eta)$. That is the thermal dispersion enhances the transport of heat along the normal direction to the wall as compared with the case where dispersion is neglected (i.e.,$Pe_\gamma = 0$). Figure 2.4(c) displays that concentration boundary layer $\phi(\eta)$ reduces with increasing value of the thermal dispersion.

Figures 2.5(a)-2.5(c) presents the non-dimensional velocity $f'(\eta)$, temperature $\theta(\eta)$ and concentration $\phi(\eta)$ profiles for different values of power-law fluid index (n) and solutal dispersion (Pe_ζ). It is observed from the Fig. 2.5(a) that non-dimensional velocity $f'(\eta)$ profile increases with an increase in the values of solutal dispersion. Also an increase in the value of the solutal dispersion slightly decreases the thermal boundary layer thickness, as shown in Fig. 2.5(b). Figure 2.5(c) depicts that the concentration $\phi(\eta)$ profile continuously increases with increasing value of the solutal dispersion. Hence the concentration boundary layer thickness enhances with an increases in the solutal dispersion parameter.

The variations of the mixed convection parameter (λ) and the power-law index (n) on the non-dimensional velocity $f'(\eta)$, temperature $\theta(\eta)$ and concentration $\phi(\eta)$ profiles for fixed value of the other parameters,have been plotted in 2.6(a)-2.6(c). It is observed from Fig. 2.6(a) that the velocity is increased with increase in the value of mixed convection parameter. It can be evident from this figure that as λ increases, the momentum boundary layer thickness increases. From Fig. 2.6(b) it is observed that the non-dimensional temperature increases with decreasing values of mixed convection parameter. Figure 2.6(c) is plotted for the effect of mixed convection on non-dimensional concentration, and reveals that an increase in the thermal dispersion leads to decrease thermal boundary layer thickness.

Figure 2.7(a)-2.7(c) explore the non-dimensional velocity $f'(\eta)$, temperature $\theta(\eta)$ and concentration $\phi(\eta)$ profiles for different values of the Newtonian and power-law fluid. It is observed that the boundary layer thickness is more for power-law fluid when compared to Newtonian fluid.

Table 2 describes the rate of heat and mass transfer for different values of power-law index (n), variable viscosity (θ_e), thermal conductivity (β), thermal dispersion (Pe_γ) and solutal dispersion (Pe_γ) parameters for fixed values of B = 1.0 and Le = 1.0. It is observed

n	θ_e	β	Pe_γ	Pe_ζ	λ	$-[1+Pe_\gamma f'(0)]\,\theta'(0)$	$-[1+Pe_\zeta f'(0)]\,\phi'(0)$
0.6	1.5	0.5	0.5	0.5	1.0	0.498329	0.576219
0.6	2.0	0.5	0.5	0.5	1.0	0.486825	0.551171
0.6	2.5	0.5	0.5	0.5	1.0	0.480030	0.537673
1.0	1.5	0.5	0.5	0.5	1.0	0.450245	0.531321
1.0	2.0	0.5	0.5	0.5	1.0	0.448707	0.523213
1.0	2.5	0.5	0.5	0.5	1.0	0.447846	0.518910
1.5	1.5	0.5	0.5	0.5	1.0	0.426502	0.508064
1.5	2.0	0.5	0.5	0.5	1.0	0.426952	0.504808
1.5	2.5	0.5	0.5	0.5	1.0	0.427307	0.503223
0.6	2.0	0.0	0.5	0.5	1.0	0.550143	0.550143
0.6	2.0	1.0	0.5	0.5	1.0	0.439824	0.552078
0.6	2.0	1.5	0.5	0.5	1.0	0.403332	0.552873
1.0	2.0	0.0	0.5	0.5	1.0	0.522349	0.522349
1.0	2.0	1.0	0.5	0.5	1.0	0.397727	0.523952
1.0	2.0	1.5	0.5	0.5	1.0	0.324591	0.526265
1.5	2.0	0.0	0.5	0.5	1.0	0.504155	0.504155
1.5	2.0	1.0	0.5	0.5	1.0	0.375254	0.504808
1.5	2.0	1.5	0.5	0.5	1.0	0.324228	0.506780
0.6	2.0	0.5	0.0	0.5	1.0	0.731247	0.542309
0.6	2.0	0.5	1.0	0.5	1.0	0.380226	0.554467
0.6	2.0	0.5	1.5	0.5	1.0	0.318587	0.556057
1.0	2.0	0.5	0.0	0.5	1.0	0.586879	0.519212
1.0	2.0	0.5	1.0	0.5	1.0	0.373234	0.525157
1.0	2.0	0.5	1.5	0.5	1.0	0.461777	0.361598
1.5	2.0	0.5	0.0	0.5	1.0	0.528253	0.502541
1.5	2.0	0.5	1.0	0.5	1.0	0.365851	0.506032
1.5	2.0	0.5	1.5	0.5	1.0	0.434350	0.361916
0.6	2.0	0.5	0.5	0.0	1.0	0.453391	0.930892
0.6	2.0	0.5	0.5	1.0	1.0	0.504292	0.425202
0.6	2.0	0.5	0.5	1.5	1.0	0.515382	0.357005
1.0	2.0	0.5	0.5	0.0	1.0	0.435381	0.760308
1.0	2.0	0.5	0.5	1.0	1.0	0.456516	0.421436
1.0	2.0	0.5	0.5	1.5	1.0	0.461777	0.361598
1.5	2.0	0.5	0.5	0.0	1.0	0.419904	0.687774
1.5	2.0	0.5	0.5	1.0	1.0	0.431316	0.416408
1.5	2.0	0.5	0.5	1.5	1.0	0.434350	0.361916
0.6	2.0	0.5	0.5	0.5	0.0	0.470829	0.520391
0.6	2.0	0.5	0.5	0.5	0.5	0.481244	0.539973
0.6	2.0	0.5	0.5	0.5	1.5	0.491378	0.560776
1.0	2.0	0.5	0.5	0.5	0.0	0.446832	0.513544
1.0	2.0	0.5	0.5	0.5	0.5	0.447748	0.518139
1.0	2.0	0.5	0.5	0.5	1.5	0.449705	0.528841
1.5	2.0	0.5	0.5	0.5	0.0	0.427982	0.528841
1.5	2.0	0.5	0.5	0.5	0.5	0.427598	0.502513
1.5	2.0	0.5	0.5	0.5	1.5	0.426312	0.508722

Table 2.2: *Variation of heat and mass transfer coefficients for varying values of n, θ_e, β, Pe_γ, Pe_ζ and λ.*

that increasing the value of power-law index (n) decreases the heat and mass transfer rates. It is noticed that enhancing the variable viscosity decreases both the heat and mass transfer coefficient. It can be seen that the increase in the value of thermal conductivity and thermal dispersion parameters decreases the heat transfer, but a reverse trend is observed in the mass transfer rate. An enhancement in the value of solutal dispersion parameter increases in heat transfer rate, but it decreases the mass transfer rate. It depicts that increase in the value of mixed convection parameter increases both heat and mass transfer rates.

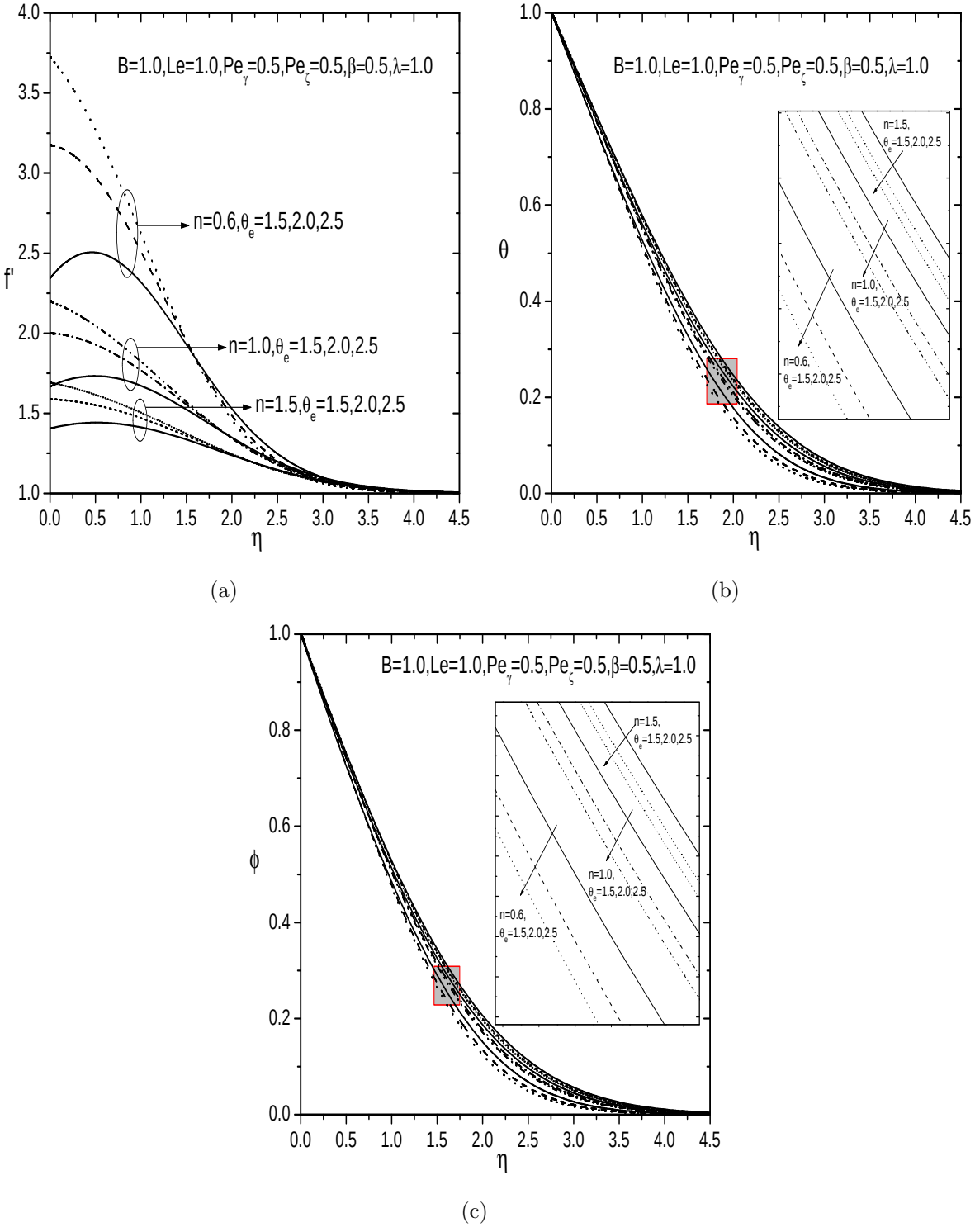

Figure 2.2: (a) velocity profile (b) temperature profile and (c) concentration profile for various value of θ_e and n.

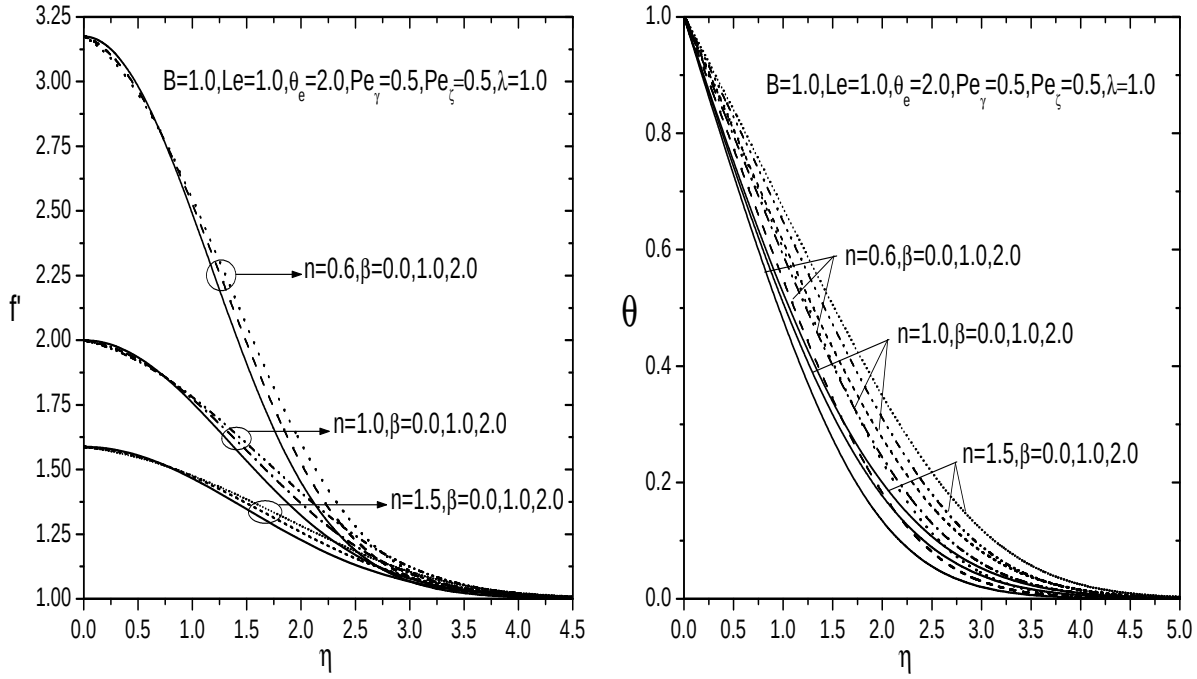

(a) (b)

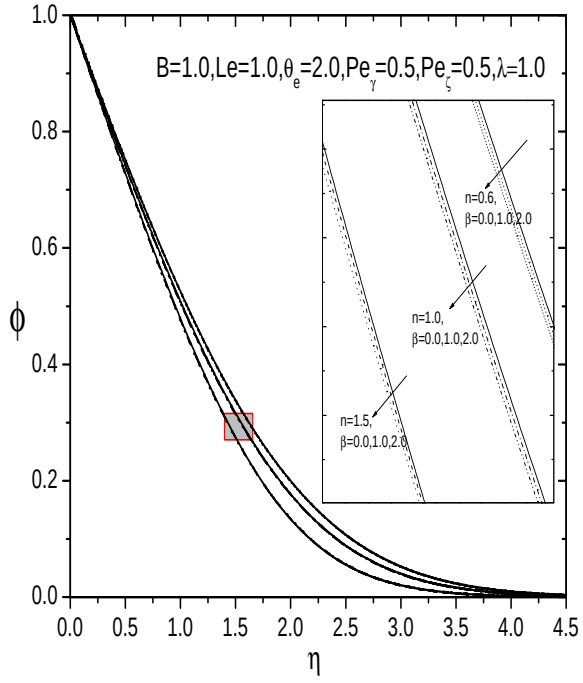

(c)

Figure 2.3: (a) velocity profile (b) temperature profile and (c) concentration profile for various value of β and n.

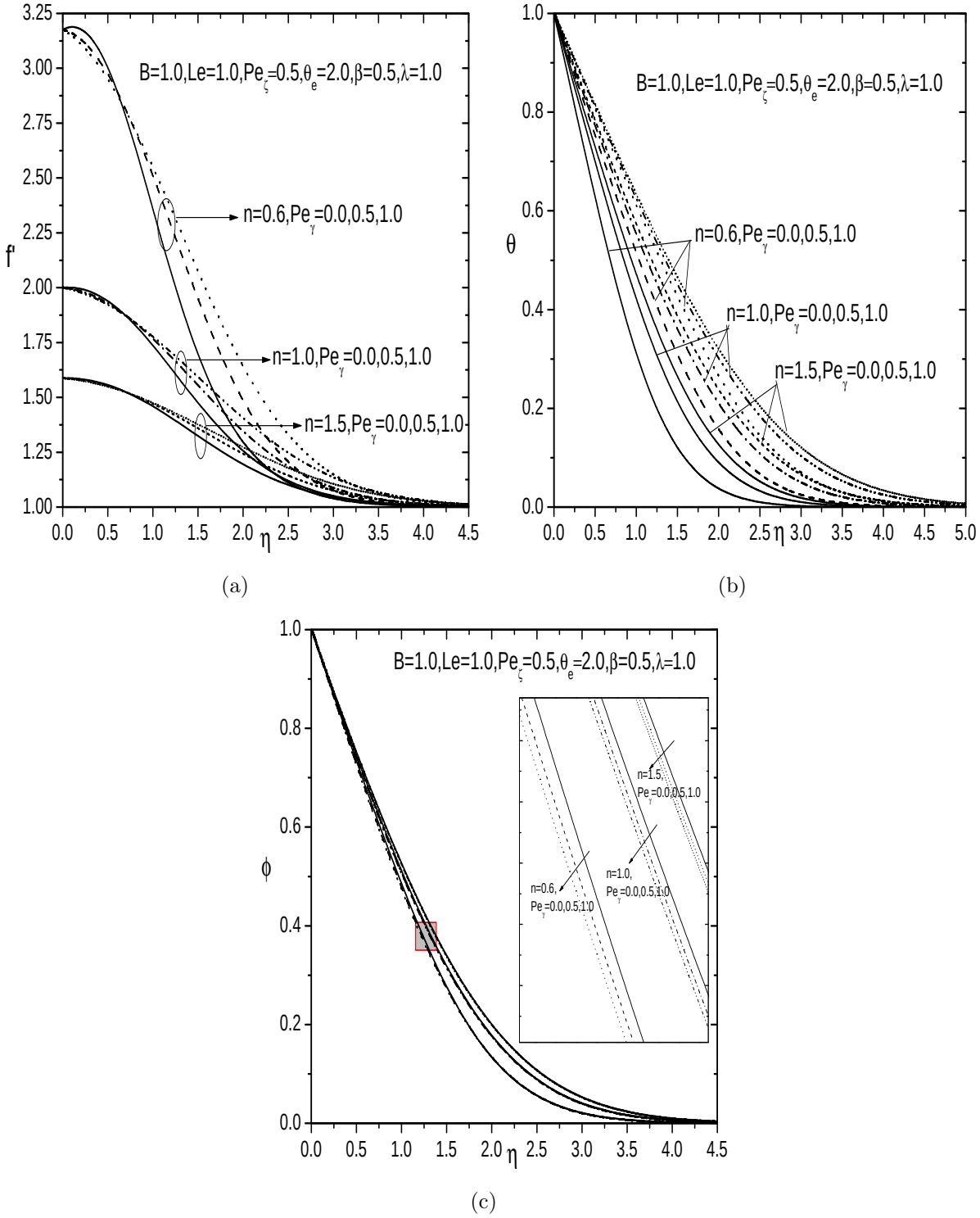

Figure 2.4: (a) velocity profile (b) temperature profile and (c) concentration profile for various value of Pe_γ and n.

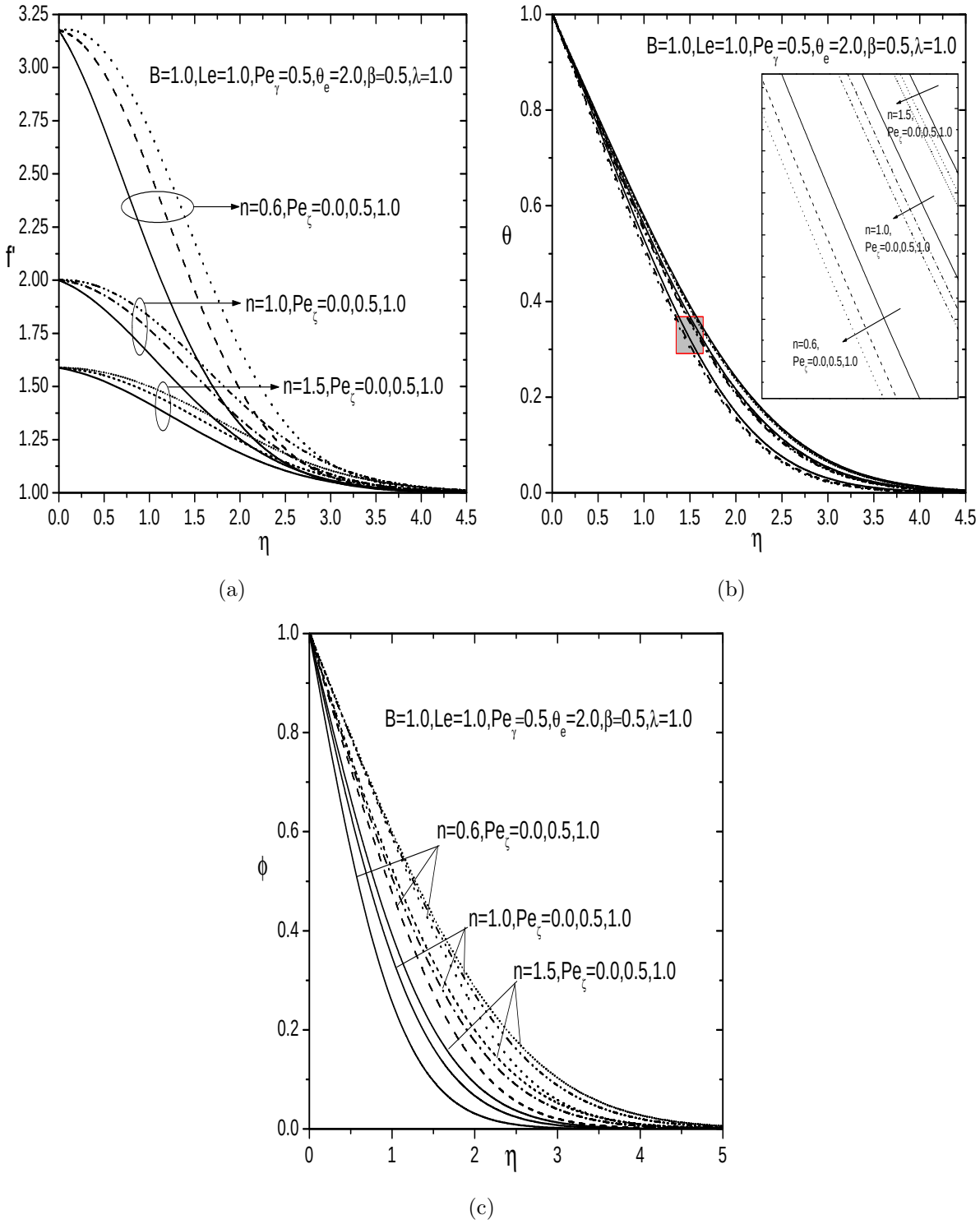

Figure 2.5: (a) velocity profile (b) temperature profile and (c) concentration profile for various value of Pe_ζ and n.

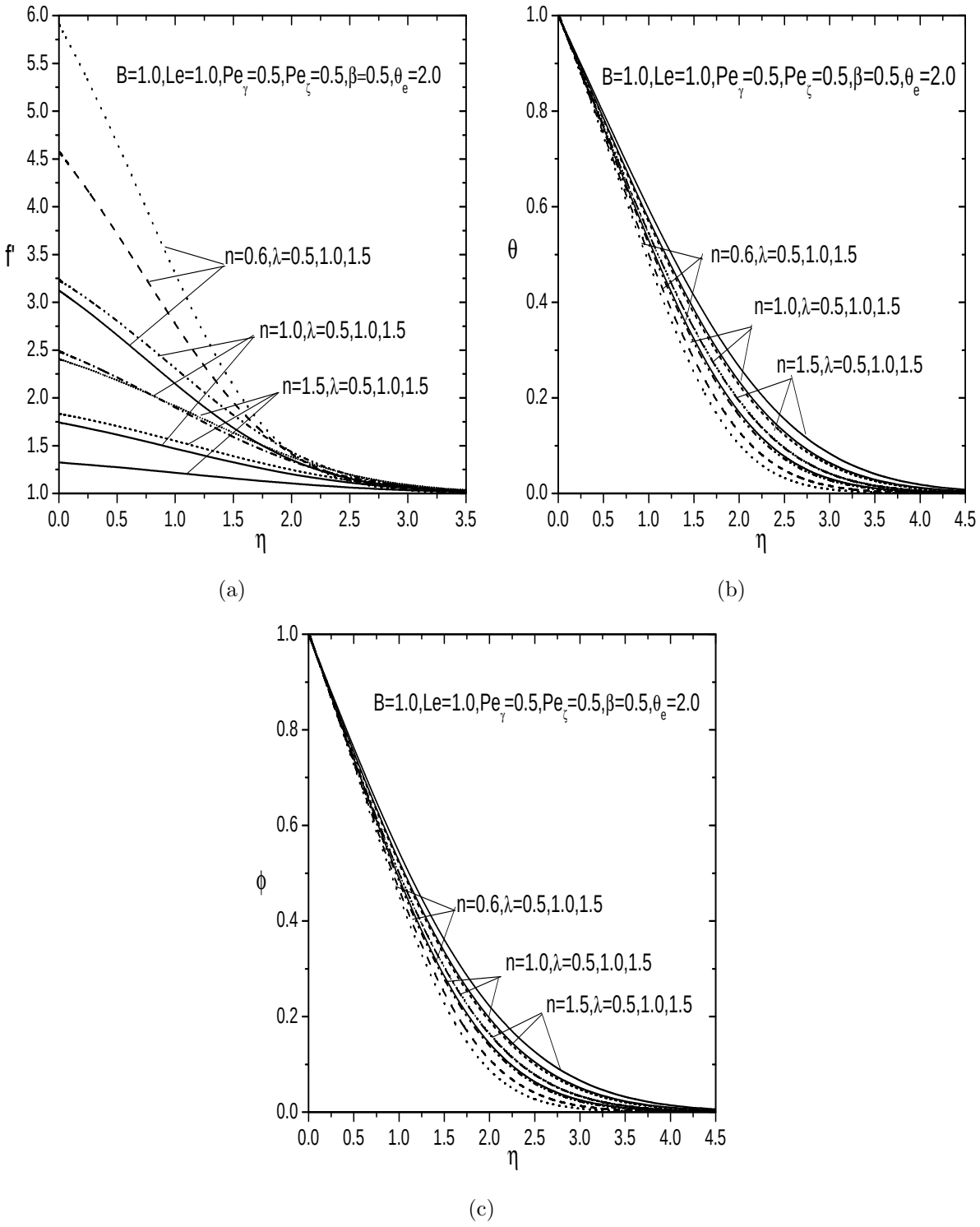

Figure 2.6: (a) velocity profile (b) temperature profile and (c) concentration profile for various value of λ and n.

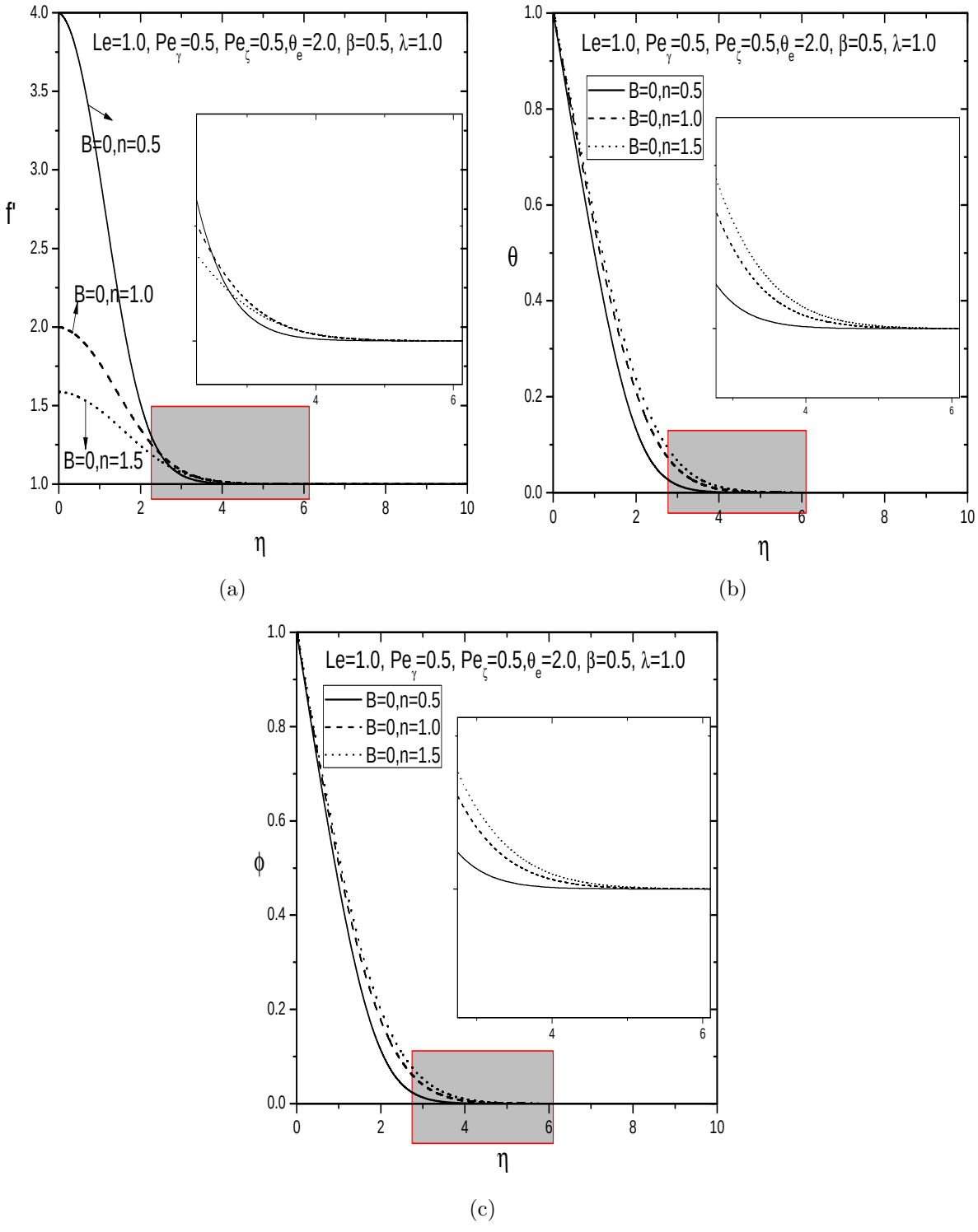

Figure 2.7: (a) velocity profile (b) temperature profile and (c) concentration profile for various value of n.

2.5 Conclusion

In this Chapter, Lie scaling group transformations are applied to find the similarity solutions of mixed convection flow over a vertical plate in a power-law fluid saturated Darcy porous medium in the presence of variable viscosity, thermal conductivity and double dispersion. The resulting equations are solved numerically by the shooting method. The main findings are summarized as follows:

- Enhancement in the value of variable viscosity increases the velocity near the plate, and slightly decreases far away from the plate and decreases in temperature, concentration, heat and mass transfer rates.
- An increase in the value of thermal conductivity decreases the concentration, heat and mass transfer rates and increases the velocity and temperature profiles.
- Higher values of the thermal dispersion parameter result in higher velocity, temperature and mass transfer distributions but lower concentration heat transfer rate.
- Velocity, concentration and heat transfer increases with increase in solutal dispersion parameter while we noticed that opposite results are reported for temperature and mass transfer rate.
- An increase in the values of the mixed convection parameter results in higher velocity, heat and mass transfer rates but lower temperature and concentration profiles.

Chapter 3

Effect of Variable Properties and Thermophoresis on a Mixed Convective Flow of Power-law Fluid Saturated Porous Medium [1]

3.1 Introduction

Thermophoresis is a phenomenon by which sub-micron particles suspended in a non-isothermal gas acquire velocity relative to the gas in the direction of decreasing temperature. It is important when the particle sizes are small and the temperature gradients are large. When the wall is cold, the particles tend to deposit on the surface, while the particles tend to repel from that surface, when the wall is hot. Here, assuming a sufficiently weak suspension sub-micron particles. Thermophoresis is of practical importance in many industrial applications (see Tsai [101]) such as in aerosol collection (thermal precipitator), micro contamination control, removing small particles from gas streams, etc. Mahdy and Hady [55] investigated the influence of MHD and thermophoretic particle deposition on the free convective flow over

[1] Accepted in "**Computational Thermal Sciences: An International Journal**"

a vertical flat plate embedded in a power-law fluid saturated porous medium. Animasaun [5] studied the effects of thermophoresis, Dufour, variable viscosity, thermal conductivity and chemical reaction on the free convection heat and mass transfer of a non-Darcian flow along an isothermal vertical porous surface in the presence of viscous dissipation and suction. Rashad *et al.* [82] discussed the influence of thermophoresis and thermal radiation effects on mixed convection heat and mass transfer from a rotating cone in a porous medium. Mondal *et al.* [60] explored the effects of thermophoresis, chemical reaction, Dufour and Soret on MHD mixed convective flow of an infinite permeable inclined flat plate in the presence of non-uniform heat source/sink.

Survey of the literature reveals that the problem of mixed convection in a power-law fluid saturated Darcy porous medium under the influence of variable properties and thermophoresis has not been investigated so far. Hence, the present chapter aims to explore the effects of variable viscosity, thermal conductivity, thermophoresis on the mixed convection in a power-law fluid saturated Darcy porous medium. In addition, the similarity representation of the system of governing non-dimensional equations is obtained using the scaling group of transformations and then solved the resultant system of equations by shooting method. The effects of pertinent parameters on the physical quantities are studied and the results are displayed graphically and tabular form.

3.2 Mathematical Formulation

Consider the two-dimensional steady, laminar, incompressible mixed convection heat and mass transfer boundary layer flow along a vertical plate embedded in a non-Newtonian power-law fluid saturated Darcy porous medium.The plate is maintained at a constant temperature $\overline{T}_w$ and concentration $\overline{C}_w$. The ambient fluid temperature is $\overline{T}_\infty$ and the concentration is $\overline{C}_\infty$. Choose the two dimensional coordinate system such that the $\overline{x}$ - axis is along the vertical plate and $\overline{y}$ - axis is normal to the plate. The physical model of the problem as given in Figure 2.1. The effects of thermophoresis is taken into account to help in the understanding of the mass deposition variation on the surface.

The governing equations of continuity, momentum, temperature and concentration under the Boussinesq approximation and the boundary layer assumptions (see Shenoy [91]) are written as:

$$\frac{\partial \overline{u}}{\partial \overline{x}} + \frac{\partial \overline{v}}{\partial \overline{y}} = 0 \tag{3.1}$$

$$n\overline{u}^{n-1}\frac{\partial \overline{u}}{\partial \overline{y}} = \frac{\partial}{\partial \overline{y}}\left[\frac{gK\rho_\infty}{\mu}\left(\beta_T^*(\overline{T}-\overline{T}_\infty)+\beta_C^*(\overline{C}-\overline{C}_\infty)\right)\right] \tag{3.2}$$

$$\overline{u}\frac{\partial \overline{T}}{\partial \overline{x}} + \overline{v}\frac{\partial \overline{T}}{\partial \overline{y}} = \frac{\partial}{\partial \overline{y}}\left(\alpha\frac{\partial \overline{T}}{\partial \overline{y}}\right) \tag{3.3}$$

$$\overline{u}\frac{\partial \overline{C}}{\partial \overline{x}} + \overline{v}\frac{\partial \overline{C}}{\partial \overline{y}} = D\frac{\partial^2 \overline{C}}{\partial \overline{y}^2} - \frac{\partial}{\partial \overline{y}}\left(V_T\overline{C}\right) \tag{3.4}$$

where $\overline{x}$ and $\overline{y}$ are the Cartesian coordinates, $\overline{u}$ and $\overline{v}$ are the velocity components in $\overline{x}$ and $\overline{y}$ directions, respectively, $\overline{T}$ is the temperature, $\overline{C}$ is the concentration, β_T^* and β_C^* are the thermal and concentration expansion coefficients respectively, ρ_∞ is the reference density, g is the acceleration due to gravity, V_T is the thermophoretic velocity, K is the permeability, α and D are the thermal and mass diffusivities of the porous medium, respectively.

The associated boundary conditions are

$$\left.\begin{aligned} &\overline{v}=0, \quad \overline{T}=\overline{T}_w, \quad \overline{C}=\overline{C}_w \quad \text{at} \quad \overline{y}=0 \\ &\overline{u}=u_\infty, \quad \overline{T}=\overline{T}_\infty, \quad \overline{C}=\overline{C}_\infty \quad \text{as} \quad \overline{y}\to\infty \end{aligned}\right\} \tag{3.5}$$

The effect of thermophoresis is usually prescribed by means of an average velocity which a particle will acquire when exposed to a temperature gradient. In the boundary layer flow, the temperature gradient in the $\overline{y}$-direction is very much larger than in the $\overline{x}$-direction, and therefore only the thermophoretic velocity in $\overline{y}$-direction is considered. In Eq. (3.4), V_T is thermophoretic velocity which can be written as (see Wu and Greif [109] and Selim *et al.* [90])

$$V_T = -\frac{K_T\mu}{\rho_\infty T_r}\frac{\partial \overline{T}}{\partial \overline{y}} \tag{3.6}$$

where K_T is the thermophoretic coefficient which ranges from 0.2 to 1.2 and is defined as

(see Talbot *et al.* [98])

$$K_T = \frac{2C_t\left(\lambda_r/\lambda_g + C_nKn\right)\left[1 + Kn(C_1 + C_2e^{-C_3/Kn})\right]}{(1+3C_mKn)(1+2\lambda_r/\lambda_g + 2C_nKn)}$$

Here λ_r and λ_g reprsents the thermal conductivities of fluid and diffused particles, Kn represents the Knudsen number and $C_1, C_2, C_3, C_m, C_t, C_n$ are constants, respectively.

Introducing the following dimensionless variables

$$\begin{gathered} x = \frac{\overline{x}}{\mathrm{L}}, \quad y = \frac{\overline{y}}{\mathrm{L}}\mathrm{Pe}^{\frac{1}{2}}, \quad u = \frac{\overline{u}\mathrm{L}}{\alpha_0\mathrm{Pe}}, \quad v = \frac{\overline{v}\mathrm{L}}{\alpha_0\mathrm{Pe}^{\frac{1}{2}}} \\ \theta(\eta) = \frac{\overline{T} - \overline{T}_\infty}{\overline{T}_w - \overline{T}_\infty}, \quad \phi(\eta) = \frac{\overline{C} - \overline{C}_\infty}{\overline{C}_w - \overline{C}_\infty} \end{gathered} \tag{3.7}$$

In view of the continuity equation (3.1), we introduce the stream function ψ by

$$u = \frac{\partial\psi}{\partial y}, \quad v = -\frac{\partial\psi}{\partial x} \tag{3.8}$$

Substituting Eq.(3.6)-(3.8) into Eqs.(3.2)-(3.4), we get the following equations

$$n\left(\frac{\partial\psi}{\partial y}\right)^{n-1}\frac{\partial^2\psi}{\partial y^2} + \frac{\lambda^n}{\theta_e}\left[\theta + \mathrm{B}\phi\right]\frac{\partial\theta}{\partial y} - \lambda^n\left[\frac{\partial\theta}{\partial y} + \mathrm{B}\frac{\partial\phi}{\partial y}\right]\left[1 - \frac{\theta}{\theta_e}\right] = 0 \tag{3.9}$$

$$\frac{\partial\psi}{\partial y}\frac{\partial\theta}{\partial x} - \frac{\partial\psi}{\partial x}\frac{\partial\theta}{\partial y} - \beta\left(\frac{\partial\theta}{\partial y}\right)^2 - (1+\beta\theta)\frac{\partial^2\theta}{\partial y^2} = 0 \tag{3.10}$$

$$\mathrm{Le}\left[\frac{\partial\psi}{\partial y}\frac{\partial\phi}{\partial x} - \frac{\partial\psi}{\partial x}\frac{\partial\phi}{\partial y}\right] - \frac{\partial^2\phi}{\partial y^2} + \tau\mathrm{Sc}\frac{\theta_e}{\theta_e - \theta}\left[\left(\frac{\partial\theta}{\partial y}\right)^2\frac{\phi}{\theta_e - \theta} + \frac{\partial^2\theta}{\partial y^2}\phi + \frac{\partial\theta}{\partial y}\frac{\partial\phi}{\partial y}\right] = 0 \tag{3.11}$$

The corresponding boundary conditions (3.5) becomes

$$\left.\begin{aligned} &\frac{\partial\psi}{\partial x} = 0, \quad \theta = 1, \quad \phi = 1 \quad \text{at} \quad y = 0 \\ &\frac{\partial\psi}{\partial y} = 1, \quad \theta = 0, \quad \phi = 0 \quad \text{as} \quad y \to \infty \end{aligned}\right\} \tag{3.12}$$

where $\mathrm{Pe} = \dfrac{u_\infty\mathrm{L}}{\alpha_0}$ represents the Péclet number, $\mathrm{B} = \dfrac{\beta_c(\overline{C}_w - \overline{C}_\infty)}{\beta_T(\overline{T}_w - \overline{T}_\infty)}$ represents the Buoyancy

ratio, $\mathrm{Sc} = \dfrac{\nu}{D}$ represents the Schmidt number, $\mathrm{Ra} = \dfrac{\mathrm{L}}{\alpha_0}\left[\dfrac{Kg\beta_T(\overline{T}_w - \overline{T}_\infty)}{\nu}\right]^{1/n}$ represents the generalized Rayleigh number, $\mathrm{Le} = \dfrac{\alpha_0}{D}$ represents the Lewis number, $\tau = -\dfrac{k}{T_r}(\overline{T}_w - \overline{T}_\infty)$ represents the thermophoretic parameter, $\theta_e = \dfrac{\overline{T}_e - \overline{T}_\infty}{\overline{T}_w - \overline{T}_\infty}$ represents the variable viscosity and $\lambda = \dfrac{\mathrm{Ra}}{\mathrm{Pe}}$ represents the mixed convection parameter.

Similarity equations via Lie group transformations

Using Lie scaling group transformations and the procedure explained in the second chapter, the following similarity transformations are obtained

$$\eta = yx^{-1/2}, \quad \psi = x^{1/2}f(\eta), \quad \theta = \theta(\eta), \quad \phi = \phi(\eta) \tag{3.13}$$

Substituting Eq.(3.13) into Eqs.(3.9)-(3.11), we obtain the following ordinary differential equations

$$n(f')^{n-1}f'' = \lambda^n\left(\theta' + \mathrm{B}\phi'\right)\left(1 - \frac{\theta}{\theta_e}\right) - \lambda^n\left(\theta + \mathrm{B}\phi\right)\frac{\theta'}{\theta_e} \tag{3.14}$$

$$\beta(\theta')^2 + (1 + \beta\theta)\,\theta'' + \frac{1}{2}f\theta' = 0 \tag{3.15}$$

$$\phi'' - \tau\mathrm{Sc}\frac{\theta_e}{\theta_e - \theta}\left[(\theta')^2\frac{\phi}{\theta_e - \theta} + \theta''\phi + \theta'\phi'\right] + \frac{1}{2}\mathrm{Le}f\phi' = 0 \tag{3.16}$$

where the primes indicate differentiation with respect to η.
The boundary conditions (3.12) becomes

$$\left.\begin{aligned} &f(0) = 0, \quad \theta(0) = 1, \quad \phi(0) = 1 \\ &f'(\infty) = 1, \quad \theta(\infty) = 0, \quad \phi(\infty) = 0 \end{aligned}\right\} \tag{3.17}$$

Heat and Mass transfer coefficients

The non-dimensional heat and mass fluxes from wall are given by

$$q_w = -\widetilde{k}\left(\frac{\partial \overline{T}}{\partial \overline{y}}\right)_{\overline{y}=0} \text{ and } \quad q_m = -D\left(\frac{\partial \overline{C}}{\partial \overline{y}}\right)_{\overline{y}=0} \tag{3.18}$$

The local Nusselt number $Nu_{\overline{x}} = \dfrac{q_w \overline{x}}{\widetilde{k}(\overline{T}_w - \overline{T}_\infty)}$ and local Sherwood number $Sh_{\overline{x}} = \dfrac{q_m \overline{x}}{D(\overline{C}_w - \overline{C}_\infty)}$ are given by

$$\frac{Nu_{\overline{x}}}{x^{1/2}} = -\theta'(0) \quad \text{and} \quad \frac{Sh_{\overline{x}}}{x^{1/2}} = -\phi'(0) \tag{3.19}$$

3.3 Results and Discussion

The system of nonlinear Eqs.(3.14)-(3.16) with the corresponding boundary conditions (3.17) are solved numerically by shooting technique that uses fourth order Runge-Kutta method and Newton-Raphson method. The integration length η_∞ varies with the parameter values and it has been suitably chosen each time such that the boundary conditions at the outer edge of the boundary layer are satisfied. In order to see the effect of step size ($\Delta\eta$), we executed the code for our model with three different step sizes as $\Delta\eta = 0.001$, $\Delta\eta = 0.01$, $\Delta\eta = 0.05$ and in each case, we found very good agreement between them on different profiles. After some trials, we imposed a maximal value of η at ∞ of 10 and a step size $\Delta\eta = 0.001$ is used to obtain the numerical solution with six-decimal place accuracy as the criterion of convergence explained in the Chapter-2. In order to check the effects of step size ($\Delta\eta$) we found the Nusselt number and Sherwood number with four different step sizes as $\Delta\eta = 0.01$, $\Delta\eta = 0.001$, $\Delta\eta = 0.0001$ and $\Delta\eta = 0.00001$. We observe from Table 1 that the results are independent with the step size ($\Delta\eta$). Hence a step size $\Delta\eta = 0.1$ is selected to be satisfactory for a convergence criterion of 10^{-6}. in all cases. In order to test the accuracy of our results, we compared our results with those of Chaoyang *et al.* [18] by taking $\mathrm{Sc} = \tau = \mathrm{B} = \beta = 0$, $\mathrm{Le} = 1.0$ and $\theta_e \to \infty$. The comparison shows a good agreement, as given in Tab. (3.1).

The effect of variable viscosity (θ_e) and power-law index (n) on the non-dimensional

Table 3.1: Grid-independence for $n = 1.0$, $\beta = 0.5$, $Le = 1.0$, $B = 1.0$, $Sc = 1$, $\tau = 1$ and $\theta_e = 2$

$\Delta\eta$(step size)	$\frac{Nu_{\overline{x}}}{x^{1/2}}$	$\frac{Sh_{\overline{x}}}{x^{1/2}}$
0.01	0.55782608039592329607359033616376	1.61103064036497278799231480661 55
0.001	0.55782608039592329607359033616376	1.61103064036497278799231480661 55
0.0001	0.55782607864904398820016240279074	1.61103064676580420844231866794 87
0.00001	0.55782608043353443250111922679935	1.61103064044689148204270168207 59

velocity $f'(\eta)$, temperature $\theta(\eta)$ and concentration $\phi(\eta)$ are illustrated in Figs. 3.1(a)-3.1(c) with fixed values of other parameters. From the Fig. 3.1(a), it is observed that the velocity increases near the plate and decreases far away from the plate with the increasing values of variable viscosity for three kinds of fluids. It can be seen from Fig. 3.1(b) that the non-dimensional temperature decreases with an increase in the value of variable viscosity for all values of n. It is revealed from Fig. 3.1(c) that an increase in the variable viscosity increases the concentration boundary layer thickness for three kinds of fluids.

Figures 3.2(a)-3.2(c) depict the non-dimensional velocity $f'(\eta)$, temperature $\theta(\eta)$ and concentration $\phi(\eta)$ profiles for various values of variable thermal conductivity (β) and power-law indices (n). It is observed that an increase in the thermal conductivity leads to increase the velocity profile for all values of n, as displayed in Fig. 3.2(a). Figure 3.2(b) shows that the non-dimensional temperature monotonically increases with the increasing values of thermal conductivity for all values of n. However, it is seen from the Fig. 3.2(c) that an increase in the value of thermal conductivity enhances the concentration near the plate and slightly reduces far away from the plate for three kinds of fluids.

The effects of thermophoresis (τ) and power-law index (n) on the non-dimensional velocity $f'(\eta)$, temperature $\theta(\eta)$ and concentration $\phi(\eta)$ profiles are plotted in Figs. 3.3(a)-3.3(c). Figure 3.3(a) indicates that the velocity decreases with an increase in the values of thermophoresis parameter for three kinds of n. It is evident from the Fig. 3.3(b) that temperature slightly increases with increasing values of thermophoresis parameter for three kinds of fluids. Physically, the temperature distribution near the surface in the presence of thermophoresis is always negative and thus the heat is always transferred from the surface. It is seen that the concentration decreases with the increase of the thermophoresis parameter for the kinds of n, as illustrates in 3.3(c). This is due to the fact that fluid particles move

away from cool surroundings with the increase in the thermophoretic parameter. Therefore, thermophoresis parameter is expected to alter the concentration boundary layer significantly.

Figures 3.4(a)-3.4(c) presents the influence of mixed convection parameter (λ) and power-law indices (n) on the non-dimensional velocity $f'(\eta)$, temperature $\theta(\eta)$ and concentration $\phi(\eta)$ profiles, respectively. It is noticed that the velocity function significantly increases with an increase in mixed convection parameter for three kinds of fluids, as presented in 3.4(a). It is clear from Fig. 3.4(b) that the non-dimensional temperature profile decreases with an increase in the mixed convection parameter for all values of n. Figure 3.4(c) reveals that, the non-dimensional concentration decreases with increasing the values of mixed convection parameter for three kinds of fluids. It is also interesting to note that the smaller values of mixed convection parameter gives strong influence on the temperature and concentration profiles.

The variations of the heat and mass transfer rates are shown in Tab.(3.2) with different values of the power-law index (n), variable viscosity (θ_e), thermal conductivity (β) and thermophoresis parameter (τ) for fixed values of B = 1.0, Le = 1.0 and Sc = 0.6. We observe that the heat and mass transfer rates decreases when power-law index increases. An increase in the value of the variable viscosity the heat transfer rate enhances, but a reverse trend is observed in the mass transfer rate. Higher value of thermophoresis parameter reduces the heat transfer rate and increases the mass transfer rate. Both heat and mass transfer rates increases for the mixed convection parameter, whereas reverse trend is noticed for thermal conductivity parameter.

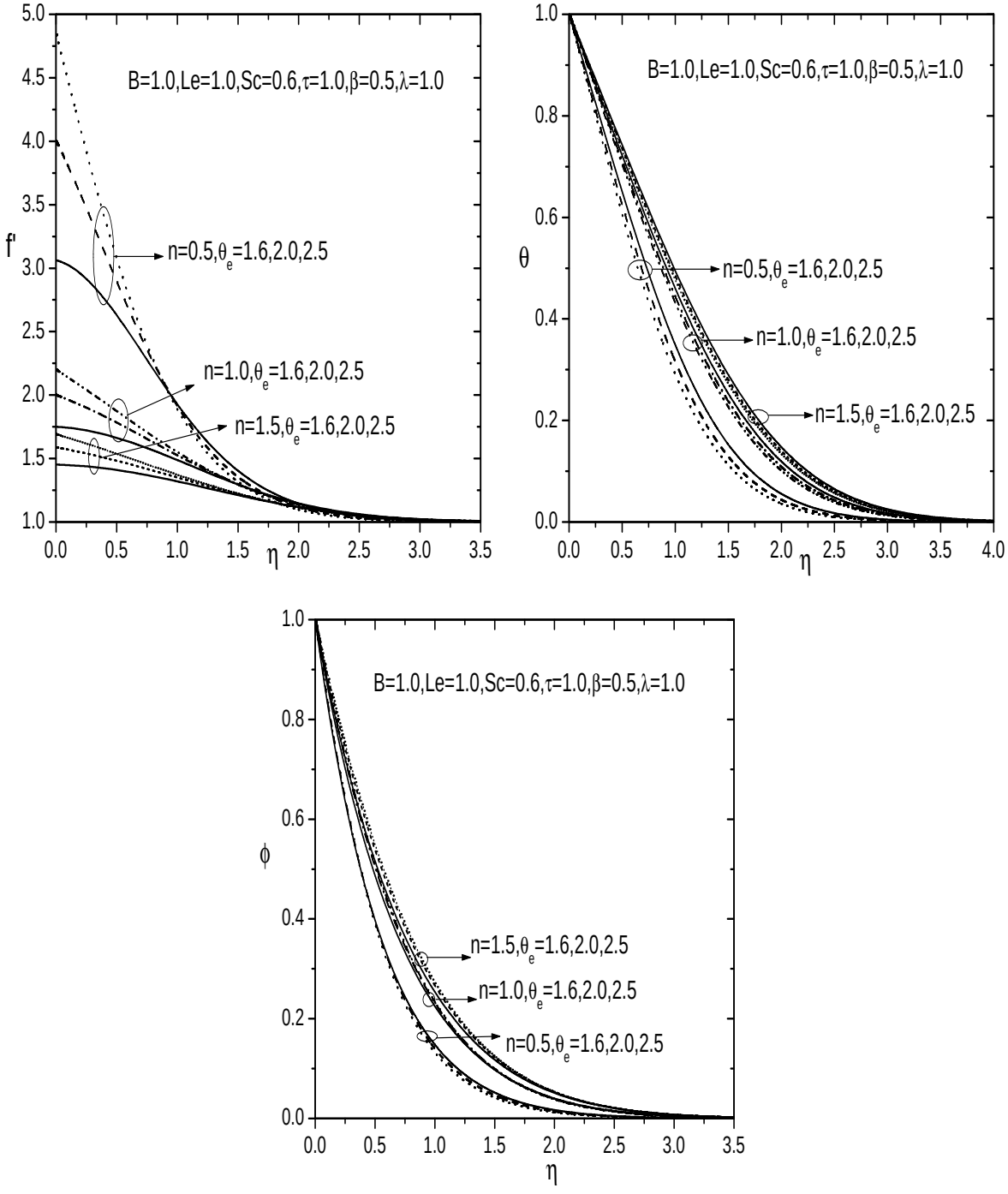

Figure 3.1: (a) velocity profile (b) temperature profile and (c) concentration profile for various value of θ_e and n.

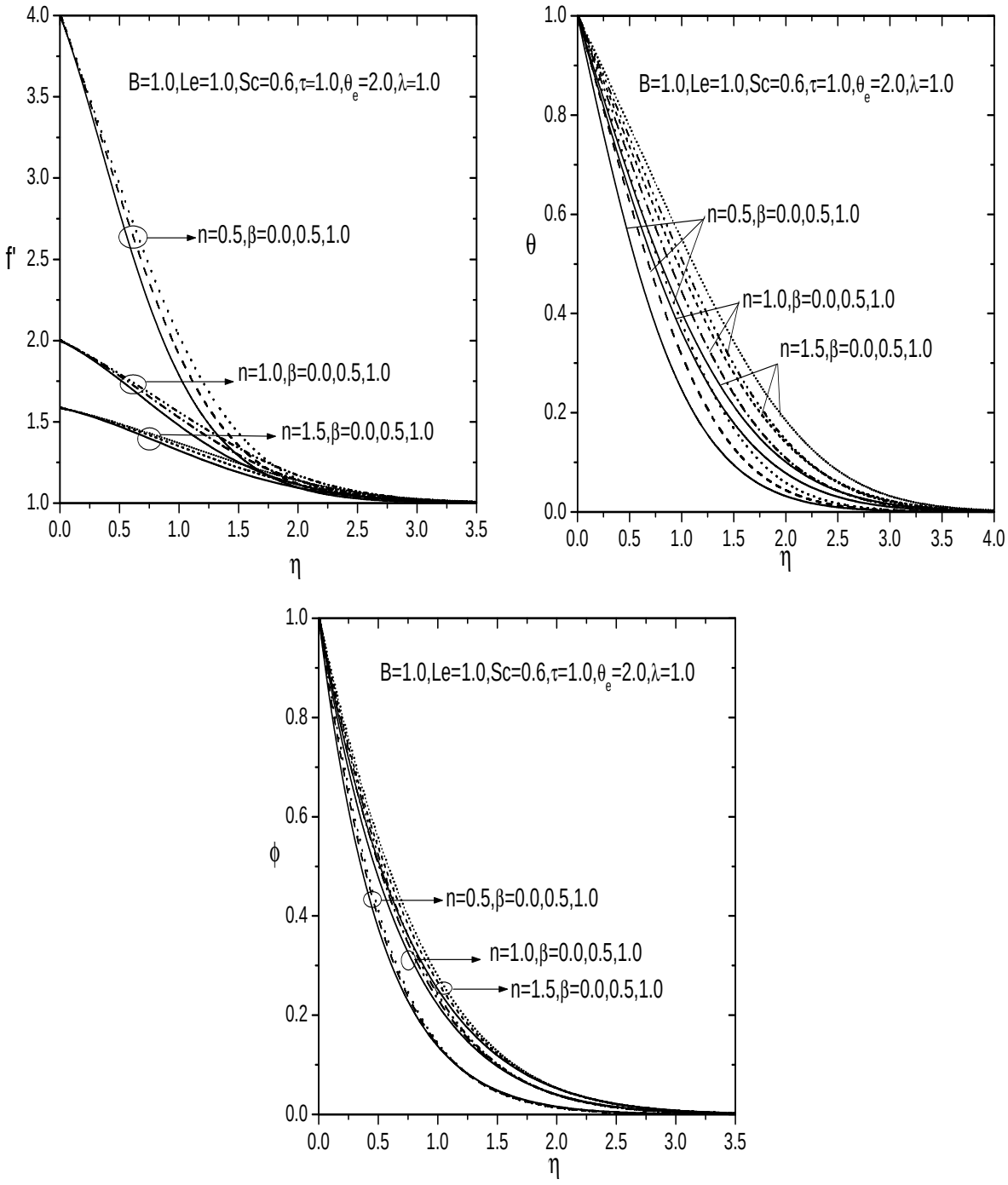

Figure 3.2: (a) velocity profile (b) temperature profile and (c) concentration profile for various value of β and n.

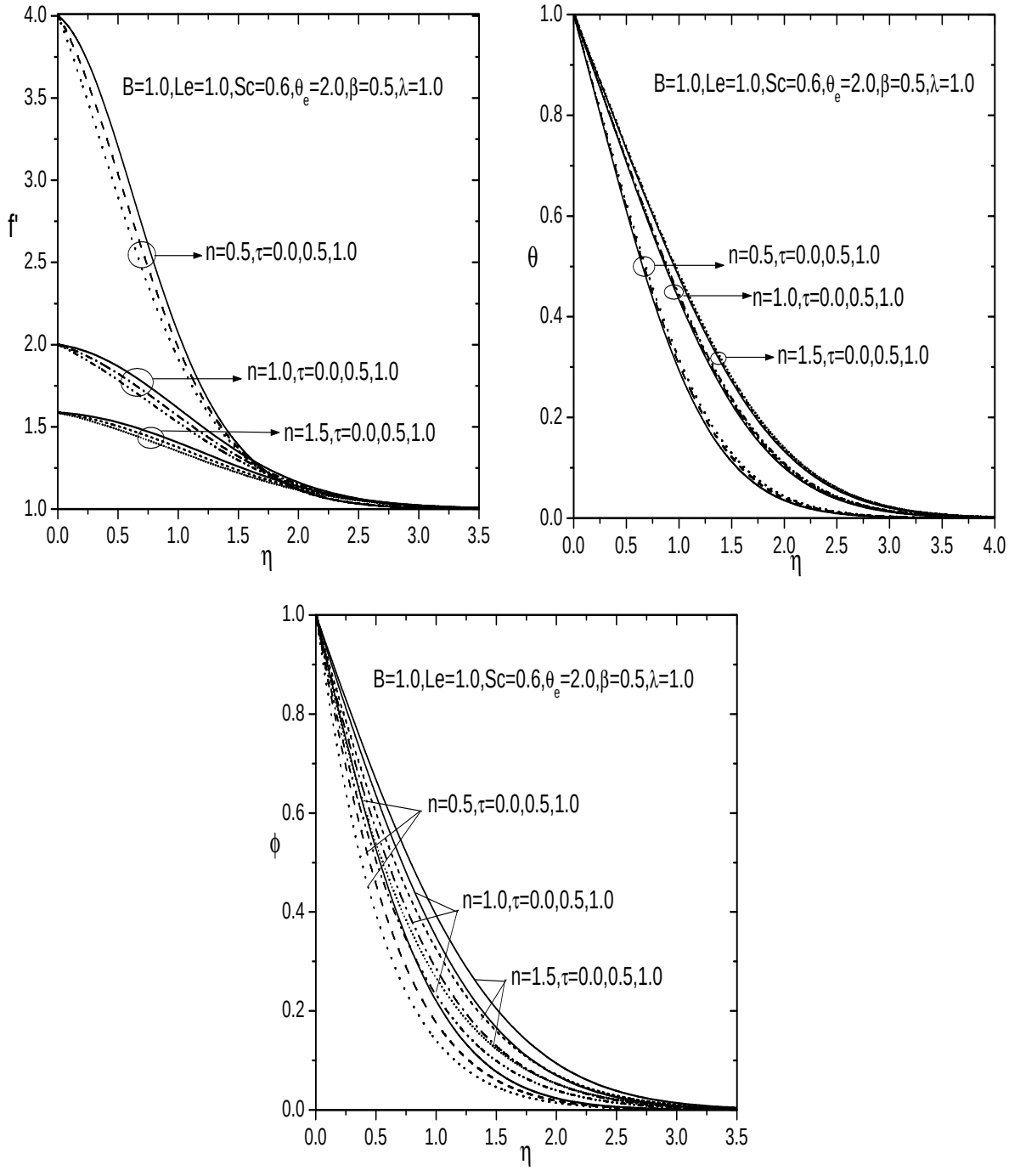

Figure 3.3: (a) velocity profile (b) temperature profile and (c) concentration profile for various value of τ and n.

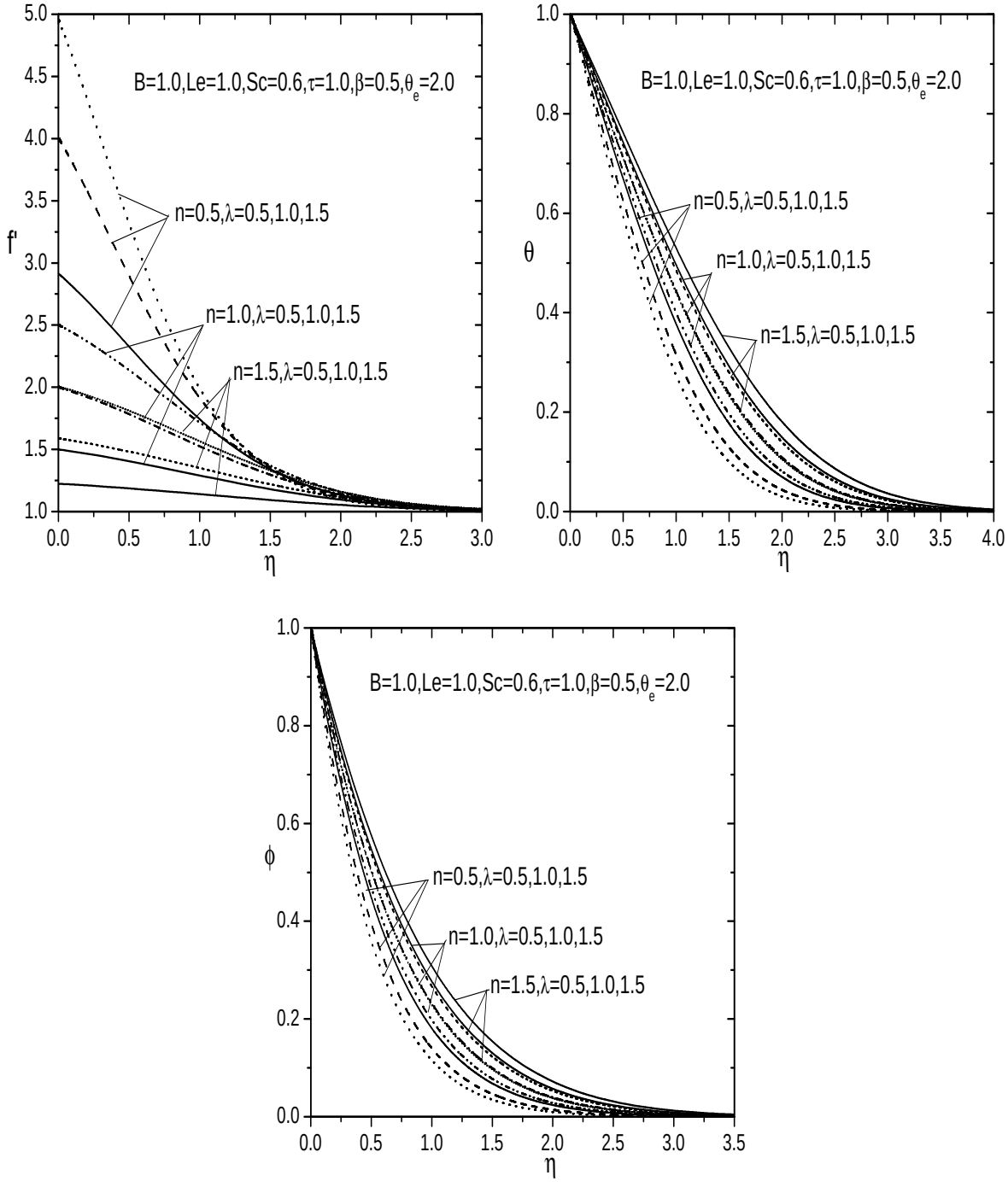

Figure 3.4: (a) velocity profile (b) temperature profile and (c) concentration profile for various value of λ and n.

Table 3.2: Variation of heat and mass transfer coefficients for varying values of n, θ_e, β, τ and λ.

n	θ_e	β	τ	λ	$-\theta'(0)$	$-\phi'(0)$
0.5	2.0	0.5	1.0	1.0	0.741640	1.674919
1.0	2.0	0.5	1.0	1.0	0.563815	1.258742
1.5	2.0	0.5	1.0	1.0	0.515349	1.145993
0.5	1.6	0.5	1.0	1.0	0.686584	1.779595
0.5	2.5	0.5	1.0	1.0	0.785708	1.648386
0.5	3.0	0.5	1.0	1.0	0.815134	1.646386
0.5	2.0	0.0	1.0	1.0	0.973910	1.914540
0.5	2.0	1.0	1.0	1.0	0.615734	1.551708
0.5	2.0	1.5	1.0	1.0	0.534856	1.475657
0.5	2.0	0.5	0.0	1.0	0.770320	1.023001
0.5	2.0	0.5	0.5	1.0	0.755064	1.345503
0.5	2.0	0.5	1.5	1.0	0.729855	2.009595
0.5	2.0	0.5	1.0	0.5	0.431598	0.952043
0.5	2.0	0.5	1.0	1.5	0.650541	1.462362
0.5	2.0	0.5	1.0	2.0	0.811640	1.838279

3.4 Conclusions

In this Chapter, the effect of variable viscosity, thermal conductivity and thermophoresis parameters on the mixed convection heat and mass transfer along a vertical plate embedded in a porous medium saturated with power-law fluid has been analyzed. From this analysis, the following conclusions are drawn.

The variable viscosity parameter increases the velocity, concentration and heat transfer rate and reduces the temperature and mass transfer rate. An increase in the value of the thermal conductivity parameter increases the velocity, temperature and concentration profiles, but decreases the heat and mass transfer rates. A rise in the value of thermophoresis parameter monotonically decreases the momentum, concentration boundary layers and heat transfer rate, but it increases the temperature boundary layer and mass transfer rate. The velocity, heat and mass transfer rates increases by increasing values of mixed convection parameter, but it continuously decreases the temperature and concentration profiles.

Chapter 4

Scaling Group Transformation for Mixed Convection in a Power-law Fluid Saturated Porous Medium with Variable Properties, Soret and Radiation Effects [1]

4.1 Introduction

The study of Soret effect (also known as thermo-diffusion), in which molecules are carried in a multi-component mixture impelled by temperature gradients, is considered in this chapter. Even though Soret effect is more significant, the literature regarding Soret effect in power-law fluid is noticed less. Narayana and Murthy [68] reported the role of free convection on power-law fluids with yield stress over a vertical flat plate in a porous media with Dufour and Soret effects. Pal and Chatterjee [74] investigated the influence of radiation, thermal conductivity, Soret and Dufour on MHD convective transport in a power-law fluid saturated

[1] Published in "**Frontiers in Heat and Mass Transfer**"9, 39 (2017)

porous medium. The influence of internal heat generation, Soret and Dufour on natural convection of power-law fluids over a vertical permeable cone in a porous medium has been discussed by Huang [39].

Several investigations have been carried out on the mixed convective flow of different fluids under the influence of thermal radiation. Grosan and Pop [31] discussed the influence of radiation on free convective flow over a vertical surface in a power-law fluid. Hayat *et al.* [34] discussed on two dimensional mixed convection stagnation-point flow of power-law fluids towards a stretching sheet with the effects of MHD and radiation. Cortell [21] scrutinized the viscous dissipation and thermal radiation effects on a power-law fluid past an infinite porous plate.

The main aim of this chapter is to explore the combined influence of Soret, variable properties and radiation effect on mixed convection flow of a power-law fluid in a porous medium. The effect of various physical parameters on the non-dimensional velocity, temperature and concentration are examined numerically and displayed graphically.

4.2 Mathematical Formulation

Consider a steady, laminar, incompressible, two dimensional, mixed convection flow of power-law fluid over a vertical surface in a porous medium. The $\overline{x}$-axis is along the vertical plate and $\overline{y}$-axis is normal to the plate. The physical model and coordinate system are displayed in Fig. (2.1). The fluid is considered to be a gray, absorbing emitting radiation but non-scattering medium and the Rosseland approximation is used to describe the radiative heat flux in the energy equation. The plate is maintained at a constant temperature $\overline{T}_w$ and concentration $\overline{C}_w$. The ambient temperature is $\overline{T}_\infty$ and the concentration is $\overline{C}_\infty$. Applying the boundary layer assumptions and Boussinesq approximations, the governing equations of the momentum, energy and concentration can be written as

$$\frac{\partial \overline{u}}{\partial \overline{x}} + \frac{\partial \overline{v}}{\partial \overline{y}} = 0, \tag{4.1}$$

$$n\overline{u}^{n-1}\frac{\partial \overline{u}}{\partial \overline{y}} = \frac{\partial}{\partial \overline{y}}\left[\frac{gK\rho_\infty}{\mu}\left(\beta_T^*(\overline{T}-\overline{T}_\infty)+\beta_C^*(\overline{C}-\overline{C}_\infty)\right)\right] \tag{4.2}$$

$$\overline{u}\frac{\partial \overline{T}}{\partial \overline{x}} + \overline{v}\frac{\partial \overline{T}}{\partial \overline{y}} = \frac{\partial}{\partial \overline{y}}\left[\alpha\frac{\partial \overline{T}}{\partial \overline{y}} - \frac{1}{\rho C_p}q_r\right] \tag{4.3}$$

$$\overline{u}\frac{\partial \overline{C}}{\partial \overline{x}} + \overline{v}\frac{\partial \overline{C}}{\partial \overline{y}} = D_m\frac{\partial^2 \overline{C}}{\partial \overline{y}^2} + \frac{D_m K_T}{T_y}\frac{\partial^2 \overline{T}}{\partial \overline{y}^2} \tag{4.4}$$

where $\overline{u}$ and $\overline{v}$ are the Darcy velocity components in $\overline{x}$ and $\overline{y}$ directions, respectively. Further, K represents the permeability, K_T indicates the thermal diffusion ratio, α represents the thermal conductivity, D_m is the mass diffusivity of the saturated porous medium, g is the acceleration due to gravity, T_y is the mean fluid temperature, C_p represents the specific heat capacity and q_r is the component of radiative heat flux.

The associated boundary conditions are

$$\left.\begin{aligned} &\overline{v}=0, \quad \overline{T}=\overline{T}_w, \quad \overline{C}=\overline{C}_w \quad \text{at} \quad \overline{y}=0 \\ &\overline{u}=u_\infty, \quad \overline{T}=\overline{T}_\infty, \quad \overline{C}=\overline{C}_\infty \quad \text{as} \quad \overline{y}\to\infty \end{aligned}\right\} \tag{4.5}$$

The quantity q_r is the radiative heat flux which is simplified by using the Rosseland diffusion approximation (see Sparrow [93]). Thus

$$q_r = \frac{-4\sigma^*}{3k^*}\frac{\partial \overline{T}^4}{\partial \overline{y}} \tag{4.6}$$

where σ^* is the Stefan-Boltzmann constant and k^* is the Rosseland mean absorption coefficient. Assuming that the temperature differences within the flow are sufficiently small such that T^4 may expressed as a linear function of temperature

$$\overline{T}^4 = 4\overline{T}_\infty^3\overline{T} - 3\overline{T}^4{}_\infty \tag{4.7}$$

Introducing the following dimensionless variables:

$$\left.\begin{aligned} x = \frac{\overline{x}}{\mathrm{L}}, \quad y = \frac{\overline{y}}{\mathrm{L}}\mathrm{Pe}^{\frac{1}{2}}, \quad u = \frac{\overline{u}\mathrm{L}}{\alpha_0 \mathrm{Pe}}, \quad v = \frac{\overline{v}\mathrm{L}}{\alpha_0 \mathrm{Pe}^{\frac{1}{2}}} \\ \theta(\eta) = \frac{\overline{T} - \overline{T}_\infty}{\overline{T}_w - \overline{T}_\infty}, \quad \phi(\eta) = \frac{\overline{C} - \overline{C}_\infty}{\overline{C}_w - \overline{C}_\infty} \end{aligned}\right\} \tag{4.8}$$

where $\mathrm{Pe} = \dfrac{u_\infty \mathrm{L}}{\alpha_0}$ is the Péclet number and L represents the characteristic length.

In view of the continuity equation (4.1), introduce the stream function ψ by

$$u = \frac{\partial \psi}{\partial y}, \quad v = -\frac{\partial \psi}{\partial x} \tag{4.9}$$

Using Eqs.(4.8)-(4.9) into Eqs.(4.2)-(4.4), we get the following momentum, energy, and concentration equations in dimensionless form as

$$n\left(\frac{\partial \psi}{\partial y}\right)^{n-1} \frac{\partial^2 \psi}{\partial y^2} + \frac{\lambda^n}{\theta_e}\left[\theta + \mathrm{B}\phi\right]\frac{\partial \theta}{\partial y} - \lambda^n \left[\frac{\partial \theta}{\partial y} + \mathrm{B}\frac{\partial \phi}{\partial y}\right]\left[1 - \frac{\theta}{\theta_e}\right] = 0 \tag{4.10}$$

$$\frac{\partial \psi}{\partial y}\frac{\partial \theta}{\partial x} - \frac{\partial \psi}{\partial x}\frac{\partial \theta}{\partial y} - \beta\left(\frac{\partial \theta}{\partial y}\right)^2 - \left(1 + \beta\theta + \frac{4\,\mathrm{R}}{3}\right)\frac{\partial^2 \theta}{\partial y^2} = 0 \tag{4.11}$$

$$\frac{\partial \psi}{\partial y}\frac{\partial \phi}{\partial x} - \frac{\partial \psi}{\partial x}\frac{\partial \phi}{\partial y} - \frac{1}{\mathrm{Le}}\frac{\partial^2 \phi}{\partial y^2} - \mathrm{Sr}\frac{\partial^2 \theta}{\partial y^2} = 0 \tag{4.12}$$

The prescribed boundary conditions (4.5) become

$$\left.\begin{aligned} \frac{\partial \psi}{\partial x} = 0, \quad \theta = 1, \quad \phi = 1 \quad \text{at} \quad y = 0 \\ \frac{\partial \psi}{\partial y} = 1, \quad \theta = 0, \quad \phi = 0 \quad \text{as} \quad y \to \infty \end{aligned}\right\} \tag{4.13}$$

where the prime indicates differentiation with respect to η, $\mathrm{R} = \dfrac{4\sigma^* \overline{T}_\infty^3}{k^* k}$ represents thermal radiation, $\mathrm{Le} = \dfrac{\alpha_0}{D_m}$ indicates the Lewis number, $\mathrm{Ra} = \dfrac{\mathrm{L}}{\alpha_0}\left[\dfrac{Kg\beta_T(\overline{T}_w - \overline{T}_\infty)}{\nu}\right]^{1/n}$ represents the generalized Rayleigh number, $\mathrm{B} = \dfrac{\beta_c(\overline{C}_w - \overline{C}_\infty)}{\beta_T(\overline{T}_w - \overline{T}_\infty)}$ represents the Buoyancy ratio, $\lambda = \dfrac{\mathrm{Ra}}{\mathrm{Pe}}$ indicates the mixed convection parameter, $\mathrm{Sr} = \dfrac{D_m K_T}{T_m \alpha_0}\left(\dfrac{\overline{T}_w - \overline{T}_\infty}{\overline{C}_w - \overline{C}_\infty}\right)$ represents the Soret

parameter and $\theta_e = \dfrac{\overline{T}_e - \overline{T}_\infty}{\overline{T}_w - \overline{T}_\infty}$ indicates the variable viscosity.

Similarity equations via Lie group transformations

Using the mathematical procedure of Lie scaling transformation explained in the second chapter, the following similarity transformations are obtained

$$\eta = yx^{-1/2}, \quad \psi = x^{1/2} f(\eta), \quad \theta = \theta(\eta), \quad \phi = \phi(\eta) \tag{4.14}$$

Using Eq. (4.14) into Eqs. (4.10)-(4.12), the following similarity equations are attained

$$n(f')^{n-1} f'' = -\lambda^n (\theta + \mathrm{B}\phi) \frac{\theta'}{\theta_e} + \lambda^n (\theta' + \mathrm{B}\phi') \left(1 - \frac{\theta}{\theta_e}\right) \tag{4.15}$$

$$\beta(\theta')^2 + \left(1 + \beta\theta + \frac{4\mathrm{R}}{3}\right)\theta'' + \frac{1}{2} f\theta' = 0 \tag{4.16}$$

$$\frac{1}{\mathrm{Le}}\phi'' + \frac{1}{2} f\phi' + \mathrm{Sr}\theta'' = 0 \tag{4.17}$$

The transformed boundary conditions (4.5) become

$$\left.\begin{aligned} &f(0) = 0, \quad \theta(0) = 1, \quad \phi(0) = 1 \\ &f'(\infty) = 1, \quad \theta(\infty) = 0, \quad \phi(\infty) = 0 \end{aligned}\right\} \tag{4.18}$$

The non-dimensional heat and mass fluxes from wall are given by

$$q_w = -\widetilde{k}\left(\frac{\partial \overline{T}}{\partial \overline{y}}\right)_{\overline{y}=0} - \frac{4\sigma^*}{3k^*}\left(\frac{\partial \overline{T}^4}{\partial \overline{y}}\right)_{\overline{y}=0} \quad \text{and} \quad q_m = -D\left(\frac{\partial \overline{C}}{\partial \overline{y}}\right)_{\overline{y}=0} \tag{4.19}$$

The Nusselt number $Nu_{\overline{x}} = \dfrac{q_w \overline{x}}{\widetilde{k}(\overline{T}_w - \overline{T}_\infty)}$ and Sherwood number $Sh_{\overline{x}} = \dfrac{q_m \overline{x}}{D(\overline{C}_w - \overline{C}_\infty)}$ are given by

$$\frac{Nu_{\overline{x}}}{x^{1/2}} = -\left(1+\frac{4\mathrm{R}}{3}\right)\theta'(0) \quad \text{and} \quad \frac{Sh_{\overline{x}}}{x^{1/2}} = -\phi'(0) \tag{4.20}$$

4.3 Results and Discussion

The coupled nonlinear Eqs.(4.15)-(4.17) along with the boundary conditions (4.18) are solved numerically using shooting method, which is explained clearly in chapter-2. In order to validate the code, we compared the present results with those of Chaoyang *et al.* [18] as a special case of Sr = R = B = $\beta = 0$, Le = 1.0, and $\theta_e \to \infty$, as shown in Tab. (3.1).

The results for the non-dimensional velocity, temperature and concentration have been computed and presented graphically in Figs. 4.1–4.5 to analyze the influence of variable viscosity (θ_e), thermal conductivity (β), radiation (R), Soret parameter (Sr) and mixed convection parameter (λ).

Figures 4.1(a)-4.1(c) exhibit the dimensionless velocity $f'(\eta)$, temperature $\theta(\eta)$ and concentration $\phi(\eta)$ distributions for different values of the variable viscosity (θ_e) and power-law index (n). Figure 4.1(a) illustrates that, the velocity $f'(\eta)$ enhances near the plate up to a certain value and then reduces far away from the plate with increasing value of variable viscosity for three types of fluids. From Figs. 4.1(b)-4.1(c), It is observe that, when the variable viscosity is increased there is a reduction in the value of temperature and concentration for three types of fluids.

The variation of thermal conductivity (β) and power-law index (n), (namely $n < 1, n = 1, n > 1$) for fixed values of other parameters on the dimensionless velocity $f'(\eta)$, temperature $\theta(\eta)$ and concentration $\phi(\eta)$ profiles, is displayed in Figs. 4.2(a)- 4.2(c). It is clear from Fig. 4.2(a) that an increase in the value of thermal conductivity reduces velocity near the plate and enhances it far away from the plate for three types of fluids. Figure 4.2(b) depicts that the temperature $\theta(\eta)$ is more pronounced with increasing values of thermal conductivity for three types of fluids. It is seen from Fig. 4.2(c) that an enhancement in the value of thermal conductivity slightly decreases the concentration profile for the three types of fluids. Because

molecular motion of the fluid reduces at a slower rate for larger values of β.

The effect of radiation parameter (R) and the power-law index (n) illustrated in Figs.4.3(a)-4.3(c). Figure 4.3(a) indicates that an enhancement in the radiation parameter reduces the velocity $f'(\eta)$ slightly near the plate and enhances it far away from the plate for the three types of fluids. In Fig. 4.3(b), temperature $\theta(\eta)$ increases monotonically with enhancing values of the radiation parameter for the three types of fluids. That is, the boundary layer thickness increases as R increases. This result can be explained by the fact that an increase in the values of $\mathrm{R} = \frac{16\sigma^*\overline{T}_\infty^3}{3k^*k}$ for given T_∞ and k means a decrease in the Rosseland radiation absorptivity k^* to Eq. (4.6), the divergence of the radiative heat flux $\frac{\partial q_r}{\partial y}$ increases as k^* decreases which in turn increases the rate of radiative heat transferred to the fluid, and hence the fluid temperature increases. In view of this explanation, the effect of radiation becomes more significant as $\mathrm{R} \to \infty$ and can be neglected when R=0. Moreover, from Fig. 4.3(c) it is visible that, for the three different types of fluids, concentration $\phi(\eta)$ reduces slightly with increasing values of radiation parameter.

Figures 4.4(a)-4.4(c) represent the variation of fluid properties for different values of the Soret parameter (Sr) and power-law index (n), with fixed values of the other parameters. Figure 4.4(a) shows that the velocity $f'(\eta)$ enhances with an enhancement of the Soret parameter (Sr) for the three different types of fluids. Moreover, an enhancement in the value of the Soret parameter (Sr) results in the increase of temperature $\theta(\eta)$ of the fluid, as displayed in Fig. 4.4(b). The influence of Soret parameter (Sr) on the concentration profile $\phi(\eta)$ is depicted in fig. 4.4(c). The concentration profile enhances with the increasing the value of Sr for the three different types of n.

Figures 4.5(a)-4.5(c) depict the variation of mixed convection parameter (λ) and power-law index (n) on the velocity $f'(\eta)$, temperature $\theta(\eta)$ and concentration $\phi(\eta)$ profiles respectively. From Fig. 4.5(a), we notice that enhancing the value of mixed convection parameter (λ) continuously raises the velocity $f'(\eta)$ for the three types of fluids. Figures 4.5(b)-4.5(c) it can be seen that the temperature $\theta(\eta)$ and concentration $\phi(\eta)$ decreases with an increase in the mixed convection parameter (λ) for the three types of fluids.

Table 4.1: *Values of heat and mass transfer rates at Le=1.0 and B=1.0 for varying values of power-law index, temperature dependent viscosity, variable thermal conductivity, radiation, Soret and mixed convection parameters.*

n	θ_e	β	R	Sr	λ	$-\theta'(0)\left(1+\frac{4\mathrm{R}}{3}\right)$	$-\phi'(0)$
0.5	2.0	0.5	0.5	0.5	1.0	1.083878	0.898871
1.0	2.0	0.5	0.5	0.5	1.0	0.811355	0.665762
1.5	2.0	0.5	0.5	0.5	1.0	0.737721	0.603112
0.5	1.5	0.5	0.5	0.5	1.0	0.985773	0.810344
0.5	2.5	0.5	0.5	0.5	1.0	1.143469	0.952729
0.5	3.0	0.5	0.5	0.5	1.0	1.183445	0.988888
0.5	2.0	0.0	0.5	0.5	1.0	1.305338	0.849427
0.5	2.0	1.0	0.5	0.5	1.0	0.939365	0.928902
0.5	2.0	1.5	0.5	0.5	1.0	0.836542	0.948922
0.5	2.0	0.5	0.0	0.5	1.0	0.790250	0.854522
0.5	2.0	0.5	1.0	0.5	1.0	1.311348	0.925503
0.5	2.0	0.5	1.5	0.5	1.0	1.501126	0.943220
0.5	2.0	0.5	0.5	0.0	1.0	1.060429	1.028426
0.5	2.0	0.5	0.5	1.0	1.0	1.107032	0.768095
0.5	2.0	0.5	0.5	1.5	1.0	1.129908	0.636080
0.5	2.0	0.5	0.5	0.5	0.5	0.945030	0.780440
0.5	2.0	0.5	0.5	0.5	1.5	1.190563	0.989876
0.5	2.0	0.5	0.5	0.5	2.0	1.280580	1.066663

Table. 4.1 displays the variations of heat and mass transfer rates for various values of the power law index (n), variable viscosity (θ_e), thermal conductivity (β), thermal radiation (R), Soret parameter (Sr) and mixed convection parameters (λ). Enhancing the value of n reduces the heat and mass transfer rates. An increase in the values of variable viscosity, radiation and mixed convection parameters raises both the heat and mass transfer rates. It is noticed that an increase in the value of the thermal conductivity decreases the heat transfer, but a reverse trend is observed in the mass transfer rate. Higher value of the Soret parameter enhance the heat transfer rate and decrease the mass transfer rate.

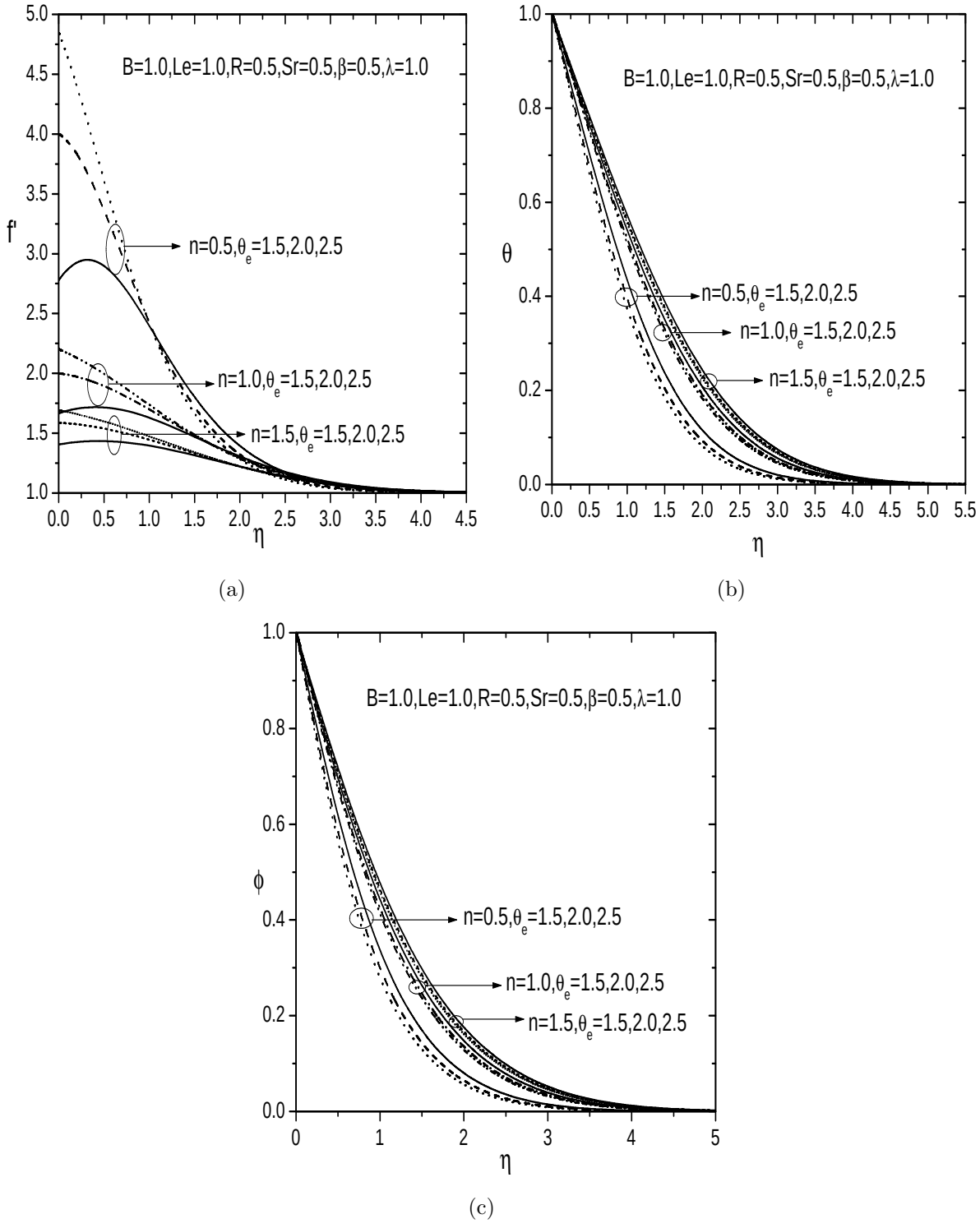

Figure 4.1: (a) velocity profile (b) temperature profile and (c) concentration profile for various value of θ_e and n.

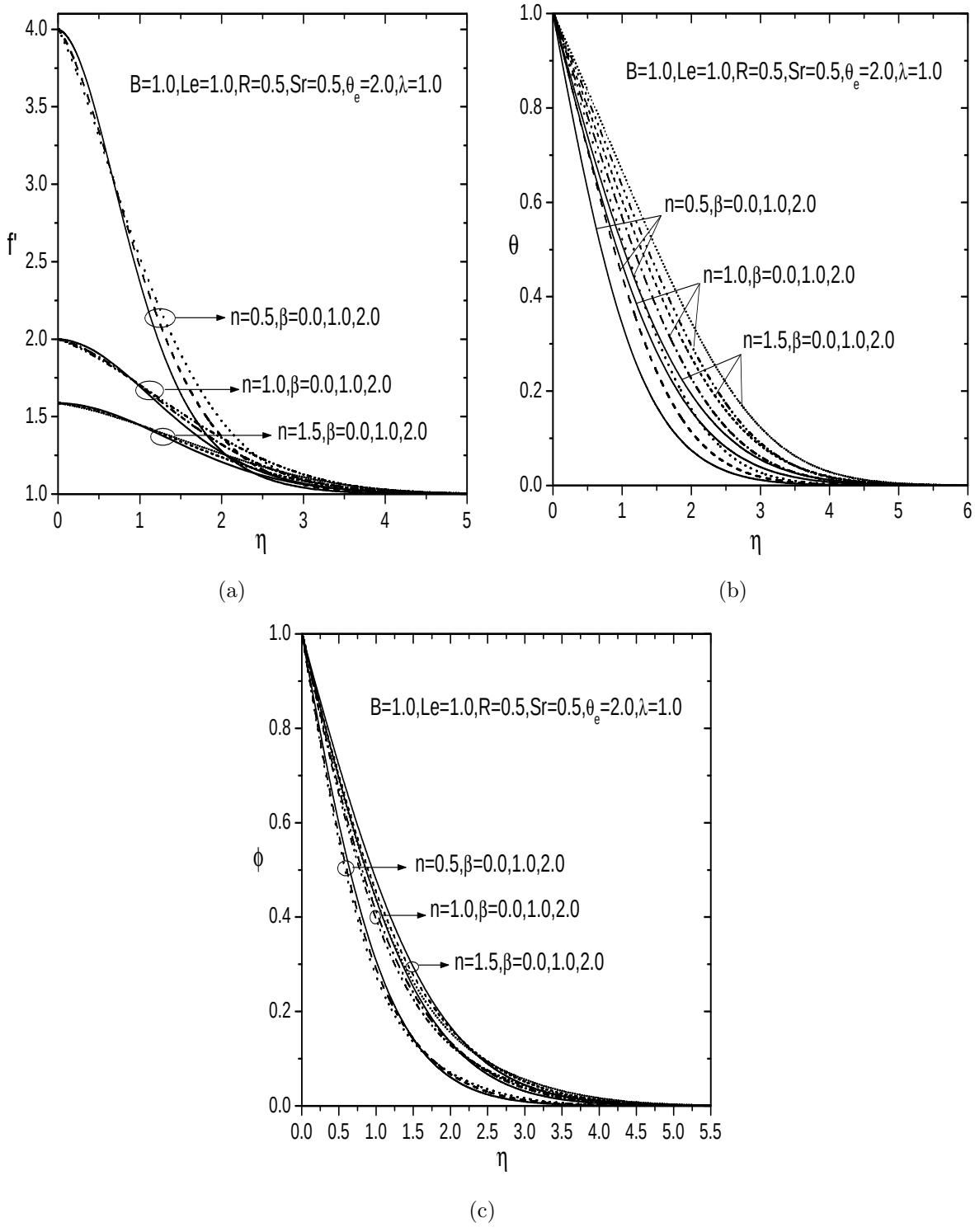

Figure 4.2: (a) velocity profile (b) temperature profile and (c) concentration profile for various value of β and n.

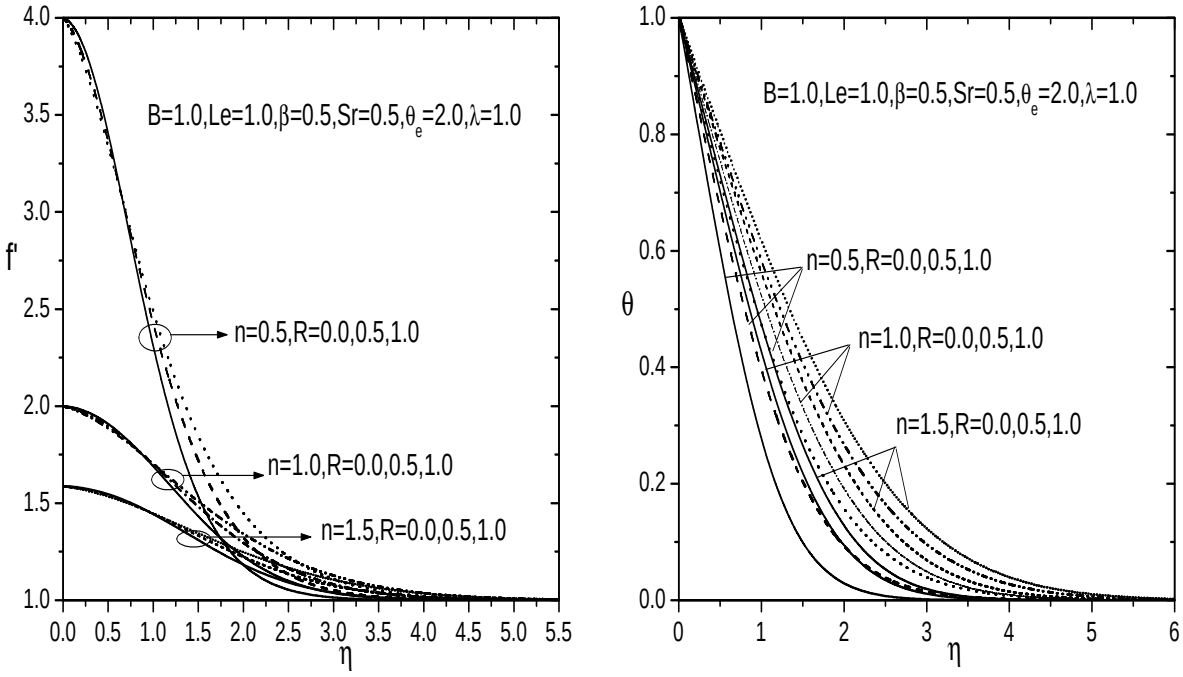

(a) (b)

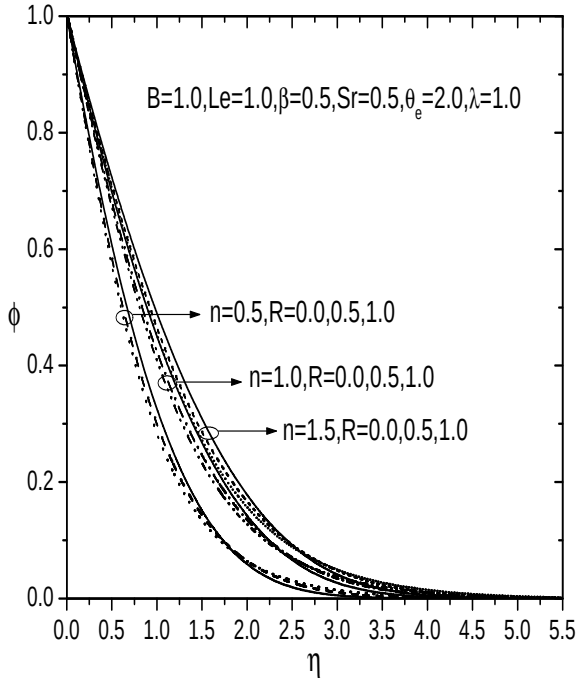

(c)

Figure 4.3: (a) velocity profile (b) temperature profile and (c) concentration profile for various value of R and n.

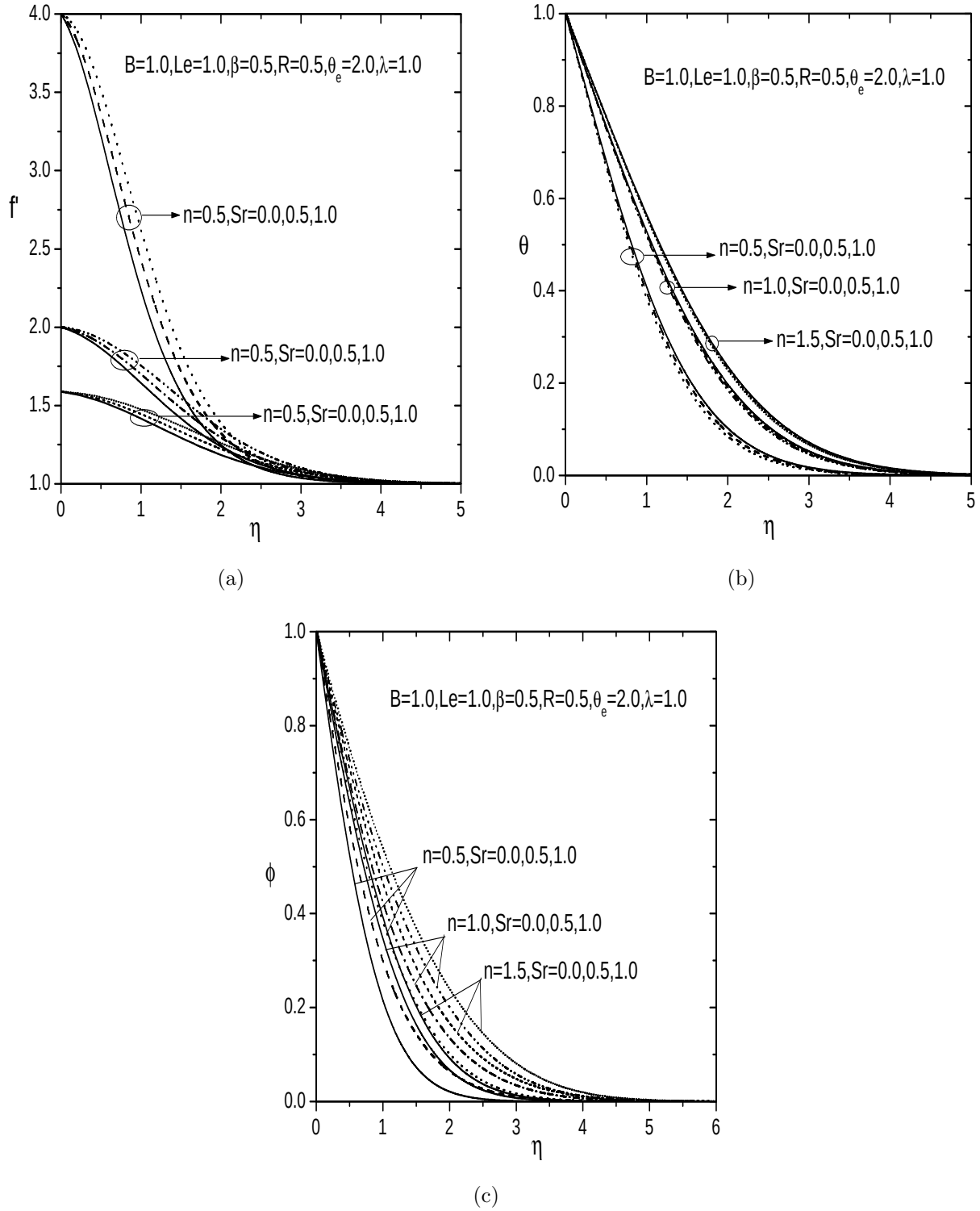

Figure 4.4: (a) velocity profile (b) temperature profile and (c) concentration profile for various value of Sr and n.

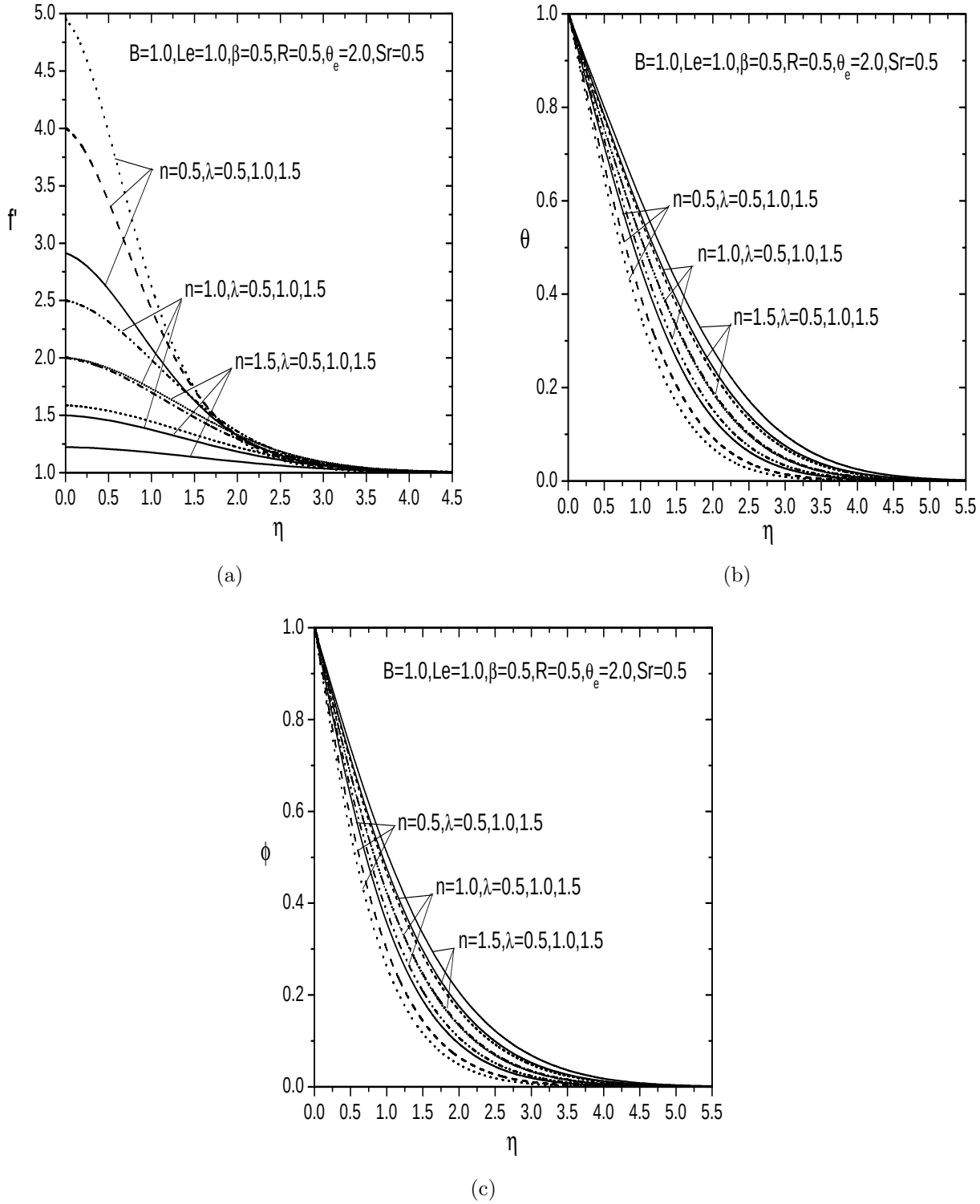

Figure 4.5: (a) velocity profile (b) temperature profile and (c) concentration profile for various value of λ and n.

4.4 Conclusions

In the present chapter, we have analyzed mixed convective flow, heat and mass transfer over a vertical surface in a porous medium saturated with power-law fluid. The numerical results were obtained for different values of the power law index (n), variable viscosity (θ_e), variable thermal conductivity (β), thermal radiation (R) and Soret parameter (Sr). The main conclusions are as follows.

- An enhancement in values of the variable viscosity parameter (θ_e) increases the velocity, heat and mass transfer rates, but decreases the temperature and concentration profiles.
- The effect of variable thermal conductivity (β) decreases the velocity, concentration and heat transfer rate, but enhances the temperature and mass transfer rates.
- The effect of the thermal radiation parameter (R) reduces the velocity and concentration profiles, but enhances the temperature, heat and mass transfer rates.
- An increasing value of the Soret parameter (Sr) decreases the temperature and mass transfer rates, but increases the velocity, concentration and heat transfer rate.
- The influence of the mixed convection parameter (λ) results in an enhancement in velocity and heat transfer rate, but reduces the temperature, concentration and mass transfer rate.

Chapter 5

Linear Stability of the Darcy-Bénard Convection of a Power-law Fluid with Local Thermal Non-Equilibrium [1]

5.1 Introduction

This Chapter is concerned with the onset of instability in a porous layer which is heated from below, and is a variation of the well-known Darcy-Bénard problem. Therefore we are considering the fate of small-amplitude disturbances when the layer is heated from below, where the upper and lower bounding surfaces are subject to constant temperature. We shall consider the combined effects of a vertical throughflow, the presence of a power-law fluid and Local Thermal non-Equilibrium between the phases. In its original and Newtonian form, convection ensures at the wave number, $k = \pi$, and when the Darcy-Rayleigh number is $4\pi^2$. Within the context of linearised theory, the stability properties of all three variations from the classical Darcy-Bénard problem are quite well-known. Wooding [108] and Sutton [97] were the first to consider vertical throughflow through the layer. Such fluid movement alters the basic temperature profile which, as the strength of the flow increases, causes that part of the

[1] Communicated to "**Transport in porous media**"

temperature field which varies rapidly (and thus is the location where destabilisation takes place) to concentrate at either the lower or the upper surface, depending on the direction of that flow. This causes both the critical wavenumber and Darcy-Rayleigh number to increase, eventually forming a deep-pool system whereby both these quantities eventually vary linearly with the transpiration velocity once it is sufficiently large. when Rayleigh number is above the critical value then small amplitude disturbances grow exponentially with time, and when it is below then they decay exponentially with time.

On the other hand, when the saturating fluid is no longer Newtonian but takes a power-law form, then certain difficulties arise when considering instability when there is no background flow. Barletta and Storesletten [9] and Barletta and Nield [8] both considered the onset of convection of a power-law fluid in the presence of a background flow, the former being a vertical flow of the type to be considered here, while the latter was a horizontal flow after Prats [78]. These authors found that when the background flows were present, then critical values could be found with ease and explained on physical grounds. However, the limit as the background flow tends to zero is singular in the sense that when the fluid is shear-thinning then critical Darcy-Rayleigh number is infinite, whereas when the fluid is shear-thickening then it is zero. Such unphysical results are due to the idealised model which is used for power-law fluids in porous media. In particular, a shear-thickening has an effective viscosity of zero when Darcy velocity is zero. In practice there will be a nonzero viscosity in the zero velocity limit, and in such cases the Carreau model will apply. However, when there is a background flow, such as we consider here, the power law and Carreau models will yield almost identical results because the effective viscosity will be essentially the same.

So the present chapter considers the combination of these three effects (Péclet number (Pe), inter-phase heat transfer parameter (H) and porosity-modified conductivity parameter (Ω)) and how they influence the onset of convection. The chapter proceeds in the obvious manner by presenting in turn the governing equations, the basic state solution (which needs to be computed, rather than having an analytical form), the linear stability analysis, a description of the numerical method and a results and discussion section.

5.2 Mathematical Formulation

We consider a plane horizontal porous layer with thickness d, which is saturated by an Ostwald-de Waele (power-law) fluid. The boundary planes at $z = 0$ and $z = d$ are permeable and the surface temperatures are $T = T_0 + \Delta T$ and $T = T_0$, respectively. The gravitational acceleration g is acting in the negative z-direction (see Fig. 5.1). Here T is the temperature field, T_0 is a reference temperature and ΔT is a positive temperature difference. The velocity components are (u, w).

The power-law fluid form of Darcy's law is modified due to the presence of buoyancy forces and subject to the Oberbeck-Boussinesq approximation, takes the form,

$$\frac{\mu^*}{K}|V|^{n-1}V = -\nabla p - \rho g \beta^* (T - T_0), \tag{5.1}$$

where μ^* is the effective consistency factor, K is the permeability, n is power law index with $n < 1$ for a thixotropic fluid, $n > 1$ for dilatant fluids and $n = 1$ the Newtonian fluids. In addition, ρ is the fluid density at the reference temperature, T_0, β^* is the thermal expansion coefficient of the fluid and p is the dynamic pressure. The ratio, $\frac{\mu^*}{K}$, depends on the consistency factor, μ, and the tortuosity factor, c_t, through the relationship

$$\frac{\mu^*}{K} = 2c_t\,\mu \left(\frac{3n+1}{n\phi}\right)^n \left(\frac{3\phi}{50K}\right)^{(n+1)/2}. \tag{5.2}$$

The tortuosity factor c_t is set equal to 25/12 (Christopher and Middleman [20]), so that, for a Newtonian fluid, μ^*/K coincides with the usual μ/K.

Darcy-Boussinesq convection is usually studied by first invoking the assumption that the solid and fluid phases of the medium are in local thermal equilibrium. In this chapter we study the case where the two-temperature model of microscopic heat transfer applies and therefore the porous medium is no longer in local thermal equilibrium. Subject to these assumptions, the governing equations are

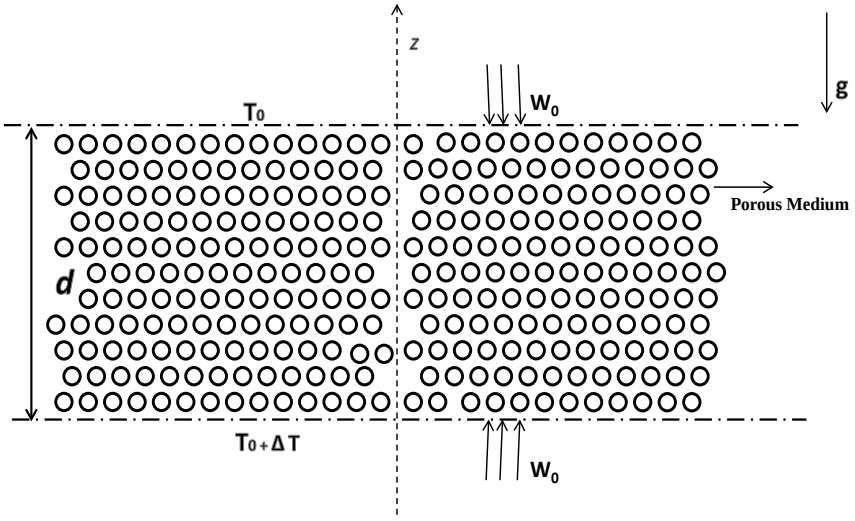

Figure 5.1: Physical model and co-ordinate system

$$\nabla.\bar{u} = 0, \tag{5.3}$$

$$\frac{\mu^*}{K}(\bar{u}^2 + \bar{w}^2)^{(\frac{n-1}{2})}\bar{u} = -\bar{p}_x, \tag{5.4}$$

$$\frac{\mu^*}{K}(\bar{u}^2 + \bar{w}^2)^{(\frac{n-1}{2})}\bar{w} = -\bar{p}_z + \frac{\rho_f g \beta^* K}{\mu}(T_f - T_0), \tag{5.5}$$

$$\epsilon(\rho_c)_f \frac{\partial T_f}{\partial \bar{t}} + (\rho_c)_f \underline{\bar{u}}.\nabla T_f = \epsilon k_f \nabla^2 T_f + h(T_s - T_f), \tag{5.6}$$

$$(1-\epsilon)(\rho_c)_s \frac{\partial T_s}{\partial \bar{t}} = (1-\epsilon)k_s \nabla^2 T_s + h(T_f - T_s), \tag{5.7}$$

where $\bar{t}$ is the time, $\bar{u}$ and $\bar{w}$ are the fluid flux velocities in the horizontal and vertical directions and $\bar{x}$ and $\bar{z}$ are the corresponding Cartesian coordinates. The f and s subscripts are the fluid and solid phases, c is the specific heat, ϵ is the porosity and h is the inter-phase heat transfer co-efficient.

A downward vertical throughflow is considered, so that the boundary conditions are given by

$$\left.\begin{aligned} &\bar{w} = -w_0, \quad T_f = T_0 + \Delta T, \quad T_s = T_0 + \Delta T \quad \text{at} \quad z = 0 \\ &\bar{w} = -w_0, \quad T_f = T_0, \quad T_s = T_0 \quad \text{at} \quad z = 1, \end{aligned}\right\} \tag{5.8}$$

where $w_0 > 0$ is the prescribed vertical through flow velocity.

Non-Dimensional analysis

The governing equations are non-dimensionalized by using the non-dimensional variables as follows:

$$\left.\begin{aligned} &(\bar{x},\bar{z}) = d(x,z), \quad (\bar{u},\bar{w}) = \tfrac{\epsilon k_f}{(\rho_c)_f d}(u,v), \quad \bar{t} = \tfrac{(\rho_c)_f d^2 t}{k_f}, \\ &\tfrac{T_f - T_0}{\Delta T} = \theta, \quad \tfrac{T_s - T_0}{\Delta T} = \phi, \quad \bar{p} = \tfrac{K}{d\mu}\left(\tfrac{(\rho_c)_f d}{\epsilon k_f}\right)^n P. \end{aligned}\right\} \tag{5.9}$$

The governing Eqs. (5.3) to (5.7), become

$$u_x + w_z = 0, \tag{5.10}$$

$$(u^2 + w^2)^{(\frac{n-1}{2})} u = -P_x, \tag{5.11}$$

$$(u^2 + w^2)^{(\frac{n-1}{2})} w = -P_z + \mathrm{Ra}\,\theta, \tag{5.12}$$

$$\theta_t + w\,\theta_z + u\,\theta_x = \nabla^2\theta + H(\phi - \theta), \tag{5.13}$$

$$\alpha\,\phi_t = \nabla^2\phi + H\gamma(\theta - \phi). \tag{5.14}$$

The boundary conditions can be written in the form,

$$\left.\begin{aligned} w = -\mathrm{Pe}, \;\; \theta = 1, \;\; \phi = 1 \;\; \text{at} \quad z = 0, \\ w = -\mathrm{Pe}, \;\; \theta = 0, \;\; \phi = 0 \;\; \text{at} \quad z = 1, \end{aligned}\right\} \tag{5.15}$$

where the Darcy-Rayleigh and Péclet numbers are given by,

$$\mathrm{Ra} = \frac{\rho_f g \beta^* K \Delta T d^n (\rho_c)_f^n}{\mu \epsilon^n {k_f}^n}, \qquad \mathrm{Pe} = \frac{w_0 (\rho_c)_f d}{\epsilon k_f}.$$

while Ra can only be positive, the Péclet number can be negative (Upward throughflow). We note that $\mathrm{Ra} > 0$ here so that it is possible for thermoconvective instability to arise, and while Pe may take either sign, we shall confine ourselves to positive values for numerical

convenience since (i) the shooting method is much easier to implement when the thermal variations are confined to the lower part of the layer and (ii) onset criteria for negative values of Pe are identical, given the inherent symmetries within the equations.

The continuity Eq.(5.10) is satisfied automatically when the stream function ψ is introduced according to

$$u = -\psi_z, \quad w = \psi_x. \tag{5.16}$$

Substitution of the expressions in equation (5.16) into equations (5.11)-(5.14) transforms the latter to,

$$({\psi_z}^2 + {\psi_x}^2)^{(\frac{n-1}{2})}\Big(\psi_{xx} + \psi_{zz}\Big) + (n-1)({\psi_z}^2 + {\psi_x}^2)^{(\frac{n-3}{2})}\Big({\psi_x}^2\psi_{xx} + {\psi_z}^2\psi_{zz} + 2\psi_x\psi_z\psi_{xz}\Big) = \mathrm{Ra}\theta_x, \tag{5.17}$$

$$\theta_t - \psi_z\theta_x + \psi_x\theta_z = \theta_{xx} + \theta_{zz} + H(\phi - \theta), \tag{5.18}$$

$$\alpha\phi_t = \theta_{xx} + \theta_{zz} + H\Omega(\theta - \phi), \tag{5.19}$$

and these are to be solved subject to the boundary conditions,

$$z = 0: \quad \psi = 0,\ \theta = \phi = 1, \qquad z = 1: \quad \psi = \theta = \phi = 0. \tag{5.20}$$

5.3 Basic state solution

The basic stationary solution of Eqs. (5.17)-(5.19) is given by a uniform through flow,

$$u_b = 0, \quad w_b = -\mathrm{Pe}, \quad \psi_b = -\mathrm{Pe}\,x, \tag{5.21}$$

where the subscript, b, denotes the basic solution. The temperature fields are now purely z-dependent and these satisfy the following equations,

$$T_b'' + \mathrm{Pe}T_b' + H(\phi_b - T_b) = 0, \tag{5.22}$$

and

$$\phi_b'' + H\Omega(T_b - \phi_b) = 0, \tag{5.23}$$

and are subject to the following boundary conditions

$$z = 0: \quad T_b = \phi_b = 1 \qquad z = 1: \quad T_b = \phi_b = 0. \tag{5.24}$$

These equations have to be solved numerically, and given that the solutions depend on the governing parameters, H, Ω and Pe, these solutions are solved simultaneously with the linearised stability equations.

5.4 Linear Stability Analysis

Disturbance equations

We perturb the basic state given by Eq. (5.21) and the solutions to Eqs. (5.22) and (5.23), by defining the following stream function and temperature disturbances,

$$\psi = -\mathrm{Pe}\, x + \varepsilon\Psi, \quad \theta = T_b + \varepsilon\Theta, \quad \phi = \phi_b + \varepsilon\Phi \tag{5.25}$$

where $|\varepsilon| \ll 1$ represents the amplitude of the perturbations, and therefore nonlinear terms in ε may be neglected. Substitution of these into Eqs. (5.17) to (5.19) and linearization yields the following equations for the disturbance,

$$n\mathrm{Pe}^{(n-1)}\Psi_{xx} + \mathrm{Pe}^{(n-1)}\Psi_{zz} = \mathrm{Ra}\,\Theta_x, \tag{5.26}$$

$$\Theta_t - \mathrm{Pe}\,\Theta_z + \Psi_x T_b' = \Theta_{xx} + \Theta_{zz} + H(\Phi - \Theta), \tag{5.27}$$

$$\alpha\Phi_t = \Phi_{xx} + \Phi_{zz} + H\Omega(\Theta - \Phi), \tag{5.28}$$

where the subscripts denote partial derivatives. All three functions satisfy homogeneous Dirichlet conditions at the bounding surfaces. This partial differential eigenvalue problem

for Ra may be transformed into ordinary differential eigenvalue form by substituting the following normal mode,

$$\Psi = f(z)\cos kx; \quad \Theta = g(z)\sin kx; \quad \Phi = h(z)\sin kx \tag{5.29}$$

where k is the wavenumber of the disturbance. The functions $f(z)$, $g(z)$ and $h(z)$ satisfy the equations,

$$f'' - nk^2 f - \mathrm{Ra}\, k\, g/\mathrm{Pe}^{(n-1)} = 0, \tag{5.30}$$

$$g'' + \mathrm{Pe}\, g' - k^2 g + kT'_{(b)} f + H(h-g) = 0, \tag{5.31}$$

$$h'' - k^2 h + H\Omega(g-h) = 0, \tag{5.32}$$

and the boundary conditions that,

$$f = g = h = 0, \quad \text{at} \quad z = 0, 1. \tag{5.33}$$

5.5 Numerical Solution

Equations (5.30)–(5.33) together with those for the basic state, Eqs. (5.22) and (5.23), were solved using two different methods, namely shooting method using the classical fourth order Runge-Kutta as its basic ODE solver, and a matrix-based method. The former was encoded first but was eventually abandoned because the governing equations become stiff when any of the following parameters are too large: Pe, H, $H\Omega$, k. The methodology performs reliably and very accurately when all of these parameters are too small. One possible route to increasing the reliability of the method is to employ the method of multiple shooting, but this was deemed to be too complicated a scheme to adopt when the latter approach, which is a direct method, performs very reliably indeed over all the parameter ranges considered.

Therefore the equations for both the eigenvalue problem and the basic state were solved

by approximating the derivatives in the above-quoted equations by second order central differences and the resulting algebraic written in matrix/vector form. A uniform grid of points of length, δ, was used where the numerical values of f at $z = z_i = i\delta$ are denoted by f_i. When there are N internal points, then $(N+1)\delta = 1$ and we denote the vector of f-values by $\underline{\mathrm{f}} = (f_1, f_2, \cdots, f_{N-1}, f_N)$. In the following, we shall illustrate the method by taking $N = 4$.

Equation (5.30) becomes,

$$\begin{bmatrix} -\frac{2}{\delta^2} - nk^2 & \frac{1}{\delta^2} & 0 & 0 \\ \frac{1}{\delta^2} & -\frac{2}{\delta^2} - nk^2 & \frac{1}{\delta^2} & 0 \\ 0 & \frac{1}{\delta^2} & -\frac{2}{\delta^2} - nk^2 & \frac{1}{\delta^2} \\ 0 & 0 & \frac{1}{\delta^2} & -\frac{2}{\delta^2} - nk^2 \end{bmatrix} \begin{bmatrix} f_1 \\ f_2 \\ f_3 \\ f_4 \end{bmatrix} = \frac{\mathrm{Ra}\, k}{\mathrm{Pe}^{(n-1)}} \begin{bmatrix} g_1 \\ g_2 \\ g_3 \\ g_4 \end{bmatrix}, \tag{5.34}$$

or, in abbreviated form,

$$\mathbf{M}_1 \underline{\mathrm{f}} = \mathrm{Ra}\, k \underline{\mathrm{g}} / \mathrm{Pe}^{(n-1)} \tag{5.35}$$

where

$$\mathbf{M}_1 = \begin{bmatrix} -\frac{2}{\delta^2} - nk^2 & \frac{1}{\delta^2} & 0 & 0 \\ \frac{1}{\delta^2} & -\frac{2}{\delta^2} - nk^2 & \frac{1}{\delta^2} & 0 \\ 0 & \frac{1}{\delta^2} & -\frac{2}{\delta^2} - nk^2 & \frac{1}{\delta^2} \\ 0 & 0 & \frac{1}{\delta^2} & -\frac{2}{\delta^2} - nk^2 \end{bmatrix}, \quad \underline{\mathrm{f}} = \begin{bmatrix} f_1 \\ f_2 \\ f_3 \\ f_4 \end{bmatrix}, \quad \mathrm{g} = \begin{bmatrix} g_1 \\ g_2 \\ g_3 \\ g_4 \end{bmatrix} \tag{5.36}$$

Equation (5.31) may be written in the form,

$$\mathbf{M}_2 \underline{\mathrm{g}} + H \underline{\mathrm{h}} + k \mathbf{A} \underline{\mathrm{f}} = 0, \tag{5.37}$$

where

$$\mathbf{M}_2 = \begin{bmatrix} -\frac{2}{\delta^2} - k^2 - H & \frac{1}{\delta^2} + \frac{\mathrm{Pe}}{2\delta} & 0 & 0 \\ \frac{1}{\delta^2} - \frac{\mathrm{Pe}}{2\delta} & -\frac{2}{\delta^2} - k^2 - H & \frac{1}{\delta^2} + \frac{\mathrm{Pe}}{2\delta} & 0 \\ 0 & \frac{1}{\delta^2} - \frac{\mathrm{Pe}}{2\delta} & -\frac{2}{\delta^2} - k^2 - H & \frac{1}{\delta^2} + \frac{\mathrm{Pe}}{2\delta} \\ 0 & 0 & \frac{1}{\delta^2} - \frac{\mathrm{Pe}}{2\delta} & -\frac{2}{\delta^2} - k^2 - H \end{bmatrix}, \tag{5.38}$$

and

$$\mathbf{A} = \begin{bmatrix} \frac{1}{2\delta}(T_2 - T_0) & 0 & 0 & 0 \\ 0 & \frac{1}{2\delta}(T_3 - T_1) & 0 & 0 \\ 0 & 0 & \frac{1}{2\delta}(T_4 - T_2) & 0 \\ 0 & 0 & 0 & \frac{1}{2\delta}(T_5 - T_3) \end{bmatrix} \tag{5.39}$$

Finally, the set of disturbance equations are completed by the following replacement of Eq. (5.32),

$$\mathbf{M}_3 \underline{\mathrm{h}} + H\Omega \underline{\mathrm{g}} = 0, \tag{5.40}$$

where

$$\mathbf{M}_3 = \begin{bmatrix} -\frac{2}{\delta^2} - k^2 - H\Omega & \frac{1}{\delta^2} & 0 & 0 \\ \frac{1}{\delta^2} & -\frac{2}{\delta^2} - k^2 - H\Omega & \frac{1}{\delta^2} & 0 \\ 0 & \frac{1}{\delta^2} & -\frac{2}{\delta^2} - k^2 - H\Omega & \frac{1}{\delta^2} \\ 0 & 0 & \frac{1}{\delta^2} & -\frac{2}{\delta^2} - k^2 - H\Omega \end{bmatrix} \tag{5.41}$$

These three discretised equations may be rearranged into the following, which is a matrix eigenvalue problem for $\mathrm{Ra}/\mathrm{Pe}^{(n-1)}$ and is written as a matrix/vector system for $\underline{\mathrm{g}}$:

$$\left[H^2\Omega\, \mathbf{M}_1\mathbf{A}^{-1}\mathbf{M}_3^{-1} - \mathbf{M}_1\mathbf{A}^{-1}\mathbf{M}_2\right] \underline{\mathrm{g}} = (\mathrm{Ra}/\mathrm{Pe}^{(n-1)})\underline{\mathrm{g}}. \tag{5.42}$$

The equations for the basic state temperature profiles may be treated in the same way,

except for the fact that they do not form an eigensystem. Thus we have,

$$\mathbf{M}_4\underline{\mathrm{T}} + H\underline{\phi} = \underline{\mathrm{V}}_1, \tag{5.43}$$

$$\mathbf{M}_5\underline{\phi} + H\Omega\underline{\mathrm{T}} = \underline{\mathrm{V}}_2, \tag{5.44}$$

where,

$$\mathbf{M}_4 = \begin{bmatrix} -\frac{2}{\delta^2} - H & \frac{1}{\delta^2} + \frac{\mathrm{Pe}}{2\delta} & 0 & 0 \\ \frac{1}{\delta^2} - \frac{\mathrm{Pe}}{2\delta} & -\frac{2}{\delta^2} - H & \frac{1}{\delta^2} + \frac{\mathrm{Pe}}{2\delta} & 0 \\ 0 & \frac{1}{\delta^2} - \frac{\mathrm{Pe}}{2\delta} & -\frac{2}{\delta^2} - H & \frac{1}{\delta^2} + \frac{\mathrm{Pe}}{2\delta} \\ 0 & 0 & \frac{1}{\delta^2} - \frac{\mathrm{Pe}}{2\delta} & -\frac{2}{\delta^2} - H \end{bmatrix}, \qquad \underline{\mathrm{V}}_1 = \begin{bmatrix} -\frac{1}{\delta^2} + \frac{\mathrm{Pe}}{2\delta} \\ 0 \\ 0 \\ 0 \end{bmatrix} \tag{5.45}$$

and

$$\mathbf{M}_5 = \begin{bmatrix} -\frac{2}{\delta^2} - H\Omega & \frac{1}{\delta^2} & 0 & 0 \\ \frac{1}{\delta^2} & -\frac{2}{\delta^2} - H\Omega & \frac{1}{\delta^2} & 0 \\ 0 & \frac{1}{\delta^2} & -\frac{2}{\delta^2} - H\Omega & \frac{1}{\delta^2} \\ 0 & 0 & \frac{1}{\delta^2} & -\frac{2}{\delta^2} - H\Omega \end{bmatrix}, \qquad V_2 = \begin{bmatrix} \frac{-1}{\delta^2} \\ 0 \\ 0 \\ 0 \end{bmatrix}. \tag{5.46}$$

The basic temperature distribution, T, for the fluid phase is:

$$\underline{\mathrm{T}} = (\mathbf{M}_5\mathbf{M}_4 - H^2\Omega\mathbf{I})^{-1}(\mathbf{M}_5\underline{\mathrm{V}}_1 - H\underline{\mathrm{V}}_2), \tag{5.47}$$

and, for the solid phase, ϕ is

$$\phi = H^{-1}(\underline{\mathrm{V}}_1 - \mathbf{M}_4\underline{\mathrm{T}}). \tag{5.48}$$

5.6 Results and Discussion

In the present study, linear stability of the vertical throughflow in a horizontal porous layer saturated by a power-law fluid with local thermal non-equilibrium is studied. The critical Rayleigh number is presented for various value of Péclet number Pe, inter-phase heat transfer parameter H, power-law index n, porosity-modified conductivity parameter Ω and wavenumber k. The results are shown in the form of variation of critical Rayleigh number with other parameters. Also, minimising values of Ra_c, $\frac{Ra_c\Omega}{(1+\Omega)}$ and k_c as shown graphically in Figs. 5.3(a)-5.7(c). Here, Péclet number range from 0.1 to 10.

Table (5.1) shows the comparison of the results of Ra of the present paper for fixed values of Pe=1.0, n=0.5, H=100000 and Ω=10000 with the results obtained by Barletta and Storesletten [9] . Also, the comparison of neutral stability critical value of Ra when Pe = 0, n=1.0, H=5402.725, k=12.69114 and Ω=0.001 with the results obtained by Banu and Rees [6] as shown in Table (5.2). It is shown that these two results are in excellent agreement.

Table 5.1: *Comparison of neutral stability values of* Ra *when n=0.5,* Pe*=1.0, H=100000 and* $\Omega = 10000$.

k	Barletta and Storesletten [9]	Present
4.0	29.803019	29.805084
6.0	36.205476	36.208314

Table 5.2: *Comparison of neutral stability values of* Ra *when* Pe*=0, n=1.0, H=5402.725, k=12.69114 and* $\Omega = 0.001$.

Banu and Rees [6]	Present
5739.522	5739.5152

Basic State Solutions

Figures 5.2(a)-5.2(e) represents the basic temperature profiles T against the z for inter phase heat transfer (H). From Figs. 5.2(a)-5.2(e) it is seen from these that, an enhancement in the inter phase heat transfer parameter (H) tends to reduce the thermal boundary layer

for the fluid phase, but no variation in solid phase. The basic temperature profile is more pronounced for small value of inter phase heat transfer parameter (H).

The Neutral stability curves

Figures 5.3(a)-5.3(f) shows that the neutral stability curves on the parametric plane Ra. In the cases considered, the Péclet number (Pe) ranges from 0.1 to 2 and the power-law index (n) from 0.5 to 2. The neutral stability curve, in each case, confines the region of linear stability laying below the curve from the region of instability above the curve. The neutral stability curve is affected by both parameters Péclet number and power-law index. The effect of an increasing n for a given power-law index is different for either smaller or larger values of Pe. As shown in Figs. 5.3(a)-5.3(f), when Péclet number 0.1 and 0.2, an increasing value of n has a destabilising effect.

This behaviour changes gradually when Péclet number is 0.5 and 0.7, as the transition to instability depends non-monotonically on n. For larger Péclet numbers, such as Pe=1 and 2, the effect of an increasing n is stabilising effect. Thus, pseudo-plastic fluids are more stable than dilatant fluids when Péclet number is small, while they become more unstable if Péclet number is larger. This behaviour is partly a consequence of the scaling with Pe^{n-1} of the Rayleigh number (Ra). However, this is just a rough aspect of the actual trend, due to the sensible dependence of $\frac{Ra}{Pe^{n-1}}$ on n at neutral stability. Those things are more complicated than the law $\frac{\mathrm{Ra}}{Pe^{n-1}}$ is made clear by the frame with Pe=1 in Figs. 5.3(a)-5.3(f), where Ra displays an evident change with n.

Figures 5.4(a)-5.4(c) display the neutral stability curves of Ra against k, for varying values of H, Ω and n. It is evident from these Figs. 5.4(a)-5.4(c) that, an increase in the H leads to increase in the Ra for pseudo-plastic, Newtonian and dilatant fluids. The reason for this is that the apparent viscosity of the pseudo-plastic fluid is infinite as shear rate tends to zero (i.e., for small Ω) while it becomes zero for dilatant fluid at low shear rate. The inhibition of convective instability for pseudo-plastic fluid is represented by the large values of Ra while an exhibition of clear instability for dilatant fluid is represented by the vanishing

values of Ra for fixed values of other parameters.

The values of Ra can be minimized with respect to k and although the condition $\frac{\partial Ra}{\partial k}$ may be written down, it appears to be impossible to obtain a straightforward closed-form explicit expression for the minimising value of k. Therefore, we used Newton-Raphson iteration scheme to obtain the minimum values of Ra and k as function of H and Ω. In Figs. 5.5(a)-5.7(c) display the minimising values of Ra_c and $\frac{Ra_c\Omega}{(1+\Omega)}$ and k_c.

The variation of the Ra_c with H for a range of values of Ω, as displayed in Fig.5.5(a)-5.5(c). At small values of H that Ra_c is close to $4\pi^2$ and is independent of Ω to leading order. The physical reason for this is that there is almost no transfer of heat between the phases and therefore the onset criterion is not affected by the properties of the solid phase. But at large values of H, the LTE limit, the onset criterion is based on the mean properties of the medium and therefore the onset criterion in terms of Ra_c is dependent on Ω.

In figs. 5.6(a)-5.6(c), we show the variation of critical Rayleigh number based on the mean properties of medium $\left(\frac{Ra_c\Omega}{(1+\Omega)}\right)$, the Ra_c which is defined in terms of the mean properties of the fluid with the H for specific values of Ω. It is interesting to note that $\frac{Ra_c\Omega}{(1+\Omega)}$ approaches a common limit of $4\pi^2$ as $H \to \infty$, although the approach to that limit depends quite strongly on the value of Ω. We also find that $\frac{Ra_c\Omega}{(1+\Omega)}$ vary monotonically as H increases. It is interesting to note that, for very small H, and large Ω, the convection can be completely suppressed. The Ra_c based on the mean properties is independent of H for large Ω. In all cases both Ra_c and $\frac{Ra_c\Omega}{(1+\Omega)}$ vary monotonically as H increases with Ω fixed.

In Figs. 5.7(a)-5.7(c) we display k_c with H for different values of the Ω. We observed that the k_c approaches a common limit for small n as $H \to 0$ and as $H \to \infty$. However for large n, k_c approaches two different limits, one as $H \to 0$ and another as $H \to \infty$. As $H \to 0$ the solid phase ceases to affect the thermal field of the fluid which is free to act independently, whereas $H \to \infty$ the solid and fluid phases may be treated as a single phase as they have nearly identical temperatures. Therefore in these two limiting cases, the Ω has little effect on the k_c. For the intermediate values of H, the k_c increases with decreasing values of Ω and that the k_c is always greater than the LTE case.

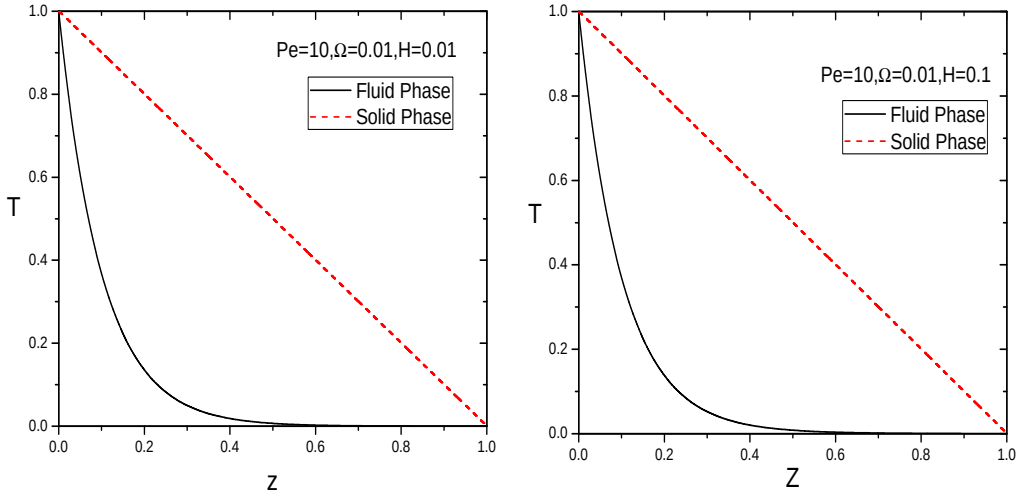

(a)

(b)

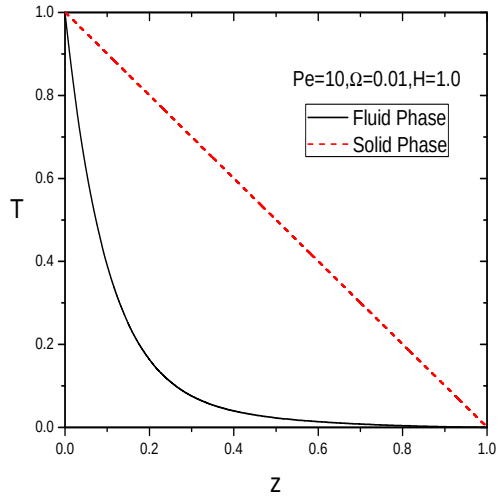

(c)

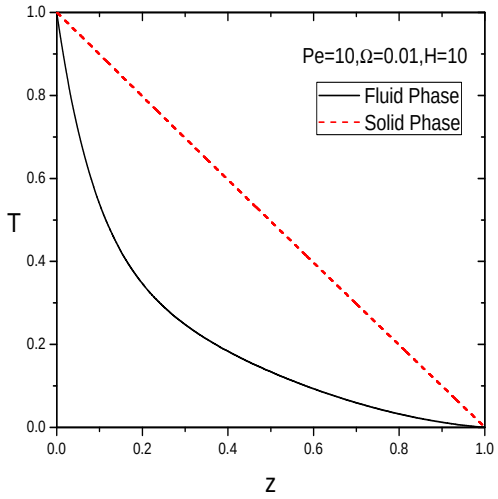

(d)

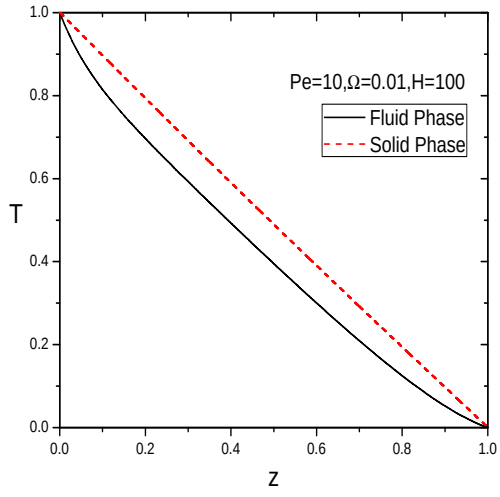

(e)

Figure 5.2: Basic state solutions of T with different values of H.

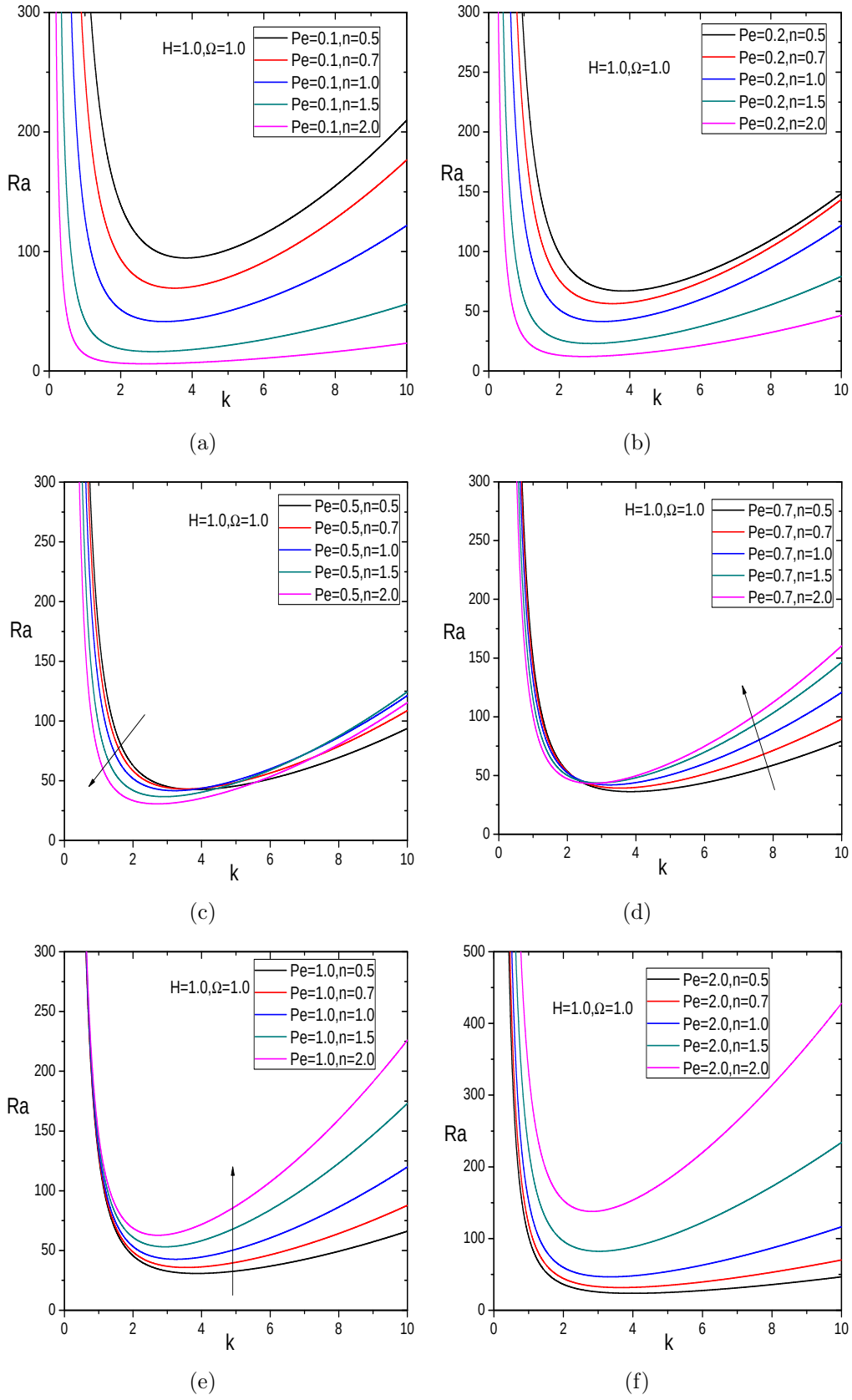

Figure 5.3: Neutral stability curves in the Plane Ra with different values of Pe and n

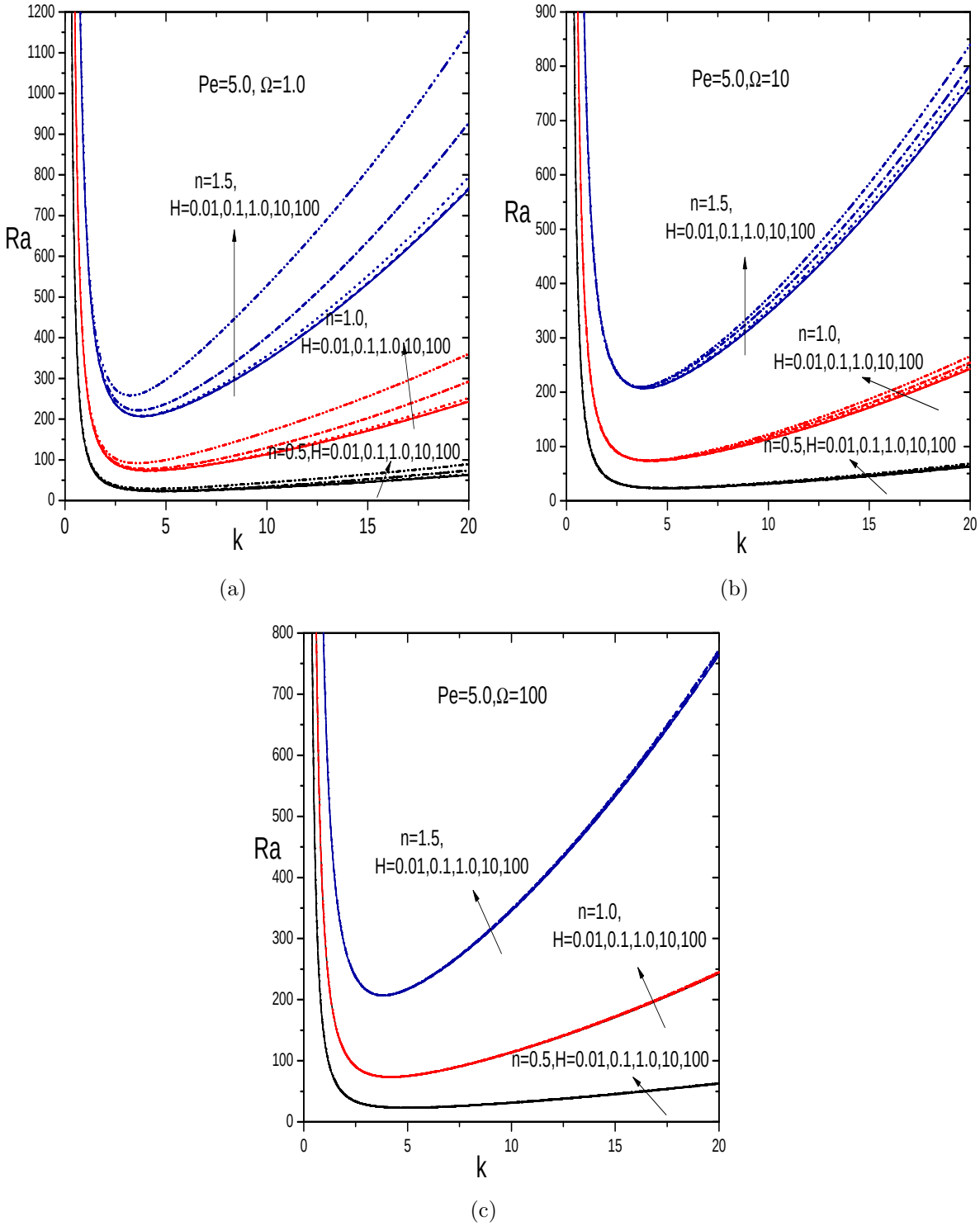

Figure 5.4: Variation of Ra with k for specific values of Ω, H and n

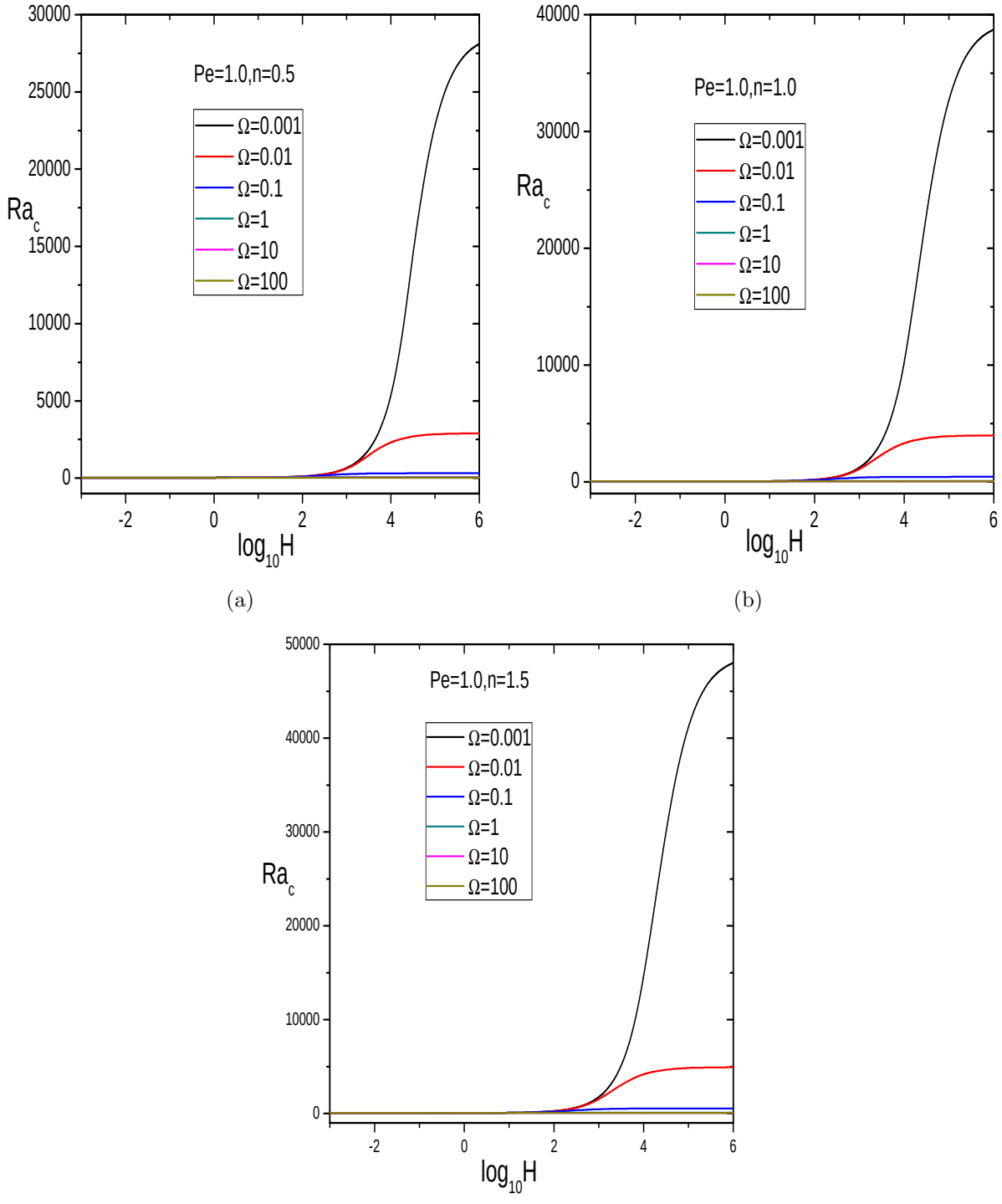

Figure 5.5: Variation of Ra_c with $log_{10}H$ for specific values of Ω and n

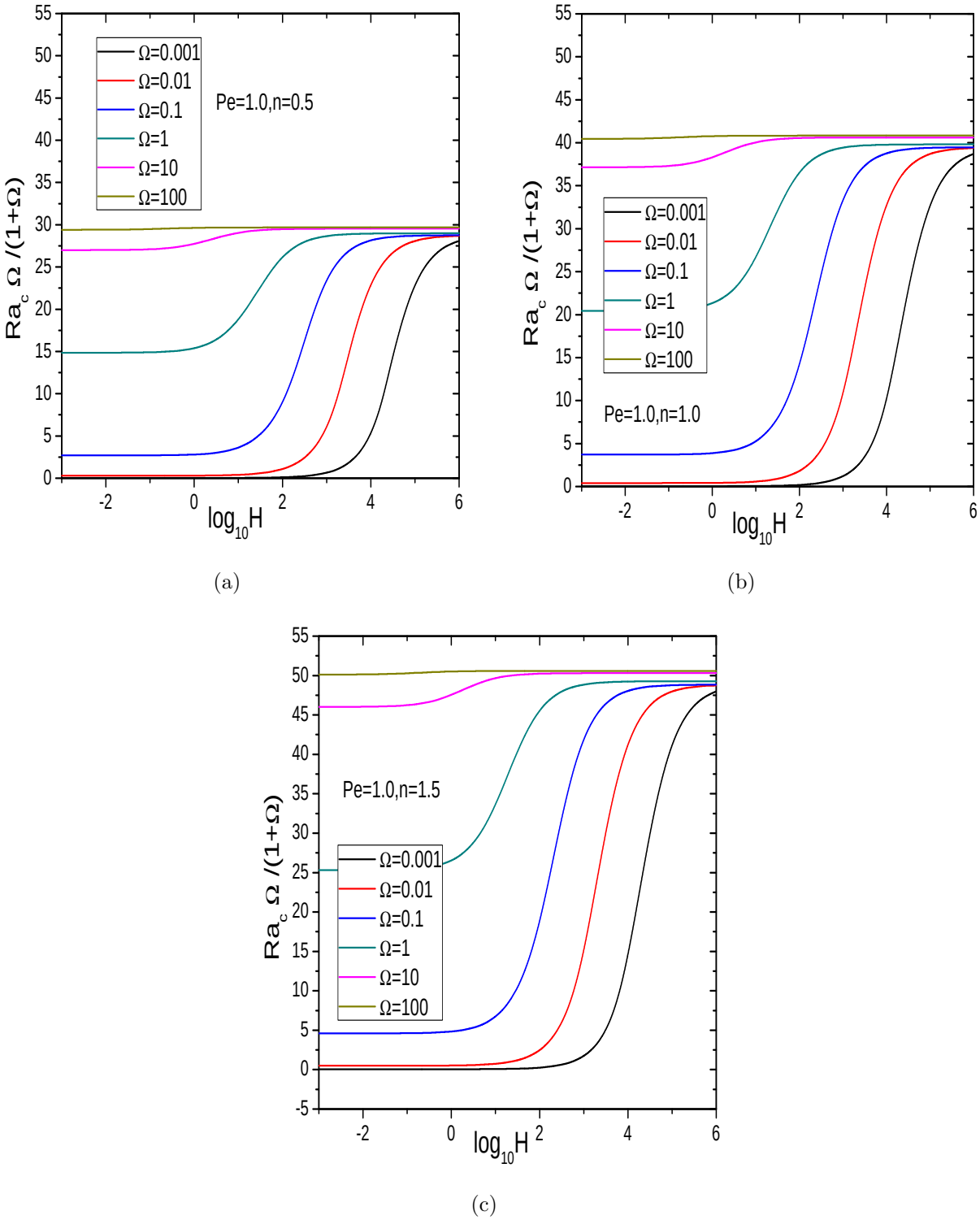

Figure 5.6: Variation of $(\frac{Ra_c\Omega}{(1+\Omega)})$ with $log_{10}H$ for specific values of Ω and n

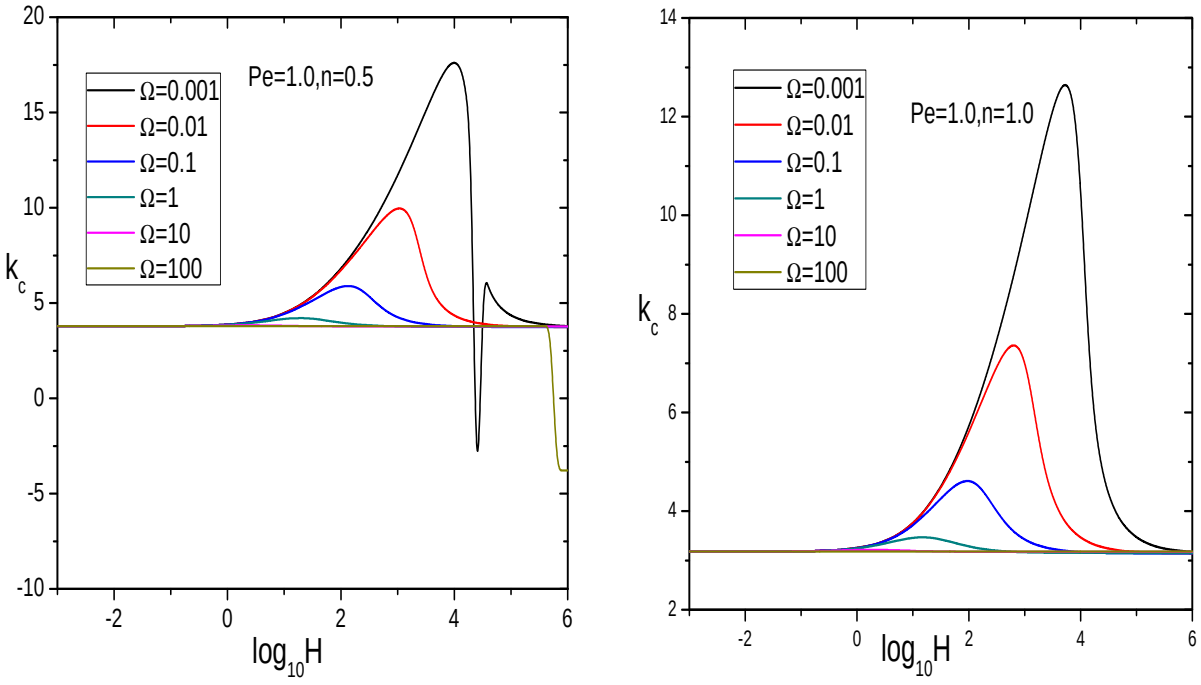

(a)

(b)

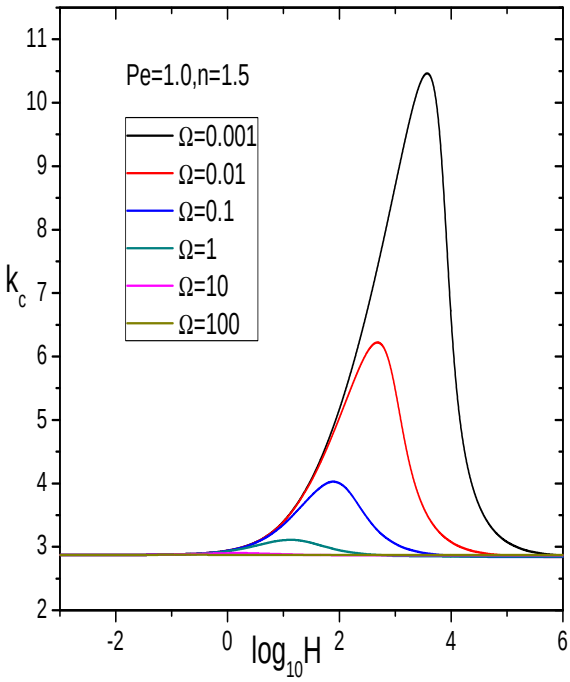

(c)

Figure 5.7: Variation of k_c with $log_{10}H$ for specific values of Ω and n

5.7 Conclusions

This chapter investigates the instability of vertical throughflow in a horizontal porous layer saturated by a power-law fluid with local non-thermal equilibrium. The lower and upper boundary planes are considered as permeable and kept at constant temperatures. Besides the Rayleigh number Ra, there are four governing dimensionless parameters in this problem, Pe, H, Ω and n. The latter parameter is proportional to the prescribed vertical throughflow velocity. The linear stability eigenvalue problem has been solved by employing a numerical solution based on the matrix based-method. From this analysis, the following conclusions can be drawn below.

- The neutral stability curve is affected by both n and Pe, while it is unaffected by the sign of Pe. The effect of an increasing n for a given Pe is different for either smaller or larger values of Pe. Generally speaking, pseudo-plastic fluids $n < 1$ are more stable than dilatant fluids $n > 1$ when Pe is small, while they become more unstable if Pe is large.

- The effect of increasing Ω is to decrease the Ra_c and hence the effect of increasing Ω is to destabilize the system. The effect is more pronounced for very small Ω. The critical Rayleigh number is independent of Ω for very small H while for large H,it decreases with increasing Ω

- It is found that the critical Rayleigh number based on the mean properties of the medium vary monotonically with H and approaches a common limit as $H \to \infty$. It is also observed that the critical wave number k_c approaches a common limit as $H \to 0$ and $H \to \infty$.

Part III

SIMILARITY SOLUTION FOR A POWER-LAW FLUID FLOW ALONG A VERTICAL PLATE IN A NON-DARCY POROUS MEDIUM.

Chapter 6

Effect of Double Dispersion, MHD and Variable Properties on Mixed Convection in a Power-law Fluid Saturated Non-Darcy Porous Medium

[1]

6.1 Introduction

The Darcy-Forchheimer model is a supplement of classical Darcian formulation obtained by adding a squared term of velocity in the momentum equation to account for the inertial effects. Modeling and analysis of a power-law fluid saturated porous medium has been an active field of research from the past few years, and it has a large number of industrial and engineering applications. Due to this importance, many of the researchers have been reported their studies on the convective transport in a power-law fluid saturated non-Darcy

[1]Published in "**Special Topics & Reviews in Porous Media-An International Journal**" 8(3), 177-195 (2017)

porous medium (see Khidir *et al.* [48], Prasad *et al.* [76], Chamkha *et al.* [16] and Mansour and El-Shaer [58]).

Magneto-hydrodynamics (MHD) flows through porous media saturated with Newtonian or non-Newtonian fluids have been analyzed by several researchers due to its significance in the different fields (see Chen [19], Kumar and Sivaraj [49], Benazir and Sivaraj [12], Zubair *et al.* [111]). The study of magneto-hydrodynamic flow, for fluid past a heated surface, has important applications in numerous engineering problems such as petroleum industries, cooling of nuclear reactors, MHD power generators, boundary layer control in aerodynamics, plasma studies, and crystal growth. Eldabe *et al.* [27] studied the influence of viscous dissipation on free convective heat and mass transfer of MHD non-Newtonian fluid flow through a porous medium. Uddin *et al.* [102] obtained the similarity representation of the problem on power-law fluid from stretching sheet with slip and MHD effects by applying lie scaling group transformations.

This chapter is an extension of second chapter by taking Darcy-Forchheimer model and MHD into account. The main objective of the present chapter is to study the influence of MHD, double dispersion and variable properties in power-law fluid saturated non-Darcy porous medium. The governing similarity equations are obtained by using the method of Lie scaling group transformations. Then, these similarity equations are solved numerically by applying Shooting technique. The effects of various parameters on the velocity, temperature and concentration profiles are presented graphically. Also, the physical quantities of the flow, heat and mass transfer rates are presented in tabular form.

6.2 Mathematical Formulation

Consider the two dimensional, laminar, steady and incompressible flow of mixed convective in a power-law fluid saturated non-Darcy porous medium. A uniform magnetic field is applied normal to the plate, as shown in Fig. (6.1). The magnetic Reynolds number is assumed to be small, so that the induced magnetic field can be neglected. The fluid and the porous

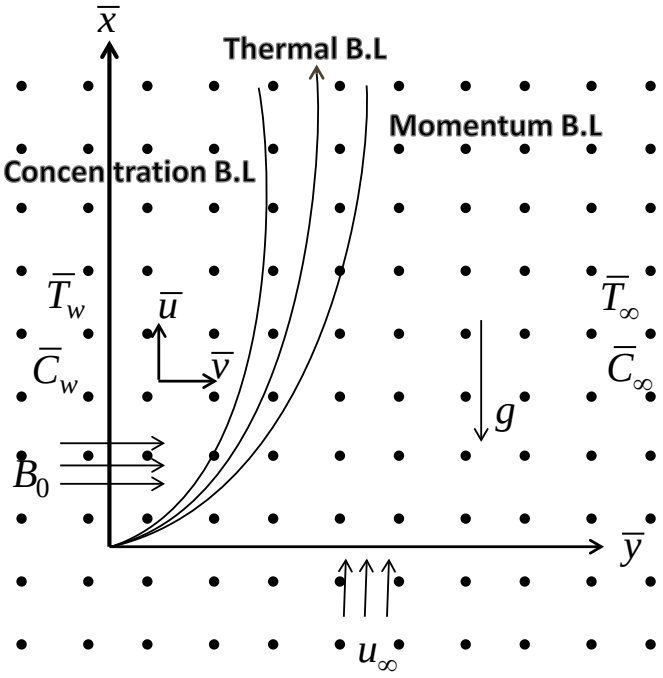

Figure 6.1: Physical geometry of the problem

structure are everywhere in local thermodynamic equilibrium and porous medium is assumed to be transparent. The fluid flow is moderate, so the pressure drop is proportional to the linear combination of fluid velocity and the square of the velocity (Forchhiemer flow model is considered). Choose the cartesian coordinate system such as $\overline{x}$-axis is taken along the vertical surface and $\overline{y}$-axis is normal to the surface. The gravitational acceleration g is in a direction opposite to the $\overline{x}$-direction. The surface is maintained at the uniform temperature and concentrations $\overline{T}_w$ and $\overline{C}_w$, respectively. These values are considered to be greater than the ambient temperature and concentrations $\overline{T}_\infty$ and $\overline{C}_\infty$, respectively.

Applying the boundary layer assumptions and Boussinesq approximations, the governing partial differential equations, such as continuity, momentum, energy and concentration equations are given by

$$\frac{\partial \overline{u}}{\partial \overline{x}} + \frac{\partial \overline{v}}{\partial \overline{y}} = 0 \tag{6.1}$$

$$n\overline{u}^{n-1}\frac{\partial \overline{u}}{\partial \overline{y}}+\frac{\partial}{\partial \overline{y}}\left[\frac{C_F\rho_\infty\sqrt{K}}{\mu}\overline{u}^2\right]=\frac{\partial}{\partial \overline{y}}\left[\frac{Kg\rho_\infty}{\mu}(\beta_T^*[\overline{T}-\overline{T}_\infty]+\beta_C^*[\overline{C}-\overline{C}_\infty])\right]-\frac{\partial}{\partial \overline{y}}\left[\frac{\sigma {B_0}^2 K {\mu_e}^2}{\mu}\overline{u}\right] \tag{6.2}$$

$$\overline{u}\frac{\partial \overline{T}}{\partial \overline{x}}+\overline{v}\frac{\partial \overline{T}}{\partial \overline{y}}=\frac{\partial}{\partial \overline{y}}\left[(\alpha+\gamma d^*\,\overline{u})\frac{\partial \overline{T}}{\partial \overline{y}}\right] \tag{6.3}$$

$$\overline{u}\frac{\partial \overline{C}}{\partial \overline{x}}+\overline{v}\frac{\partial \overline{C}}{\partial y}=\frac{\partial}{\partial \overline{y}}\left[(D+\zeta d^*\,\overline{u})\frac{\partial \overline{C}}{\partial \overline{y}}\right] \tag{6.4}$$

where $\overline{x}$ and $\overline{y}$ are the cartesian coordinates, $\overline{u}$ and $\overline{v}$ are the velocity components in $\overline{x}$ and $\overline{y}$ directions, respectively. Further, $\overline{T}$ is the temperature, $\overline{C}$ is the concentration, g is the acceleration due to gravity, ρ_∞ is the reference density, K is the permeability, μ_e is the magnetic permeability and B_0 represents the magnetic field and σ_∞ represents the electrical conductivity of the fluid, d^* represents the pore diameter, γ and ζ are the coefficients of the thermal and solutal dispersions, β_T^* and β_C^* are the thermal and concentration expansion coefficients, respectively. The boundary conditions are

$$\left.\begin{aligned}&\overline{v}=0,\ \ \overline{T}=\overline{T}_w,\ \ \overline{C}=\overline{C}_w \quad \text{at} \quad \overline{y}=0\\&\overline{u}=u_\infty,\ \ \overline{T}=\overline{T}_\infty,\ \ \overline{C}=\overline{C}_\infty \quad \text{as} \quad \overline{y}\to\infty\end{aligned}\right\} \tag{6.5}$$

The dimensionless variables are defined as follows:

$$\left.\begin{aligned}&x=\frac{\overline{x}}{\mathrm{L}},\quad y=\frac{\overline{y}}{\mathrm{L}}\mathrm{Pe}^{\frac{1}{2}},\quad u=\frac{\overline{u}\mathrm{L}}{\alpha_0\mathrm{Pe}},\quad u=\frac{\overline{v}\mathrm{L}}{\alpha_0\mathrm{Pe}^{\frac{1}{2}}}\\&\theta(\eta)=\frac{\overline{T}-\overline{T}_\infty}{\overline{T}_w-\overline{T}_\infty},\quad \phi(\eta)=\frac{\overline{C}-\overline{C}_\infty}{\overline{C}_w-\overline{C}_\infty}\end{aligned}\right\} \tag{6.6}$$

where $\mathrm{Pe}=\dfrac{u_\infty \mathrm{L}}{\alpha_0}$ represents the Péclet number and L represents the characteristic length. In view of the continuity Eq.(6.1), we introduce a stream function $\psi(x,y)$ as

$$u=\frac{\partial \psi}{\partial y},\qquad v=-\frac{\partial \psi}{\partial x} \tag{6.7}$$

Using the Eqs.(6.6)–(6.7) into equations (6.2)-(6.4) reduces the following dimensionless mo-

mentum, energy and concentration equations are obtained as follows.

$$n\left(\frac{\partial\psi}{\partial y}\right)^{n-1}\frac{\partial^2\psi}{\partial y^2}+2\mathrm{G}\left(\frac{\partial\psi}{\partial y}\right)\frac{\partial^2\psi}{\partial y^2}\left(\frac{\theta_e-\theta}{\theta_e}\right)-\frac{\mathrm{G}}{\theta_e}\left(\frac{\partial\psi}{\partial y}\right)^2\frac{\partial\theta}{\partial y}+\mathrm{M}\left(\frac{\partial^2\psi}{\partial y^2}\right)\left(\frac{\theta_e-\theta}{\theta_e}\right) \tag{6.8}$$
$$-\frac{\mathrm{M}}{\theta_e}\left(\frac{\partial\psi}{\partial y}\right)\left(\frac{\partial\theta}{\partial Y}\right)-\lambda^n\left(\frac{\partial\theta}{\partial y}+\mathrm{B}\frac{\partial\phi}{\partial y}\right)\left(\frac{\theta_e-\theta}{\theta_e}\right)+\frac{\lambda^n}{\theta_e}\left(\theta+\mathrm{B}\phi\right)\left(\frac{\partial\theta}{\partial y}\right)=0$$

$$\frac{\partial\psi}{\partial y}\frac{\partial\theta}{\partial x}-\frac{\partial\psi}{\partial x}\frac{\partial\theta}{\partial y}-\beta\left(\frac{\partial\theta}{\partial y}\right)^2-(1+\beta\theta)\frac{\partial^2\theta}{\partial y^2}-Pe_\gamma\left[\frac{\partial\psi}{\partial y}\frac{\partial^2\theta}{\partial y^2}+\frac{\partial^2\psi}{\partial y^2}\frac{\partial\theta}{\partial y}\right]=0 \tag{6.9}$$

$$\frac{\partial\psi}{\partial y}\frac{\partial\phi}{\partial x}-\frac{\partial\psi}{\partial x}\frac{\partial\phi}{\partial y}-\frac{1}{\mathrm{Le}}\frac{\partial^2\phi}{\partial y^2}-Pe_\zeta\left[\frac{\partial\psi}{\partial y}\frac{\partial^2\phi}{\partial y^2}+\frac{\partial^2\psi}{\partial y^2}\frac{\partial\phi}{\partial y}\right]=0 \tag{6.10}$$

The boundary conditions (6.5) transform into the following form

$$\left.\begin{aligned}&\frac{\partial\psi}{\partial x}=0,\quad\theta=1,\quad\phi=1\quad\text{at}\quad y=0\\&\frac{\partial\psi}{\partial y}=1,\quad\theta=0,\quad\phi=0\quad\text{as}\quad y\to\infty\end{aligned}\right\} \tag{6.11}$$

In usual definition $\mathrm{M}=\dfrac{\sigma {B_0}^2{\mu_e}^2K}{\mu_\infty}\left(\dfrac{\mathrm{L}}{\alpha_0}\right)^{(n-1)}\mathrm{Pe}^{-(n-1)}$ represents the magnetic field parameter, $\theta_e=\dfrac{\overline{T}_e-\overline{T}_\infty}{\overline{T}_w-\overline{T}_\infty}$ is the variable viscosity, $\mathrm{G}=\dfrac{C_F\sqrt{K}}{\nu_\infty}\left(\dfrac{\mathrm{L}}{\alpha_0}\right)^{(n-2)}\mathrm{Pe}^{-(n-2)}$ indicates modified non-Darcy parameter, $\mathrm{B}=\dfrac{\beta_c^*(\overline{C}_w-\overline{C}_\infty)}{\beta_T^*(\overline{T}_w-\overline{T}_\infty)}$ is the buoyancy ratio, $\lambda=\dfrac{\mathrm{Ra}}{\mathrm{Pe}}$ is the mixed convection parameter, $\mathrm{Ra}=\dfrac{\mathrm{L}}{\alpha_0}\left(\dfrac{gK\beta_T(\overline{T}_w-\overline{T}_\infty)}{\nu}\right)^{1/n}$ is the generalized Rayleigh number, $\mathrm{Le}=\dfrac{\alpha_0}{D}$ is the Lewis number, $Pe_\gamma=\dfrac{\gamma u_\infty d^*}{\alpha_0}$ is the thermal dispersion and $Pe_\zeta=\dfrac{\zeta u_\infty d^*}{\alpha_0}$ is the solutal dispersion.

Similarity equations via Lie group transformations

Using Lie scaling group transformations and procedure explained in the second chapter, the following similarity transformations are obtained:

$$\psi=x^{\frac{1}{2}}f(\eta),\quad\eta=yx^{-\frac{1}{2}},\quad\theta=\theta(\eta),\quad\phi=\phi(\eta). \tag{6.12}$$

Using Eq. (6.12) into Eqs.(6.8)-(6.10), we obtain the following similarity equations.

$$f''\left[n(f')^{n-1}+2\mathrm{G}f'\left(\frac{\theta_e-\theta}{\theta_e}\right)+\mathrm{M}\left(\frac{\theta_e-\theta}{\theta_e}\right)\right]=\frac{f'\theta'}{\theta_e}\left(\mathrm{G}f'+\mathrm{M}\right) \\ +\lambda^n\left(\theta'+\mathrm{B}\phi'\right)\left(\frac{\theta_e-\theta}{\theta_e}\right)-\lambda^n\left(\theta+\mathrm{B}\phi\right)\frac{\theta'}{\theta_e} \tag{6.13}$$

$$\beta(\theta')^2+(1+\beta\theta)\,\theta''+Pe_\gamma\left(f'\theta''+f''\theta'\right)+\frac{1}{2}f\theta'=0 \tag{6.14}$$

$$\frac{1}{\mathrm{Le}}\phi''+Pe_\zeta\left(f'\phi''+f''\phi'\right)+\frac{1}{2}f\phi'=0 \tag{6.15}$$

The boundary conditions (6.11) in terms of f',θ and ϕ become

$$f(0)=0,\quad \theta(0)=1,\quad \phi(0)=1 \tag{6.16a}$$

$$f'(\infty)=1,\quad \theta(\infty)=0,\quad \phi(\infty)=0. \tag{6.16b}$$

The physical quantities of present interest obtained by the local Nusselt and Sherwood number, which are given as follows

$$\frac{Nu_{\overline{x}}}{\mathrm{Pe}_{\overline{x}}^{1/2}}=-\left[1+Pe_\gamma f'(0)\right]\theta'(0)\quad\text{and}\quad\frac{Sh_{\overline{x}}}{\mathrm{Pe}_{\overline{x}}^{1/2}}=-\left[1+Pe_\zeta f'(0)\right]\phi'(0) \tag{6.17}$$

6.3 Results and Discussion

The system of nonlinear ordinary differential Eqs. (6.13)-(6.15) along with the corresponding boundary conditions (6.16) are solved using the shooting method, which is explained clearly in chapter-2. To validate the code, the current results are correlated with previously available results in the literature. The Eqs. (6.13)-(6.15) coincide with equations presented by Chaoyang [18], by excluding concentration equation with $\mathrm{B}=\mathrm{M}=Pe_\gamma=Pe_\zeta=\beta=0$, $\mathrm{Le}=1.0$ and $\theta_e\to\infty$. The comparison in the above case seems to be good and the results are accurate, as presented in Tab. (2.1).

Figures 6.2-6.7 represent the variation of non-dimensional velocity $f'(\eta)$, temperature $\theta(\eta)$, and concentration $\phi(\eta)$ profiles with the influence of variable viscosity (θ_e), variable

thermal conductivity (β), magnetic field parameter (M), thermal dispersion (Pe_γ), solutal dispersion (Pe_ζ) and non-Darcy parameter (G) for three values of power-law index (n).

The effect of variable viscosity (θ_e) and power-law index (n) on non-dimensional velocity $f(\eta)$, temperature $\theta(\eta)$ and concentration $\phi(\eta)$ is portrayed in Figs.6.2(a)-6.2(c). Figure 6.2(a) depicts that the momentum boundary layer reduces with the rise of variable viscosity parameter for pseudo-plastic, Newtonian and dilatant fluids. Figure 6.2(b) illustrates that an increase in variable viscosity parameter increases the thermal boundary layer thickness for all three kinds of fluids. The effect of variable viscosity on the concentration profile for different types of power-law fluids is depicted in Fig. 6.2(c). From this figure, it is seen that the concentration increases with increase in variable viscosity for all three values of n.

Figures 6.3(a)-6.3(c) explore the influence of the variable thermal conductivity (β) and power-law index (n) on the non-dimensional velocity $f'(\eta)$, temperature $\theta(\eta)$ and concentration $\phi(\eta)$ profiles, respectively. Figures 6.3(a)-6.3(b) depict that the velocity and the temperature increase with increasing the thermal conductivity for pseudo-plastic, Newtonian and dilatant fluids. This is due to the enhancement of thermal boundary layer thickness as a result of the enhancement of the thermal conductivity parameter. Figure 6.3(c) presents the effect of β and n on the concentration profile. It is observed that the concentration increases with decrease in the value of the variable thermal conductivity for all three kinds of fluids. So, it is evident that molecular motion of the fluid decreases at a slower rate for larger values of thermal conductivity parameters.

Figures 6.4(a)-6.4(c) illustrate the effect of thermal dispersion and power-law index (n) on non-dimensional velocity $f'(\eta)$, temperature $\theta(\eta)$ and concentration $\phi(\eta)$ distributions, respectively. Figure 6.4(a) describes the influence of thermal dispersion and power-law index (n) on the velocity profile. It is observed that the velocity profile increases with increasing values of thermal dispersion for pseudo-plastic, Newtonian and dilatant fluids. Figure 6.4(b) reveals that the temperature monotonically rises with enhancement in the value of thermal dispersion for all three kinds of fluids. Moreover, from Fig. 6.4(c), it is noticed that the concentration decreases as the thermal dispersion parameter increases, for all three types of fluids.

The influence of solutal dispersion parameter and power-law index on non-dimensional velocity $f'(\eta)$, temperature $\theta(\eta)$ and concentration $\phi(\eta)$ profiles is depicted in Figs. 6.5(a)-6.5(c). Figure 6.5(a) illustrates the effect of solutal dispersion on the velocity field. It can be observed that the increase in the solutal dispersion leads to enhance the velocity profile for pseudo-plastic, Newtonian and dilatant fluids. The effect of solutal dispersion on temperature for different power-law fluids is shown in Fig. 6.5(b). The thermal boundary layer thickness diminishes with an enhancement of the solutal dispersion for all three different fluids. Figure 6.5(c) describes the enhancement of concentration boundary layer with an increase in the value of solutal dispersion parameter for all three fluids.

Figures 6.6(a)-6.6(c) display the result of magnetic parameter (M) and power-law indices (see pseudo-plastic, dilatant and Newtonian fluid) on dimensionless velocity $f'(\eta)$, temperature $\theta(\eta)$, and concentration $\phi(\eta)$ profiles, respectively. It can be perceived from Fig. 6.6(a) that as M increases, the velocity profile decreases for pseudo-plastic and Newtonian fluid, but increases near the plate and reduces far away from the plate for dilatant fluid. Figure 6.6(b) demonstrates that a rise in M substantially increases the temperature profiles for $n < 1$ and $n = 1.0$ but there is a slight decrease for the index $n > 1$. This behavior in the fluid is because of the presence of a transverse magnetic field that has a tendency to make the Lorentz drag which resists the flow. Due to increase in the magnetic parameter, the non-dimensional concentration increases for pseudo-plastic and Newtonian fluid but slightly depreciates for dilatant fluids, as shown Fig. 6.6(c).

The variation of dimensionless velocity $f'(\eta)$, temperature $\theta(\eta)$ and concentration $\phi(\eta)$ distribution for various values of non-Darcy parameter (G) and power-law index [see $(n < 1, n = 1, n > 1)$] are plotted in Figures 6.7(a)-6.7(c). From Fig. 6.7(a) reveals that the velocity reduces as G increases for all kinds of fluids. Since (G) demonstrates inertial drag, thus an increase in the Forchheimer number increments the imperviousness to the flow and reduces the fluid velocity to develop. Figure 6.7(b) exhibits that the temperature increases with an increase in G for all kinds of fluids. Figure 6.7(c) explores that concentration increases with an increase in non-Darcy parameter G for all three kinds of fluids. The increase in G decreases the intensity of the flow and raises the temperature and concentration

Table 6.1: *The heat and mass transfer coefficients for varying values of power-law index, variable viscosity, thermal conductivity, thermal and solutal dispersion, magnetic field and non-Darcy porous medium parameters.*

n	θ_e	β	Pe_γ	Pe_ζ	G	M	$-[1+Pe_\gamma f'(0)]\,\theta'(0)$	$-[1+Pe_\zeta f'(0)]\,\phi'(0)$
0.6	2.0	0.5	0.5	0.5	0.1	1.0	0.433746	0.500456
1.0	2.0	0.5	0.5	0.5	0.1	1.0	0.427097	0.498653
1.5	2.0	0.5	0.5	0.5	0.1	1.0	0.419431	0.494501
0.6	1.5	0.5	0.5	0.5	0.1	1.0	0.435564	0.500356
0.6	2.5	0.5	0.5	0.5	0.1	1.0	0.432135	0.499538
0.6	3.0	0.5	0.5	0.5	0.1	1.0	0.430972	0.498719
0.6	2.0	0.0	0.5	0.5	0.1	1.0	0.495944	0.495944
0.6	2.0	1.0	0.5	0.5	0.1	1.0	0.389290	0.504245
0.6	2.0	1.5	0.5	0.5	0.1	1.0	0.355630	0.507475
0.6	2.0	0.5	0.0	0.5	0.1	1.0	0.596362	0.486367
0.6	2.0	0.5	1.0	0.5	0.1	1.0	0.354689	0.508685
0.6	2.0	0.5	1.5	0.5	0.1	1.0	0.306122	0.514225
0.6	2.0	0.5	0.5	0.0	0.1	1.0	0.424461	0.790510
0.6	2.0	0.5	0.5	1.0	0.1	1.0	0.438843	0.388123
0.6	2.0	0.5	0.5	1.5	0.1	1.0	0.442182	0.325106
0.6	2.0	0.5	0.5	1.0	0.0	1.0	0.438136	0.503041
0.6	2.0	0.5	0.5	1.0	0.2	1.0	0.430195	0.498079
0.6	2.0	0.5	0.5	1.0	0.3	1.0	0.427276	0.496004
0.6	2.0	0.5	0.5	1.0	0.1	0.0	0.461055	0.528752
0.6	2.0	0.5	0.5	1.0	0.1	0.5	0.443134	0.510141
0.6	2.0	0.5	0.5	1.0	0.1	1.5	0.427971	0.494524

boundary layer thickness.

Table 6.1 shows the effect of various parameters on the local heat and the local mass transfer coefficient for different physical parameters. It is clear that enhancement in n and θ_e reduces the Nusselt number and Sherwood numbers. It is noticed that an increase in β and Pe_γ depreciates the Nusselt number, but increases the Sherwood number. Higher values of Pe_ζ raise the Nusselt number, but reduce the Sherwood numbers. The influence of G and M results in a decrease of both Nusselt and Sherwood numbers.

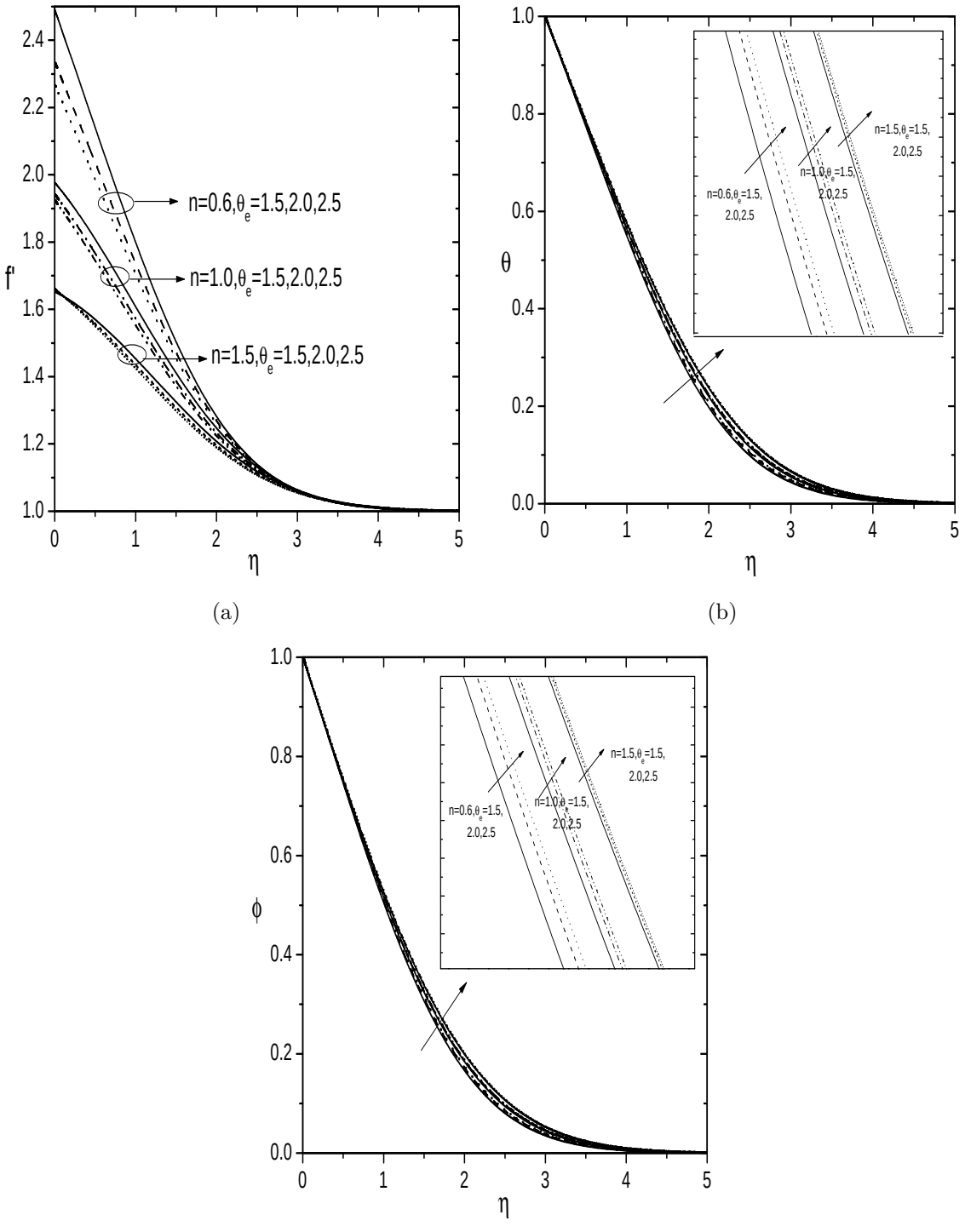

Figure 6.2: Effect of θ_e and n on (a)velocity profile (b)temperature profile and (c)concentration profile for B = 1.0, Le = 1.0, Pe_γ=0.5, Pe_ζ=0.5, β = 0.5, M = 1.0, G = 0.1 and λ = 1.0.

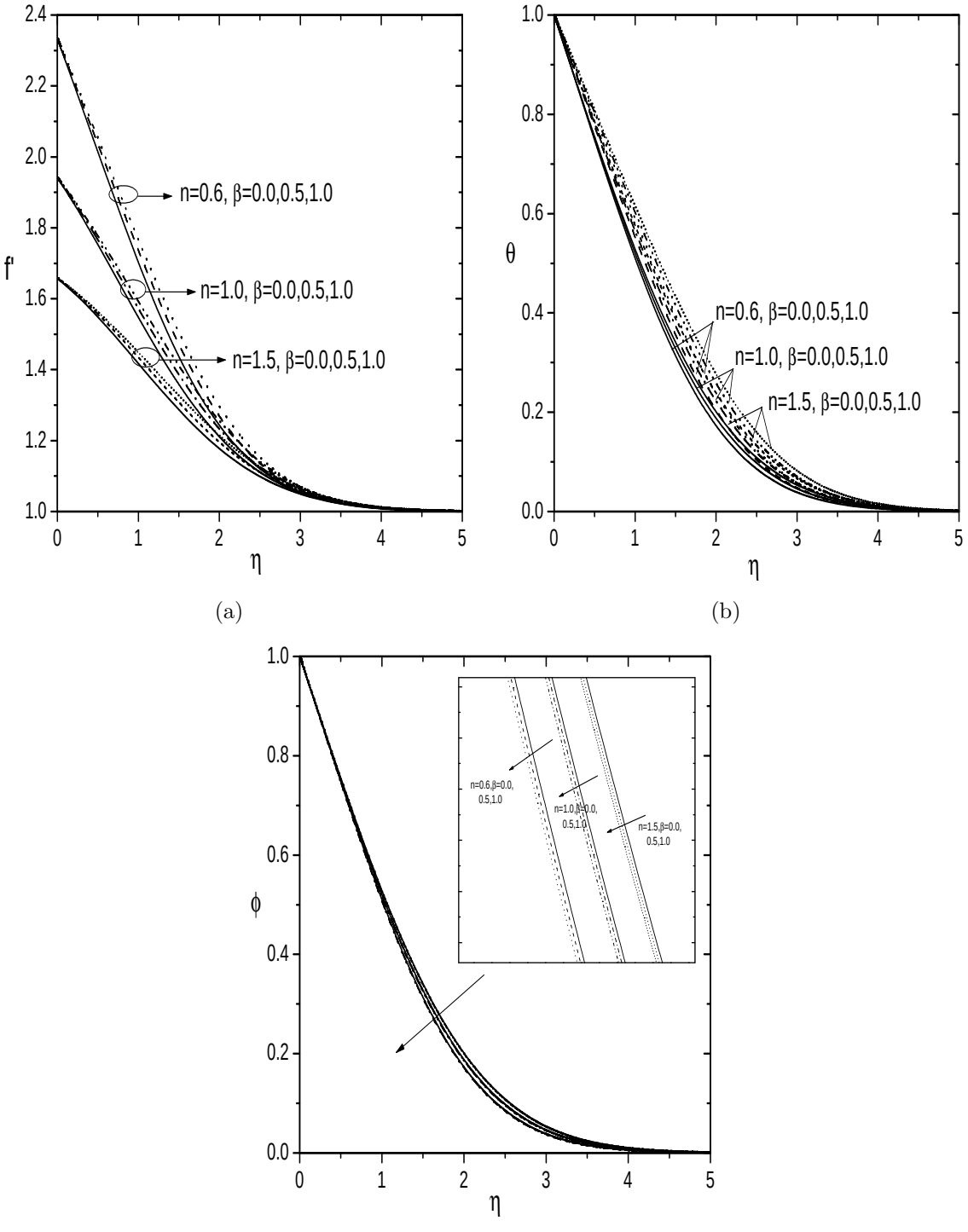

Figure 6.3: Effect of β and n on (a)velocity profile (b)temperature profile and (c)concentration profile for B = 1.0, Le = 1.0, $Pe_\gamma = 0.5$, $Pe_\zeta = 0.5$, $\theta_e = 2.0$, M = 1.0, G = 0.1 and $\lambda = 1.0$.

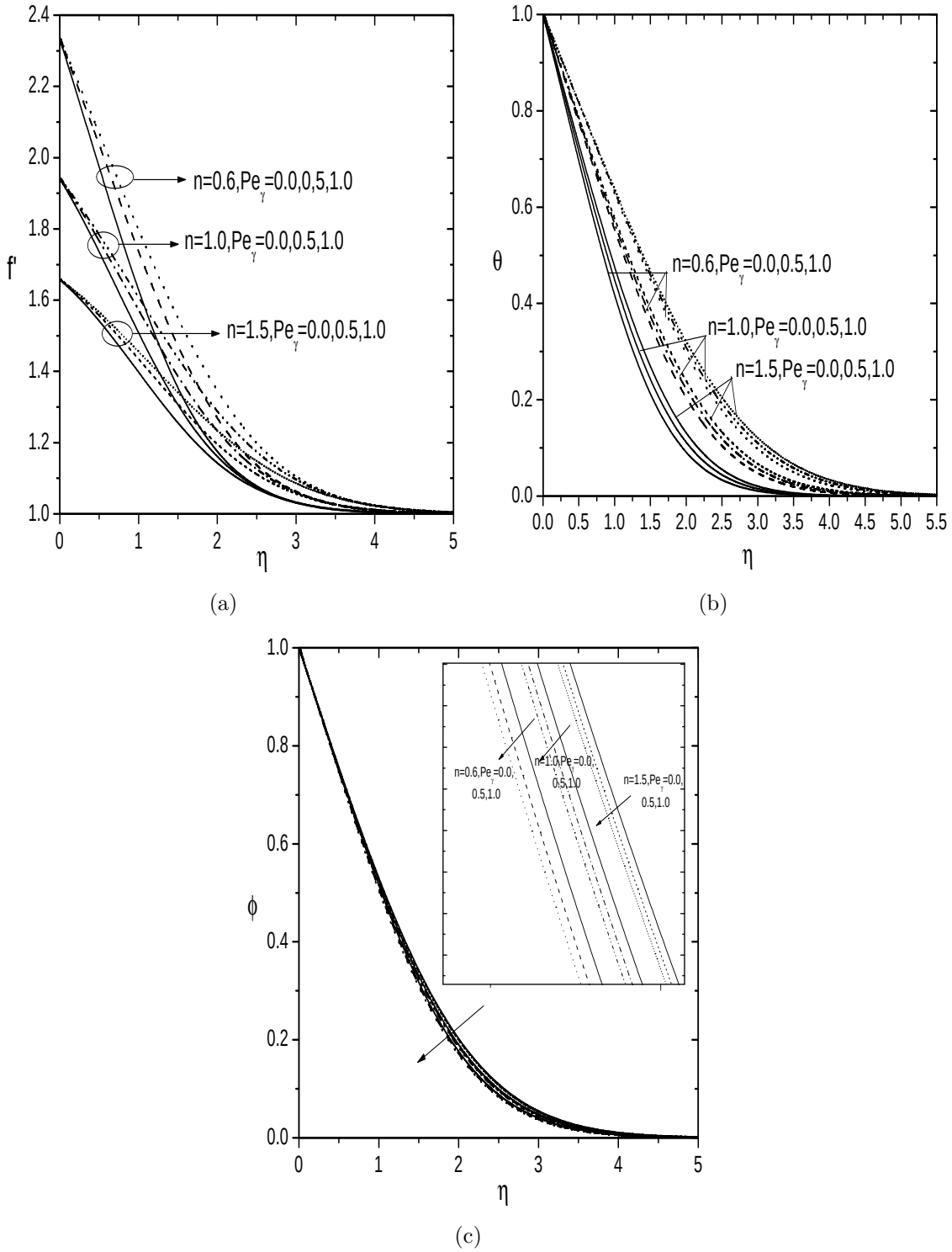

Figure 6.4: Effect of Pe_γ and n on (a)velocity profile (b)temperature profile and (c)concentration profile for B = 1.0, Le = 1.0, $\beta = 0.5$, $Pe_\zeta = 0.5$, $\theta_e = 2.0$, M = 1.0, G = 0.1 and $\lambda = 1.0$.

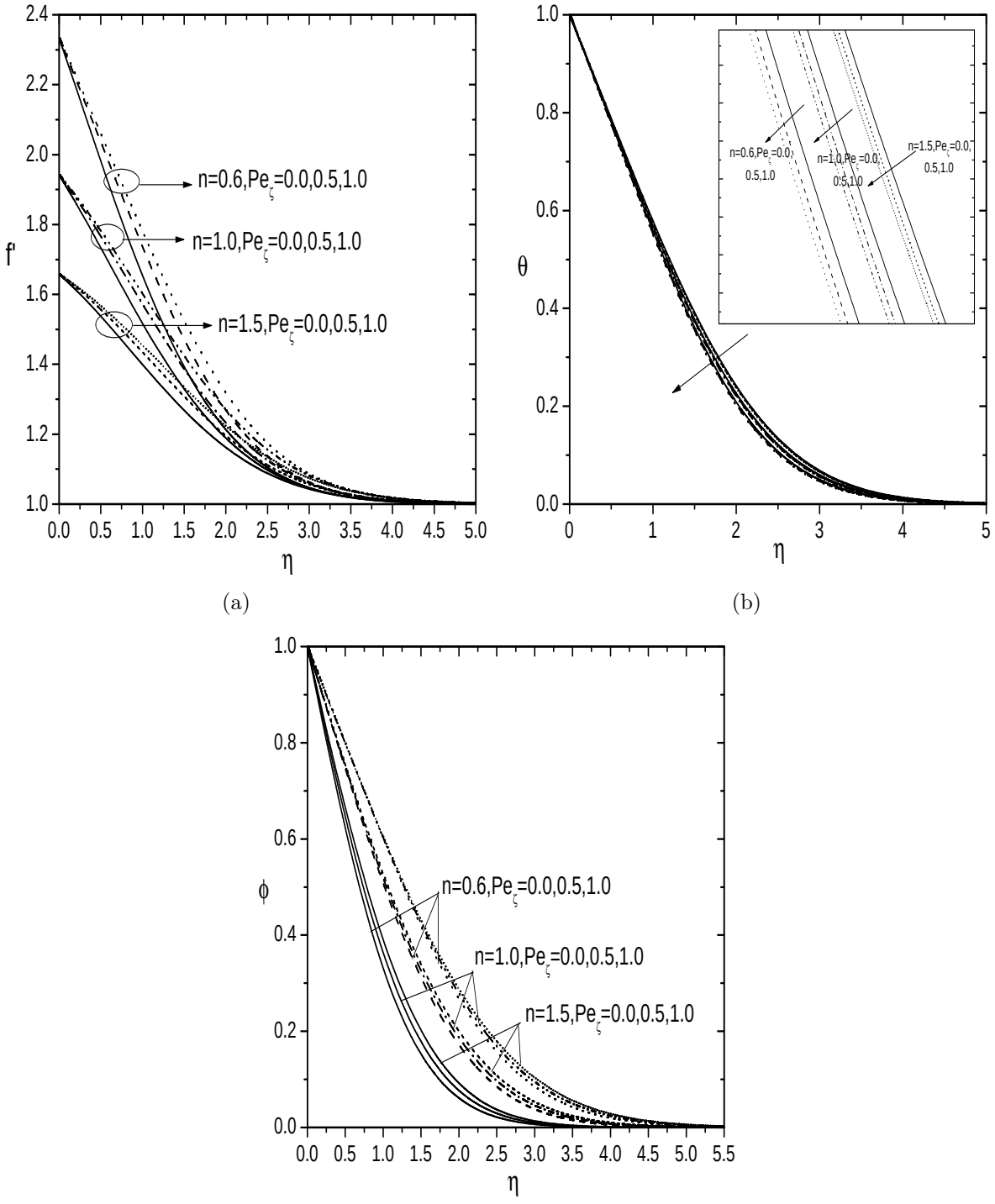

(a) (b)

(c)

Figure 6.5: Effect of Pe_ζ and n on (a)velocity profile (b)temperature profile and (c)concentration profile for B = 1.0, Le = 1.0, $\beta = 0.5$, $Pe_\gamma = 0.5$, $\theta_e = 2.0$, M = 1.0, G = 0.1 and $\lambda = 1.0$.

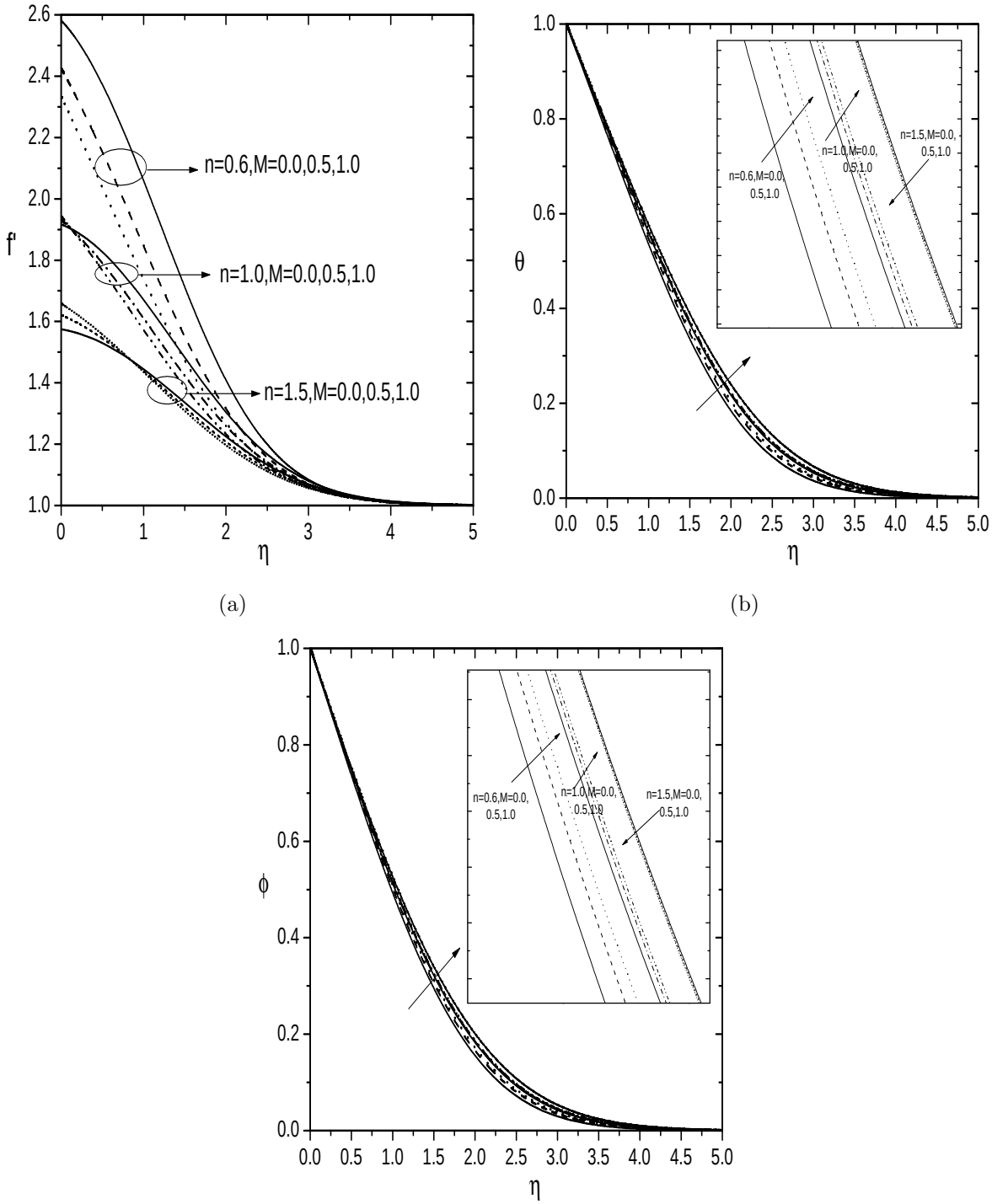

(a)

(b)

(c)

Figure 6.6: Effect of M and n on (a)velocity profile (b)temperature profile and (c)concentration profile for B = 1.0, Le = 1.0, $\beta = 0.5$, $Pe_\gamma = 0.5$, $Pe_\zeta = 0.5$, $\theta_e = 2.0$, G = 0.1 and $\lambda = 1.0$.

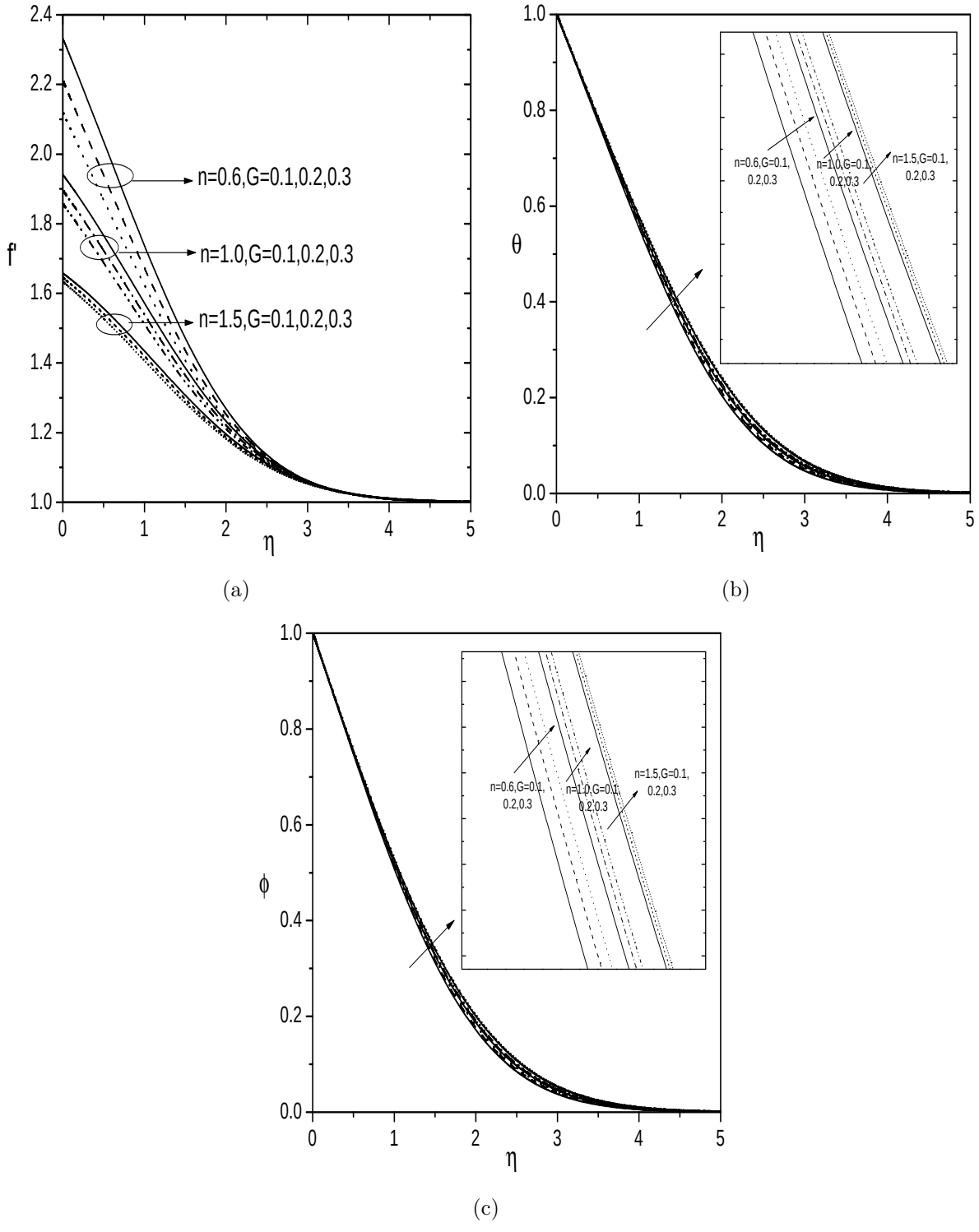

Figure 6.7: Effect of G and n on (a)velocity profile (b)temperature profile and (c)concentration profile for B = 1.0, Le = 1.0, $\beta = 0.5$, $Pe_\gamma = 0.5$, $Pe_\zeta = 0.5$, $\theta_e = 2.0$, M = 1.0 and $\lambda = 1.0$.

6.4 Conclusions

This chapter aims to compute numerical results of mixed convective flow of power-law fluid with the influence of variable properties, MHD and double dispersion along a vertical surface. The governing system of higher order non-linear differential equations is transformed into ordinary differential equations by using Lie scaling group transformations and numerical solutions are attained by the shooting method. The representative set of results is reported graphically to demonstrate the details of velocity, temperature, and concentration on some of the physical parameters.

- An increase in variable viscosity cause a decrease in velocity profile, heat and mass transfer rates, but increases the temperature and concentration profiles.
- The coefficients of velocity and temperature are found to enhance strongly with a rise in thermal conductivity, but depreciation in concentration, heat and mass transfer rates.
- The effect of thermal dispersion is to increase the velocity, temperature and mass transfer rate, but reduces the concentration and the heat transfer rate.
- Enhancement in the solutal dispersion decreases the velocity, concentration and mass transfer rate, but raises the temperature and heat transfer rate.
- The influence of the non-Darcy parameter enhances the temperature and concentration, but reduces the velocity, heat and mass transfer rates.
- The higher values of the magnetic field result in lower velocity, heat and mass transfer rates, but higher temperature and concentration profiles.

Chapter 7

Influence of MHD, Thermophoresis and Variable Properties on Mixed Convection Flow over a Vertical Plate in a Non-Darcy Porous Medium Saturated with a Power-law Fluid [1]

7.1 Introduction

Thermophoresis is a mechanism in which small particles migrate in the direction of decreasing thermal gradient. It is quite significant in radioactive particle deposition in nuclear reactor safety simulations, aerosol particle sampling, deposition of silicon thin films etc. Fagbade *et al.* [28] studied the effects of thermophoresis, viscous dissipation and magnetic field on mixed convection over a vertical plate in fluid saturated non-Darcy porous medium. Helal and Saif [35] investigated the effect of thermophoresis on free convective boundary layer flow

[1] Published in "**International Journal of Pure and Applied Mathematics**", Vol.113, no.12, pp.160-168, 2017.

along an inclined surface in a power-law fluid. Magnetic field, thermophoresis and thermal radiation effects on natural convection from a vertical plate embedded in porous media have been reported by Rashad [81].

This chapter is an extension of Chapter-3 by considering the effects of MHD and non-Darcy porous medium. The problem of MHD mixed convection flow along a vertical surface in a power-law fluid saturated non-Darcy porous medium with the thermophoresis and variable properties, are considered in this chapter. In addition, the similarity representation of the system of governing non-dimensional equations is obtained using the scaling group of transformations and then solved the resultant system of equations by shooting method. The present study mainly focused on exploring the effects of thermophoresis, MHD and variable properties, non-Darcy parameter. Further, the numerical data for heat and mass transfer rates are shown in tabular form.

7.2 Mathematical Formulation

Consider steady, laminar, incompressible mixed convection flow along a vertical plate embedded in a power-law fluid saturated non-Darcy porous medium. Choose the two dimensional coordinate system such that the $\overline{x}$-axis is along the vertical plate and the $\overline{y}$-axis is normal to the plate. The physical model of the system is shown Fig. (6.1). A uniform magnetic field is applied normal to the plate. The gravitational acceleration g acts in a downward direction. The plate is maintained at a constant temperature $\overline{T}_w$ and concentration $\overline{C}_w$. The ambient fluid temperature is $\overline{T}_\infty$ and the concentration is $\overline{C}_\infty$. Using the Boussinesq approximation and boundary layer assumptions, the governing equations of continuity, momentum, energy and concentration are given by:

$$\frac{\partial \overline{u}}{\partial \overline{x}} + \frac{\partial \overline{v}}{\partial \overline{y}} = 0 \tag{7.1}$$

$$n\overline{u}^{n-1}\frac{\partial \overline{u}}{\partial \overline{y}} + \frac{\partial}{\partial \overline{y}}\left[\frac{C_F \rho_\infty \sqrt{K}}{\mu}\overline{u}^2\right] = \frac{\partial}{\partial \overline{y}}\left[\frac{Kg\rho_\infty}{\mu}(\beta_T^*[\overline{T} - \overline{T}_\infty] + \beta_C^*[\overline{C} - \overline{C}_\infty])\right] - \frac{\partial}{\partial \overline{y}}\left[\frac{\sigma {B_0}^2 K {\mu_e}^2}{\mu}\overline{u}\right] \tag{7.2}$$

$$\overline{u}\frac{\partial \overline{T}}{\partial \overline{x}} + \overline{v}\frac{\partial \overline{T}}{\partial \overline{y}} = \frac{\partial}{\partial \overline{y}}\left[\alpha \frac{\partial \overline{T}}{\partial \overline{y}}\right] \tag{7.3}$$

$$\overline{u}\frac{\partial \overline{C}}{\partial \overline{x}} + \overline{v}\frac{\partial \overline{C}}{\partial \overline{y}} = D\frac{\partial^2 \overline{C}}{\partial \overline{y}^2} + \frac{\partial}{\partial \overline{y}}\left[\frac{K_T \mu}{\rho_\infty T_r}\frac{\partial \overline{T}}{\partial \overline{y}}(\overline{C} - \overline{C}_\infty)\right] \tag{7.4}$$

The associated boundary conditions are

$$\overline{v} = 0, \quad \overline{T} = \overline{T}_w, \quad \overline{C} = \overline{C}_w \text{ at } \quad y = 0, \tag{7.5a}$$

$$\overline{u} = u_\infty, \quad \overline{T} = \overline{T}_\infty, \quad \overline{C} = \overline{C}_\infty \quad \text{as} \quad y \to \infty \tag{7.5b}$$

where $\overline{u}$ and $\overline{v}$ are Darcy velocity components along the $\overline{x}$ and $\overline{y}$- axes, respectively, ρ_∞ is the density, β_T^* and β_C^* are coefficients of thermal and concentration expansions respectively, g represents the acceleration due to gravity, $\overline{T}$ indicates temperature, K indicates permeability, B_0 represents the strength of the magnetic field, $\overline{C}$ indicates concentration, μ_e indicates magnetic permeability, D is the mass diffusivities of the medium.

Introducing the non-dimensional transformation variables:

$$\left.\begin{aligned} x = \frac{\overline{x}}{\mathrm{L}}, \quad y = \frac{\overline{y}}{\mathrm{L}}\mathrm{Pe}^{\frac{1}{2}}, \quad u = \frac{\overline{u}\mathrm{L}}{\alpha_0 \mathrm{Pe}}, \quad u = \frac{\overline{v}\mathrm{L}}{\alpha_0 \mathrm{Pe}^{\frac{1}{2}}} \\ \theta(\eta) = \frac{\overline{T} - \overline{T}_\infty}{\overline{T}_w - \overline{T}_\infty}, \quad \phi(\eta) = \frac{\overline{C} - \overline{C}_\infty}{\overline{C}_w - \overline{C}_\infty} \end{aligned}\right\} \tag{7.6}$$

where $\mathrm{Pe} = \dfrac{u_\infty \mathrm{L}}{\alpha_0}$ is the Péclet number and L represents the characteristic length.

By introducing the non-dimensional stream function $\psi(x, y)$ the continuity Eq. (7.1) satisfies automatically, and it is defined as

$$u = \frac{\partial \psi}{\partial y}, \quad v = -\frac{\partial \psi}{\partial x} \tag{7.7}$$

Substituting Eqs.(7.6)-(7.7) into Eqs.(7.2)-(7.4), we obtain the following system of equa-

tions

$$n\left(\frac{\partial\psi}{\partial y}\right)^{n-1}\frac{\partial^2\psi}{\partial y^2}+2\mathrm{G}\left(\frac{\partial\psi}{\partial y}\right)\frac{\partial^2\psi}{\partial y^2}\left(\frac{\theta_e-\theta}{\theta_e}\right)-\frac{\mathrm{G}}{\theta_e}\left(\frac{\partial\psi}{\partial y}\right)^2\frac{\partial\theta}{\partial y}-\frac{\mathrm{M}}{\theta_e}\left(\frac{\partial\psi}{\partial y}\right)\left(\frac{\partial\theta}{\partial y}\right) \tag{7.8}$$
$$+\mathrm{M}\left(\frac{\partial^2\psi}{\partial y^2}\right)\left(\frac{\theta_e-\theta}{\theta_e}\right)-\lambda^n\left(\frac{\partial\theta}{\partial y}+\mathrm{B}\frac{\partial\phi}{\partial y}\right)\left(\frac{\theta_e-\theta}{\theta_e}\right)+\frac{\lambda^n}{\theta_e}\left(\theta+\mathrm{B}\phi\right)\left(\frac{\partial\theta}{\partial y}\right)=0$$

$$\frac{\partial\psi}{\partial y}\frac{\partial\theta}{\partial x}-\frac{\partial\psi}{\partial x}\frac{\partial\theta}{\partial y}-\beta\left(\frac{\partial\theta}{\partial y}\right)^2-\left(1+\beta\theta\right)\frac{\partial^2\theta}{\partial y^2}=0 \tag{7.9}$$

$$\mathrm{Le}\left[\frac{\partial\psi}{\partial y}\frac{\partial\phi}{\partial x}-\frac{\partial\psi}{\partial x}\frac{\partial\phi}{\partial y}\right]-\frac{\partial^2\phi}{\partial y^2}+\tau\mathrm{Sc}\frac{\theta_e}{\theta_e-\theta}\left[\left(\frac{\partial\theta}{\partial y}\right)^2\frac{\phi}{\theta_e-\theta}+\phi\frac{\partial^2\theta}{\partial y^2}+\frac{\partial\theta}{\partial y}\frac{\partial\phi}{\partial y}\right]=0 \tag{7.10}$$

The boundary conditions are

$$\left.\begin{aligned}&\frac{\partial\psi}{\partial x}=0,\quad \theta=1,\quad \phi=1\quad \text{at}\quad y=0\\&\frac{\partial\psi}{\partial y}=1,\quad \theta=0,\quad \phi=0\quad \text{as}\quad y\to\infty\end{aligned}\right\} \tag{7.11}$$

where $\mathrm{B}=\dfrac{\beta_c^*(\overline{C}_w-\overline{C}_\infty)}{\beta_T^*(\overline{T}_w-\overline{T}_\infty)}$ is the Buoyancy ratio, $\mathrm{M}=\dfrac{\sigma {B_0}^2{\mu_e}^2K}{\mu_\infty}\left(\dfrac{\mathrm{L}}{\alpha_0}\right)^{(n-1)}\mathrm{Pe}^{-(n-1)}$ is the magnetic field parameter, $\lambda=\dfrac{\mathrm{Ra}}{\mathrm{Pe}}$ is the mixed convection parameter, $\tau=-\dfrac{k}{T_r}(T_w-T_\infty)$ is the thermophoresis parameter, $\theta_e=\dfrac{\overline{T}_e-\overline{T}_\infty}{\overline{T}_w-\overline{T}_\infty}$ is the variable viscosity, $\mathrm{Le}=\dfrac{\alpha_0}{D}$ is the Lewis number, $\mathrm{G}=\dfrac{C_F\sqrt{K}}{\nu_\infty}\left(\dfrac{\mathrm{L}}{\alpha_0}\right)^{(n-2)}\mathrm{Pe}^{-(n-2)}$ is the modified non-Darcy parameter and $\mathrm{Ra}=\dfrac{\mathrm{L}}{\alpha_0}\left(\dfrac{gK\beta_T(\overline{T}_w-\overline{T}_\infty)}{\nu}\right)^{1/n}$ is the Rayleigh number.

Now, we introduce the one-parameter scaling group of transformations which is a simplified form of Lie group transformation. We will get the following similarity transformations

$$\psi=x^{\frac{1}{2}}f(\eta),\quad \eta=yx^{-\frac{1}{2}},\quad \theta=\theta(\eta),\quad \phi=\phi(\eta). \tag{7.12}$$

Substituting equation (7.12) into Eqs.(7.8)-(7.10), we obtain the following ordinary dif-

ferential equations.

$$f''\left[n(f')^{n-1}+2\mathrm{G}f'\left(\frac{\theta_e-\theta}{\theta_e}\right)+\mathrm{M}\left(\frac{\theta_e-\theta}{\theta_e}\right)\right]=\frac{f'\theta'}{\theta_e}\left(\mathrm{G}f'+\mathrm{M}\right) \\ +\lambda^n\left(\theta'+\mathrm{B}\phi'\right)\left(\frac{\theta_e-\theta}{\theta_e}\right)-\lambda^n\left(\theta+\mathrm{B}\phi\right)\frac{\theta'}{\theta_e} \tag{7.13}$$

$$\beta(\theta')^2+\left(1+\beta\theta\right)\theta''+\frac{1}{2}f\theta'=0 \tag{7.14}$$

$$\phi''-\tau\mathrm{Sc}\frac{\theta_e}{\theta_e-\theta}\left[(\theta')^2\frac{\phi}{\theta_e-\theta}+\theta''\phi+\theta'\phi'\right]+\frac{1}{2}\mathrm{Le}f\phi'=0 \tag{7.15}$$

The transformed boundary conditions (7.11) becomes

$$f(0)=0,\ \ \theta(0)=1,\ \ \phi(0)=1,\ \ f'(\infty)=1,\ \ \theta(\infty)=0,\ \ \phi(\infty)=0. \tag{7.16}$$

The Nusselt number $Nu_{\overline{x}}$ and the Sherwood number $Sh_{\overline{x}}$ are respectively given by:

$$\frac{Nu_{\overline{x}}}{x^{1/2}}=-\theta'(0)\quad\text{and}\quad\frac{Sh_{\overline{x}}}{x^{1/2}}=-\phi'(0) \tag{7.17}$$

7.3 Results and Discussion

The coupled nonlinear ordinary differential equations (7.13)-(7.15) along with the boundary conditions (7.16) are solved numerically using shooting method, as discussed in the Chapter-2. In order to test the accuracy of our results, we compared the present results with those of Chaoyang *et al.* [18] by taking Sc = 0, $\tau = 0$, B = 0, Le = 1.0, $\theta_e \to \infty$ and $\beta = 0$. The comparison show good agreement, as presented in Table (3.1).

The solutions for the non-dimensional velocity $f'(\eta)$, temperature $\theta(\eta)$, and concentration $\phi(\eta)$ are computed and are displayed graphically in Figs.7.1(a)-7.5(c) with varying variable viscosity (θ_e), thermal conductivity (β), thermophoresis (τ), magnetic field (M) and non-Darcy porous medium (G) for power-law index (n) (see pseudo-plastic, dilatants and Newtonian fluids).

Figures 7.1(a)-7.1(c) represent the non-dimensional velocity $f'(\eta)$, temperature $\theta(\eta)$, and concentration $\phi(\eta)$ for various values of variable viscosity (θ_e) and power-law index (n), respectively. We observed from Fig. 7.1(a) that the velocity depreciates with the rise of variable viscosity for three kinds of fluids. Furthermore, Fig. 7.1(b) and Fig. 7.1(c) perceives the non-dimensional temperature and concentration profiles for different values of θ_e and n. From these figures, we observe that the enhancement in variable viscosity tends to rise the temperature and concentration for three kinds of fluids.

The influence of thermal conductivity (β) and power-law index (n) on the non-dimensional velocity $f'(\eta)$, temperature $\theta(\eta)$, and concentration $\phi(\eta)$ profiles are exhibited in Figs. 7.2(a)-7.2(c). It is noted that an increase in the value of thermal conductivity tends to enhance the velocity, temperature and concentration profiles for three kinds of fluids as displayed in Figs. 7.2(a)-7.2(c).

Figures 7.3(a)-7.3(c) explore the influence of thermophoresis (τ) and power-law index (n) on the non-dimensional velocity $f'(\eta)$, temperature $\theta(\eta)$, and concentration $\phi(\eta)$ profiles, respectively. It is observed that, an enhancement in the value of thermophoresis tends to reduce the velocity and increase the temperature for three kinds of fluids, as portrayed in Figs. 7.3(a)-7.3(b). This is due to the fact that, an increase in the thermophoresis parameter increases the thermophoresis force, which tends to move particles from the hot zone to the cold zone, which results in the increase in temperature. It can be seen from Fig. 7.3(c) that the concentration enhances with the rise of thermophoresis parameter for three kinds of fluids.

Figures 7.4(a)-7.4(c) depict the influence of magnetic field parameter (M) and power-law index (n) on the dimensionless velocity $f'(\eta)$, temperature $\theta(\eta)$, and concentration $\phi(\eta)$ profiles, respectively. It is interesting to note from Fig. 7.4(a) that the velocity profile decrease across the boundary layer with increase of M for pseudo-plastic, Newtonian and dilatants fluids. The influence of M leads to increase the temperature for $n < 1, n = 1$, but an opposite trend is observed for $n > 1$, as given 7.4(b). This is due to the fact that introduction of magnetic field to an electrically conducting fluid gives rise to a rise in resistive force known as Lorentz force. This force has a tendency to slow down the motion of the fluid

in the boundary layer and to increase the temperature distribution. It is observed from Fig. 7.4(c) that the concentration boundary layer thickness enhances with enhance in the value of (M) for pseudo-plastic, Newtonian fluid but reverse trend is observed for the dilatant fluids.

The variation of non-dimensional velocity $f'(\eta)$, temperature $\theta(\eta)$, and concentration $\phi(\eta)$ for different values of non-Darcy parameter (G) and power-law index (n) are plotted in Figures 7.5(a)-7.5(c). It is observed that the velocity decreases with increase in the value of non-Darcy parameter for three kinds of fluids, as presented in 7.5(a). As the non-Darcy parameter decreases, the porous medium offers less resistance to the fluid flow and hence, the velocity is less in the non-Darcy porous medium. Moreover, the temperature increase with an increase in the value of non-Darcy parameter for three kinds of fluids in plotted on 7.5(b). Further, from Fig. 7.5(c), it can be observed that concentration enhances with the enhancing the non-Darcy parameter.

The rate of heat and mass transfers are presented Tab. 7.1. for different values of power-law index (n), variable viscosity (θ_e), thermal conductivity (β), thermophoresis (τ), magnetic field (M), non-Darcy parameter (G). The higher value of power-law index, variable viscosity, thermal conductivity, magnetic field, non-Darcy parameters reduces the heat and mass transfer rates. The influence of thermophoresis decreases the heat transfer but increases the mass transfer rates. Moreover, increase in the value of mixed convection parameter increases the heat transfer and mass transfer coefficients.

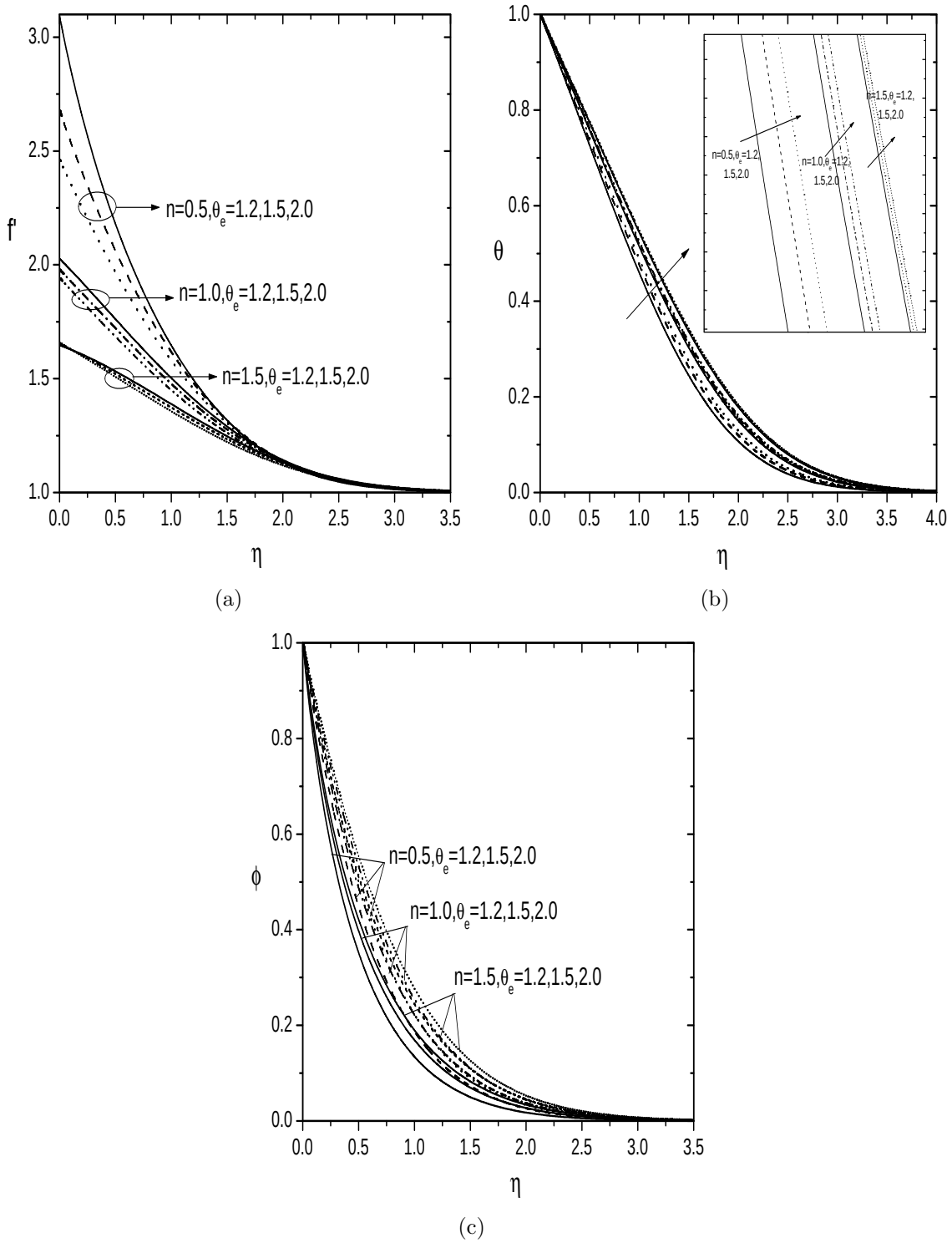

Figure 7.1: Effect of θ_e and n on (a)velocity profile (b)temperature profile and (c)concentration profile for B = 1.0, Le = 1.0, τ = 1.0, Sc = 0.6, β = 0.5, M = 1.0, G = 0.1 and λ = 1.0.

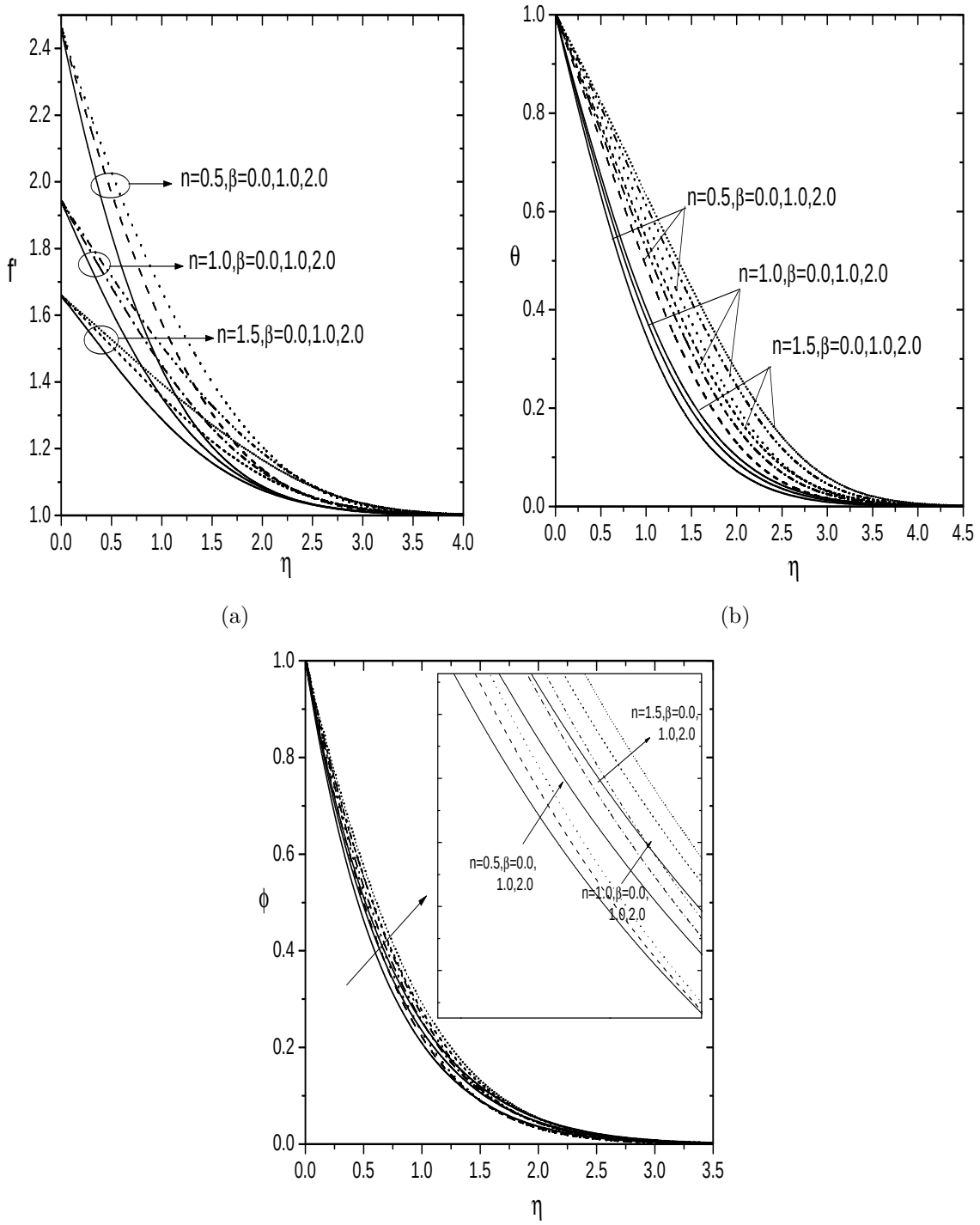

Figure 7.2: Effect of β and n on (a)velocity profile (b)temperature profile and (c)concentration profile for B = 1.0, Le = 1.0, τ = 1.0, Sc = 0.6, θ_e = 2.0, M = 1.0, G = 0.1 and $\lambda = 1.0$.

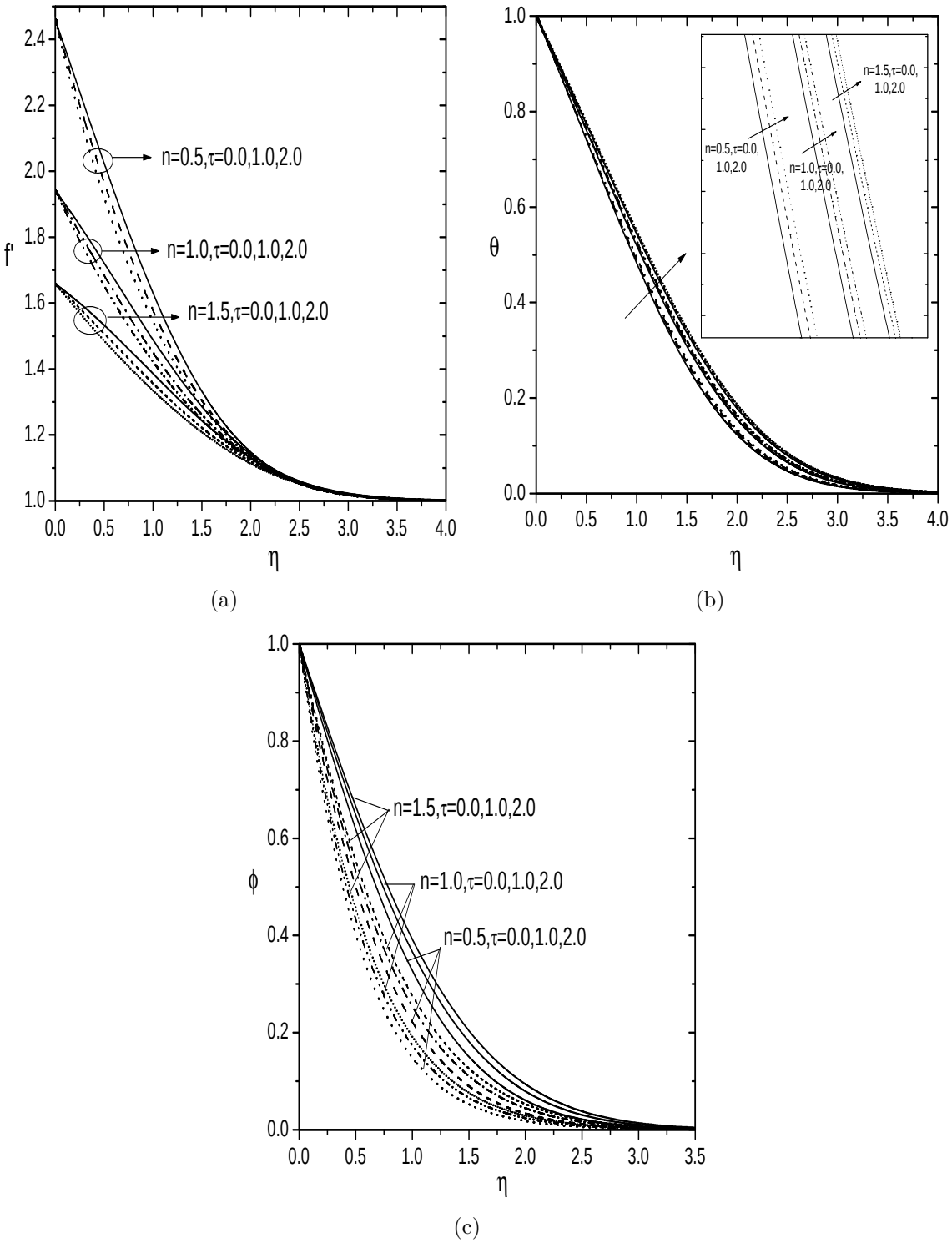

Figure 7.3: Effect of τ and n on (a)velocity profile (b)temperature profile and (c)concentration profile for B = 1.0, Le = 1.0, θ_e = 2.0, Sc = 0.6, β = 0.5, M = 1.0, G = 0.1 and λ = 1.0."

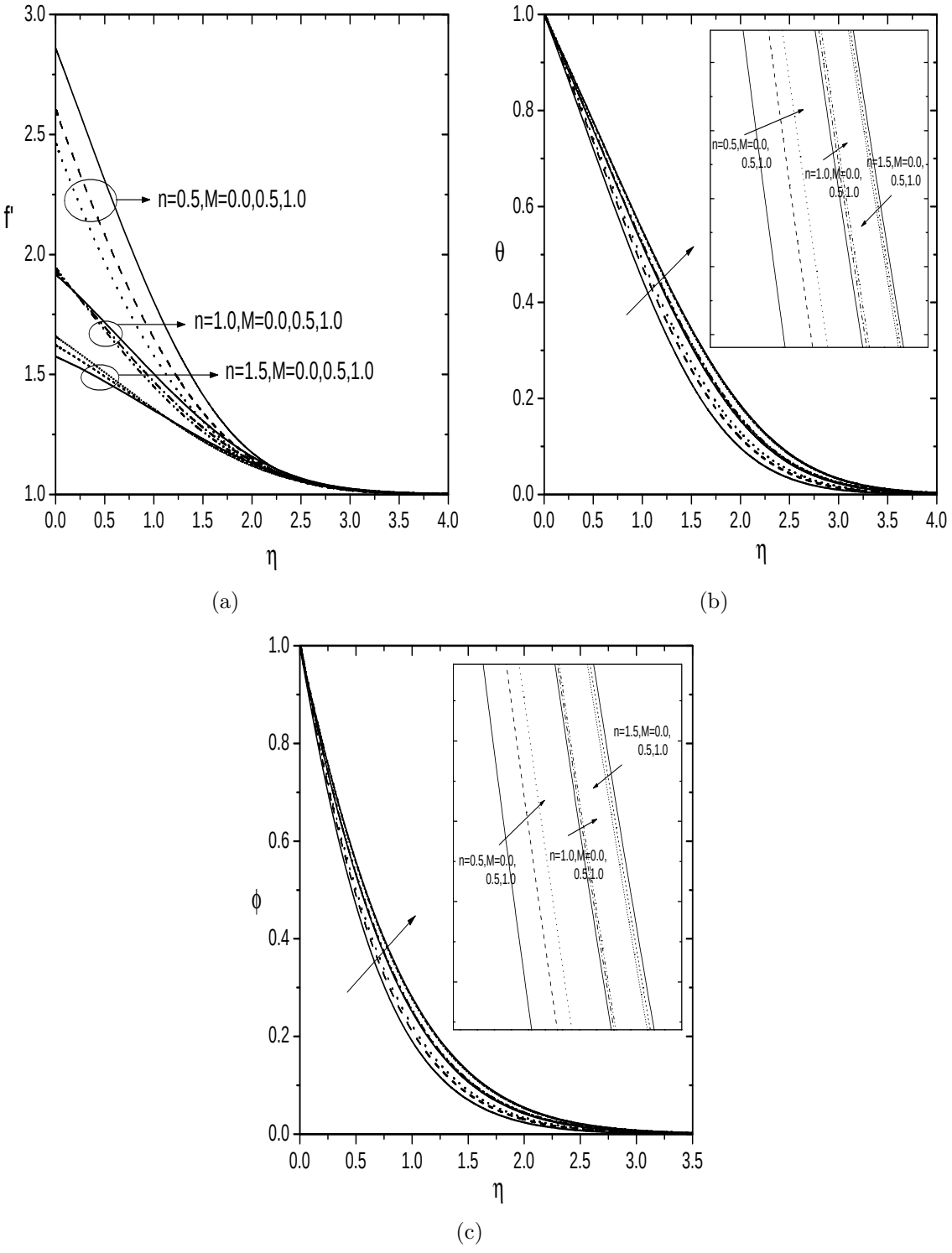

Figure 7.4: Effect of M and n on (a)velocity profile (b)temperature profile and (c)concentration profile for B = 1.0, Le = 1.0, τ = 1.0, Sc = 0.6, β = 0.5, θ_e = 2.0, G = 0.1 and λ = 1.0.

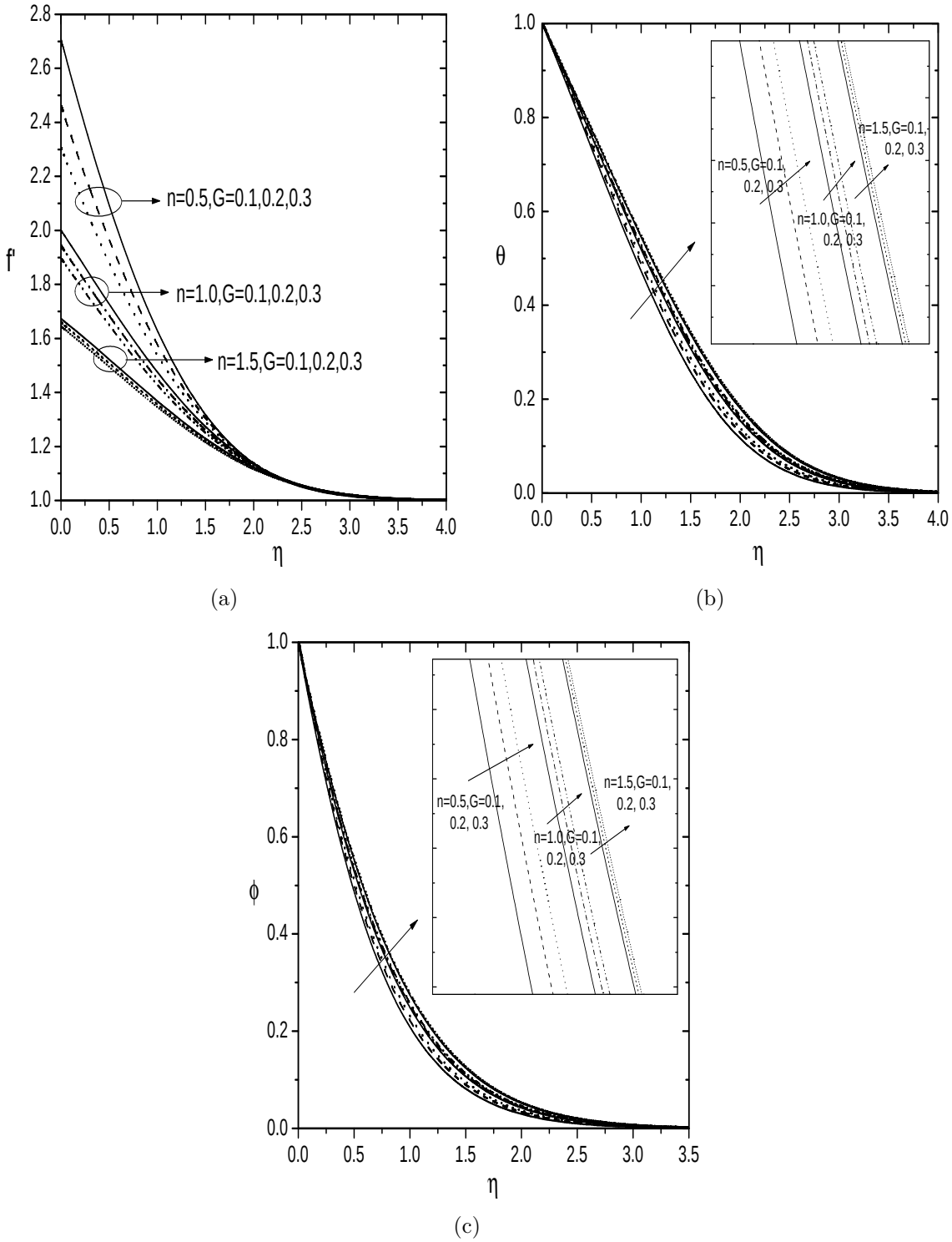

Figure 7.5: Effect of G and n on (a)velocity profile (b)temperature profile and (c)concentration profile for B = 1.0, Le = 1.0, τ = 1.0, Sc = 0.6, β = 0.5, M = 1.0, $\theta_e = 2.0$ and $\lambda = 1.0$.

Table 7.1: *Variation of heat and mass transfer coefficients for varying values of n, θ_e, β, τ, M, G and λ.*

n	θ_e	β	τ	M	G	λ	$-\theta'(0)$	$-\phi'(0)$
0.5	2.0	1.0	1.0	1.0	0.1	1.0	0.493546	1.233965
1.0	2.0	1.0	1.0	1.0	0.1	1.0	0.455366	1.130993
1.5	2.0	1.0	1.0	1.0	0.1	1.0	0.431721	1.067471
0.5	1.5	1.0	1.0	1.0	0.1	1.0	0.507206	1.532350
0.5	2.5	1.0	1.0	1.0	0.1	1.0	0.487059	1.135921
0.5	3.0	1.0	1.0	1.0	0.1	1.0	0.483245	1.087144
0.5	2.0	0.0	1.0	1.0	0.1	1.0	0.770098	1.509194
0.5	2.0	0.5	1.0	1.0	0.1	1.0	0.590767	1.326813
0.5	2.0	1.5	1.0	1.0	0.1	1.0	0.431038	1.177192
0.5	2.0	1.0	0.0	1.0	0.1	1.0	0.499397	0.799997
0.5	2.0	1.0	0.5	1.0	0.1	1.0	0.496319	1.012543
0.5	2.0	1.0	1.5	1.0	0.1	1.0	0.491057	1.462918
0.5	2.0	1.0	1.0	0.0	0.1	1.0	0.535660	1.340347
0.5	2.0	1.0	1.0	0.5	0.1	1.0	0.507915	1.270581
0.5	2.0	1.0	1.0	1.5	0.1	1.0	0.484766	1.211439
0.5	2.0	1.0	1.0	1.0	0.0	1.0	0.510795	1.280454
0.5	2.0	1.0	1.0	1.0	0.2	1.0	0.481842	1.202650
0.5	2.0	1.0	1.0	1.0	0.3	1.0	0.473161	1.179517
0.5	2.0	1.0	1.0	1.0	0.1	0.0	0.411074	1.015310
0.5	2.0	1.0	1.0	1.0	0.1	0.5	0.471042	1.174444
0.5	2.0	1.0	1.0	1.0	0.1	1.5	0.510026	1.277478

7.4 Conclusions

Mixed convective transport over the vertical plate in a non-Darcy porous medium saturated by a power-law fluid is analyzed, in this chapter. From this computational analysis, the following conclusions are drawn below.

Increase in the value of variable viscosity causes an enhancement in the fluid temperature and concentration and consequently, the fluid velocity, heat and mass transfer rates are decreases. By rising the thermal conductivity causes an enhancement in the fluid velocity, temperature and concentrations but local Nusselt number and local Sherwood numbers show an opposite trend. The influence of thermophoresis decreases the fluid velocity, concentration and heat transfer but increases the temperature and mass transfer. The effect of magnetic field reduces the fluid velocity, heat and mass transfer rates, but enhances the temperature and concentrations. Moreover, an increase in the value of non-Darcy parameter enhances the temperature, concentration, Nusselt number, and Sherwood, but velocity shown revers trend.

Chapter 8

Mixed Convection in a Power-law Fluid Saturated Non-Darcy Porous Medium with Effect of MHD, Thermal Radiation and Variable Properties [1]

8.1 Introduction

The effect of thermal radiation on the fluid flow and heat transfer, has received significant attention due to their applications in the design of many advanced energy conversion systems operating at high temperature. The thermal radiation occurs because of the emission by the hot walls and working fluid. Hence, several investigations have been carried out their research on the mixed convective transport in different fluids under the influence of thermal radiation. Merely, it is essential to study the effect of thermal radiation due to its relevance to various applications involving high temperatures such as nuclear power plant, gas turbines missiles,

[1] Communicated to "**Journal of Nanofluid**"

satellites, space vehicles, and aircrafts, etc. Hamad *et al.* [32] considered the MHD forced convective flow over a permeable at plate in the presence of thermal radiation, variable properties and convective boundary conditions. Megahed [59] explored the influence of thermal radiation, variable viscosity and velocity slip of a non-Newtonian power-law fluid over a stretching surface.

In this chapter, the effects of MHD, thermal radiation and variable properties on the mixed convective flow of power-law fluid in a non-Darcy porous medium is discussed. The influence of pertinent parameters on physical quantities for non-dimensional velocity, temperature and concentrations are examined numerically and shown through graphs. In addition, the heat and mass transfer rates are tabulated.

8.2 Mathematical Formulation

Consider a steady, laminar and two-dimensional mixed convective flow of an incompressible power-law fluid along a vertical plate. Choose the cartesian coordinate system such that $\overline{x}$- axis is taken along the vertical direction and $\overline{y}$-axis normal to the plate as shown in Fig. (6.1). The temperature and concentration of the plate are $\overline{T}_w$ and $\overline{C}_w$, respectively, and these values are greater than the ambient temperature and concentrations $\overline{T}_\infty$ and $\overline{C}_\infty$ respectively. The fluid is considered to be a gray, absorbing emitting radiation but non-scattering medium. The Rosseland approximation is used to describe the radiative heat flux in the energy equation. By implementing boundary layer assumptions and Boussinesq approximation, the governing equations for the power-law fluid are given by

$$\frac{\partial \overline{u}}{\partial \overline{x}} + \frac{\partial \overline{v}}{\partial \overline{y}} = 0 \tag{8.1}$$

$$n\overline{u}^{n-1}\frac{\partial \overline{u}}{\partial \overline{y}} + \frac{\partial}{\partial \overline{y}}\left[\frac{C_F \rho_\infty \sqrt{K}}{\mu}\overline{u}^2\right] + \frac{\partial}{\partial \overline{y}}\left[\frac{\sigma {B_0}^2 K {\mu_e}^2}{\mu}\overline{u}\right] = \frac{\partial}{\partial \overline{y}}\left[\frac{Kg\rho_\infty}{\mu}(\beta_T^*[\overline{T}-\overline{T}_\infty] + \beta_C^*[\overline{C}-\overline{C}_\infty])\right] \tag{8.2}$$

$$\overline{u}\frac{\partial \overline{T}}{\partial \overline{x}} + \overline{v}\frac{\partial \overline{T}}{\partial \overline{y}} = \frac{\partial}{\partial \overline{y}}\left[\alpha \frac{\partial \overline{T}}{\partial \overline{y}}\right] + \frac{4\sigma^*}{3k^*\rho C_p}\frac{\partial^2}{\partial \overline{y}^2}\left[4\overline{T}_\infty^3 \overline{T} - 3\overline{T}^4{}_\infty\right] \tag{8.3}$$

$$\overline{u}\frac{\partial \overline{C}}{\partial \overline{x}} + \overline{v}\frac{\partial \overline{C}}{\partial \overline{y}} = D_0\frac{\partial^2 \overline{C}}{\partial \overline{y}^2} \tag{8.4}$$

where $\overline{u}$ and $\overline{v}$ are velocity components along the $\overline{x}$ and $\overline{y}$ axes, respectively. ρ_∞ is the density, β_T^* indicates the coefficient of thermal expansion, β_C^* represents the coefficient of concentration expansion, g is the acceleration due to gravity, $\overline{T}$ indicates the temperature, K represents the permeability, B_0 indicates the strength of the magnetic field, $\overline{C}$ is the concentration, k^* indicates the mean absorption coefficient, σ represents the electrical conductivity of the fluid, μ_e represents the magnetic permeability, D_0 indicates the mass diffusivities of the medium, Cp represents the specific heat capacity and σ^* is the stefan-Boltzmann constant. The associated boundary conditions are

$$\left.\begin{aligned} &\overline{v} = 0, \quad \overline{T} = \overline{T}_w, \quad \overline{C} = \overline{C}_w \quad \text{at} \quad \overline{y} = 0 \\ &\overline{u} = u_\infty, \quad \overline{T} = \overline{T}_\infty, \quad \overline{C} = \overline{C}_\infty \quad \text{as} \quad \overline{y} \to \infty \end{aligned}\right\} \tag{8.5}$$

We introduce the following dimensionless variables:

$$\left.\begin{aligned} &x = \frac{\overline{x}}{\mathrm{L}}, \quad y = \frac{\overline{y}}{\mathrm{L}}\mathrm{Pe}^{\frac{1}{2}}, \quad u = \frac{\overline{u}\mathrm{L}}{\alpha_0 \mathrm{Pe}}, \quad u = \frac{\overline{v}\mathrm{L}}{\alpha_0 \mathrm{Pe}^{\frac{1}{2}}} \\ &\theta(\eta) = \frac{\overline{T} - \overline{T}_\infty}{\overline{T}_w - \overline{T}_\infty}, \quad \phi(\eta) = \frac{\overline{C} - \overline{C}_\infty}{\overline{C}_w - \overline{C}_\infty} \end{aligned}\right\} \tag{8.6}$$

where $\mathrm{Pe} = \dfrac{u_\infty \mathrm{L}}{\alpha_0}$ is the Péclet number and L represents the characteristic length.

In view of the continuity equation (8.1), we introduce the stream function ψ by

$$u = \frac{\partial \psi}{\partial y}, \quad v = -\frac{\partial \psi}{\partial x} \tag{8.7}$$

Using (8.6)-(8.7) into (8.2)-(8.4), we get the following momentum, energy, and concentration equations

$$\begin{aligned} n\left(\frac{\partial \psi}{\partial y}\right)^{n-1}\frac{\partial^2 \psi}{\partial y^2} + 2\mathrm{G}\left(\frac{\partial \psi}{\partial y}\right)\frac{\partial^2 \psi}{\partial y^2}\left(\frac{\theta_e - \theta}{\theta_e}\right) - \frac{\mathrm{G}}{\theta_e}\left(\frac{\partial \psi}{\partial y}\right)^2\frac{\partial \theta}{\partial y} + \mathrm{M}\left(\frac{\partial^2 \psi}{\partial y^2}\right)\left(\frac{\theta_e - \theta}{\theta_e}\right) \\ -\frac{\mathrm{M}}{\theta_e}\left(\frac{\partial \psi}{\partial y}\right)\left(\frac{\partial \theta}{\partial Y}\right) - \lambda^n\left(\frac{\partial \theta}{\partial y} + \mathrm{B}\frac{\partial \phi}{\partial y}\right)\left(\frac{\theta_e - \theta}{\theta_e}\right) + \frac{\lambda^n}{\theta_e}(\theta + \mathrm{B}\phi)\left(\frac{\partial \theta}{\partial y}\right) = 0 \end{aligned} \tag{8.8}$$

$$\frac{\partial\psi}{\partial y}\frac{\partial\theta}{\partial x}-\frac{\partial\psi}{\partial x}\frac{\partial\theta}{\partial y}-\beta\left(\frac{\partial\theta}{\partial y}\right)^2-\left(1+\beta\theta+\frac{4\,\mathrm{R}}{3}\right)\frac{\partial^2\theta}{\partial y^2}=0 \tag{8.9}$$

$$\frac{\partial\psi}{\partial y}\frac{\partial\phi}{\partial x}-\frac{\partial\psi}{\partial x}\frac{\partial\phi}{\partial y}-\frac{1}{\mathrm{Le}}\frac{\partial^2\phi}{\partial y^2}=0 \tag{8.10}$$

The prescribed boundary conditions (8.5) become

$$\left.\begin{aligned}&\frac{\partial\psi}{\partial x}=0,\quad \theta=1,\quad \phi=1\quad \text{at}\quad y=0\\&\frac{\partial\psi}{\partial y}=1,\quad \theta=0,\quad \phi=0\quad \text{as}\quad y\to\infty\end{aligned}\right\} \tag{8.11}$$

where $\theta_e=\dfrac{\overline{T}_e-\overline{T}_\infty}{\overline{T}_w-\overline{T}_\infty}$ represents the variable viscosity parameter, $\mathrm{R}=\dfrac{4\sigma^*T_\infty^3}{k^*k}$ represents the thermal radiation parameter, $\mathrm{M}=\dfrac{\sigma {B_0}^2{\mu_e}^2K}{\mu_\infty}\left(\dfrac{\mathrm{L}}{\alpha_0}\right)^{(n-1)}\mathrm{Pe}^{-(n-1)}$ represents the magnetic field parameter, $\mathrm{Le}=\dfrac{\alpha_0}{D_0}$ represents the Lewis number, $\mathrm{Ra}=\dfrac{\mathrm{L}}{\alpha_0}\left(\dfrac{gK\beta_T(\overline{T}_w-\overline{T}_\infty)}{\nu}\right)^{1/n}$ represents the generalized Rayleigh number, $\mathrm{G}=\dfrac{C_F\sqrt{K}}{\nu_\infty}\left(\dfrac{\mathrm{L}}{\alpha_0}\right)^{(n-2)}\mathrm{Pe}^{-(n-2)}$ represents the non-Darcy parameter, $\mathrm{B}=\dfrac{\beta_c^*(\overline{C}_w-\overline{C}_\infty)}{\beta_T^*(\overline{T}_w-\overline{T}_\infty)}$ represents the Buoyancy ratio parameter and $\lambda=\dfrac{\mathrm{Ra}}{\mathrm{Pe}}$ represents the mixed convection parameters.

Now, we introduce the one-parameter scaling group transformations which is simplified form of Lie scaling group transformations. We will get the following similarity transformations

$$\eta=yx^{-1/2},\quad \psi=x^{1/2}f(\eta),\quad \theta=\theta(\eta),\quad \phi=\phi(\eta) \tag{8.12}$$

Using Eq. (8.12) into Eqs. (8.8)-(8.10), the following similarity equations are attained

$$\begin{aligned}f''\left[n(f')^{n-1}+2\mathrm{G}f'\left(\frac{\theta_e-\theta}{\theta_e}\right)+\mathrm{M}\left(\frac{\theta_e-\theta}{\theta_e}\right)\right]&=\frac{f'\theta'}{\theta_e}\left(\mathrm{G}f'+\mathrm{M}\right)\\&+\lambda^n\left(\theta'+\mathrm{B}\phi'\right)\left(\frac{\theta_e-\theta}{\theta_e}\right)-\lambda^n\left(\theta+\mathrm{B}\phi\right)\frac{\theta'}{\theta_e}\end{aligned} \tag{8.13}$$

$$\beta(\theta')^2+\left(1+\beta\theta+\frac{4\mathrm{R}}{3}\right)\theta''+\frac{1}{2}f\theta'=0 \tag{8.14}$$

$$\frac{1}{\mathrm{Le}}\phi'' + \frac{1}{2}f\phi' = 0 \tag{8.15}$$

The transformed boundary conditions (8.11) become

$$\left.\begin{aligned} &f(0) = 0, \quad \theta(0) = 1, \quad \phi(0) = 1 \\ &f'(\infty) = 1, \quad \theta(\infty) = 0, \quad \phi(\infty) = 0 \end{aligned}\right\} \tag{8.16}$$

The non-dimensional heat and mass flux are given by:

$$q_w = -\widetilde{k}\left(\frac{\partial \overline{T}}{\partial \overline{y}}\right)_{\overline{y}=0} - \frac{4\sigma^*}{3k^*}\left(\frac{\partial \overline{T}^4}{\partial \overline{y}}\right)_{\overline{y}=0} \quad and \quad q_m = -D\left(\frac{\partial \overline{C}}{\partial \overline{y}}\right)_{\overline{y}=0} \tag{8.17}$$

The Nussult number $Nu = \dfrac{q_w \overline{x}}{\widetilde{k}(\overline{T}_w - \overline{T}_\infty)}$ and Sherwood number $Sh = \dfrac{q_m \overline{x}}{D(\overline{C}_w - \overline{C}_\infty)}$ are given by

$$\frac{Nu_{\overline{x}}}{x^{1/2}} = -\left(1 + \frac{4\mathrm{R}}{3}\right)\theta'(0) \quad \text{and} \quad \frac{Sh_{\overline{x}}}{x^{1/2}} = -\phi'(0) \tag{8.18}$$

8.3 Results and Discussion

The coupled nonlinear Eqs.(8.13)-(8.15) along with the boundary conditions (8.16) are solved numerically using shooting method, which is explained clearly in chapter-2. In order to assess the accuracy of the code generated the results of the present problem have been compared with that of the results obtained by Chaoyang *et al.* [18] as a special case by taking G = B = R = M = β = 0, Le = 1 and $\theta_e \to \infty$ and found that they are in good agreement, as presented in Tab. (3.1).

Figures 8.1(a)-8.1(c) describe the effect of temperature-dependent viscosity (θ_e) and power-law index (n) on the dimensionless velocity $f'(\eta)$, temperature $\theta(\eta)$ and the concentration $\phi(\eta)$ distribution, respectively. Figure 8.1(a) depicts that the enhancement in the value of temperature-dependent viscosity tends to reduce the velocity profile for pseudo-plastic, dilatant and Newtonian fluids. The temperature increases with increasing the values

of θ_e for all three kinds of fluids, as plotted in Fig. 8.1(b). Thus, the enhancement of viscosities accelerate the fluid motion and decreases the temperature of the fluid along the wall. Moreover, Fig. 8.1(c) illustrates that, as increase in θ_e increases the concentration for the three cases of pseudo-plastic, dilatant and Newtonian fluid. Here, it is inferred that the variable viscosity has a significant effect on the velocity, temperature and concentration.

The influence of thermal conductivity (β) and power-law index (pseudo-plastic, dilatant and Newtonian fluid) on dimensionless velocity $f'(\eta)$, temperature $\theta(\eta)$ and concentration $\phi(\eta)$ distribution can be seen in Figs. 8.2(a)-8.2(c). Figure 8.2(a) reveals the enhancement in thermal conductivity parameter rises the velocity for three kinds of fluids. Figure 8.2(b) shows that the temperature enhances with the raise in thermal conductivity for three kinds of fluids. From this plot it is noticed that the concentration slightly reduces with increase in the variation of β for three kinds of fluids as shown in Fig. 8.2(c).

Figures 8.3(a)-8.3(c) explore the dimensionless velocity $f'(\eta)$, temperature $\theta(\eta)$ and concentration $\phi(\eta)$ profiles for thermal radiation (R) and power-law index ($n = 0.5$, $n = 1.0$, $n = 1.5$), respectively. Figure 8.3(a) illustrates that the velocity $f'(\eta)$ enhances with raise in R for three kinds of fluids (pseudo-plastic, Newtonian and dilatant fluids). Fig.8.3(b) explores that increasing the value of R results an increase in temperature $\theta(\eta)$ profile for three kinds of fluids. This is due to fact that the slope of the temperature distribution near the surface is always negative, in the presence of R and thus heat is always transferred from the surface. Fig. 8.3(c) depicts that increasing R slightly reduces the concentration for three kinds of fluids.

Figures 8.4(a)-8.4(c) illustrate the combined effect of magnetic parameter M and pseudo-plastic, dilatant and Newtonian fluid on dimensionless velocity $f'(\eta)$, temperature $\theta(\eta)$ and concentration $\phi(\eta)$ profiles, respectively. Figure 8.4(a) exhibits that, as M increases, the velocity profile decreases for pseudo-plastic and Newtonian fluids. But for dilatant fluid it is observed that effect of magnetic field increases near the plate and reduces far away from the plate. Figure 8.4(b) demonstrates that a rise in M substantially increases the temperature profiles for index $n < 1$ and $n = 1$ but slightly decreases for index $n > 1$. This behaviour in the fluid is because of the presence of a transverse magnetic field has a tendency to make the

Lorentz drag which resists the flow. Accordingly, the vertical temperature and concentration profiles increases as M increases. Due to the increase in the magnetic parameter, the non dimensional concentration increases for index $n < 1$ and $n = 1$ but slightly reduces for dilatant fluids as shown in Fig. 8.4(c).

Figures 8.5(a)-8.5(c) depict the dimensionless velocity $f'(\eta)$, temperature $\theta(\eta)$ and concentration $\phi(\eta)$ distributions for varying values of non-Darcy parameter (G) and power law index (n), respectively. Figure 8.5(a) reveals that the velocity reduces as G increases for all kinds of fluids. Since G demonstrates inertial drag, thus an increase in the Forchheimer number increments the imperviousness to the flow, reduces the fluid velocity to develop. The enhancement in G shows that the porous medium is offering more resistance to the fluid flow. Figure 8.5(b) exhibits that the temperature increases with an increase in G for all kinds of fluids. Figure 8.5(c) explores that the concentration increases with increase in non-Darcy parameter (G) for all kinds of fluids. The increase in G decreases the intensity of the flow and raises the temperature and concentration boundary layer thicknesses.

Table 8.1 shows the variation of the heat and mass transfer coefficients for various values of power-law indices (n), temperature-dependent viscosity (θ_e), thermal conductivity (β), thermal radiation (R), modified non-Darcy parameter (G) and magnetic field parameter (M). Higher the values of n lower the heat and mass transfer coefficients. An increase in the variable viscosity reduce both the heat and mass transfer coefficients. It is observed that increase in the thermal conductivity reduces the heat transfer but a reverse trend is observed for the mass transfer coefficients. It is seen that an enhancement in R raises the heat and mass transfer coefficients. An increase in the magnetic parameter decrease the heat and mass transfer coefficients. It can be seen that the heat and mass transfer coefficients reduce with increasing the value of modified non-Darcy parameter.

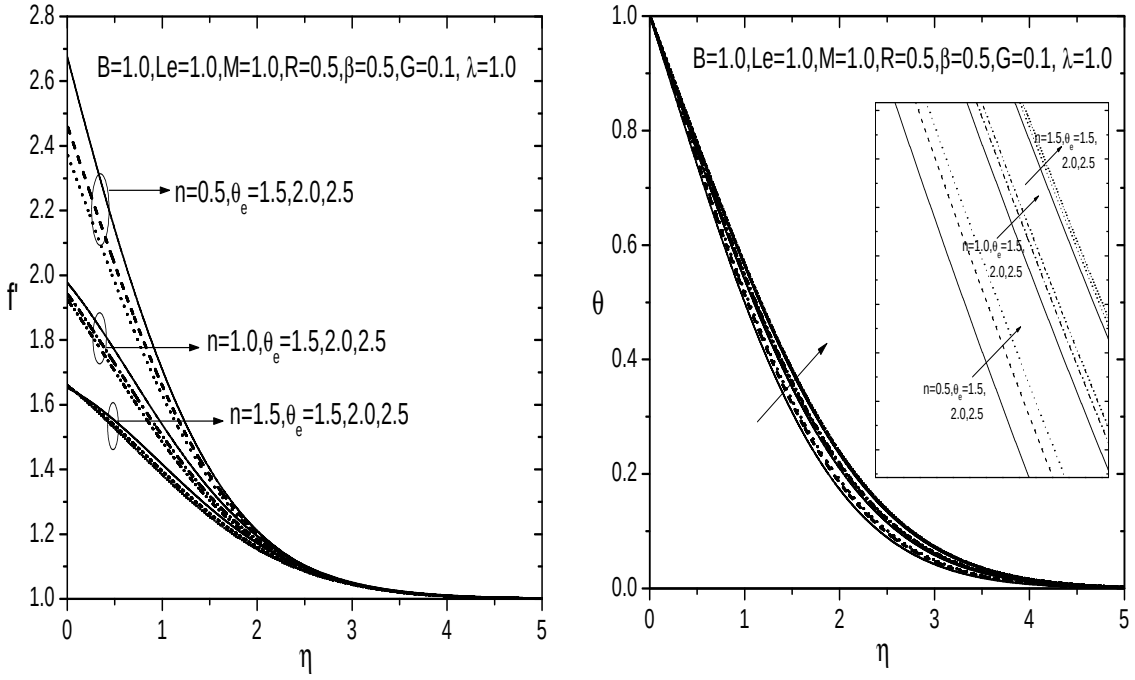

(a) (b)

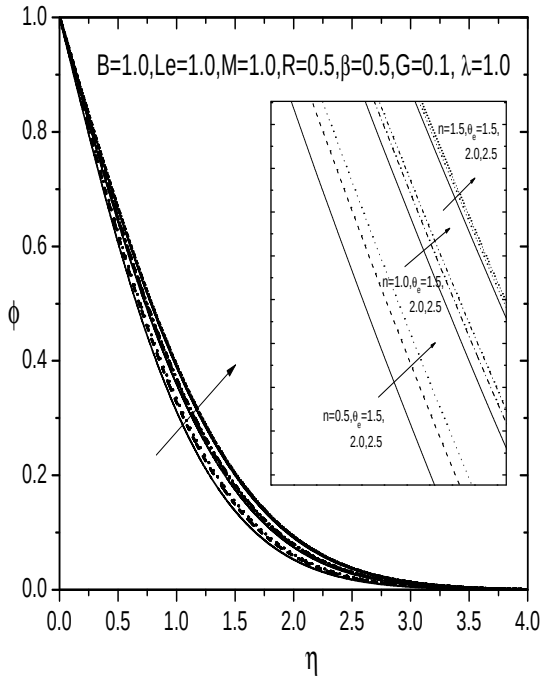

(c)

Figure 8.1: (a) velocity profile (b) temperature profile and (c) concentration profile for various value of θ_e and n.

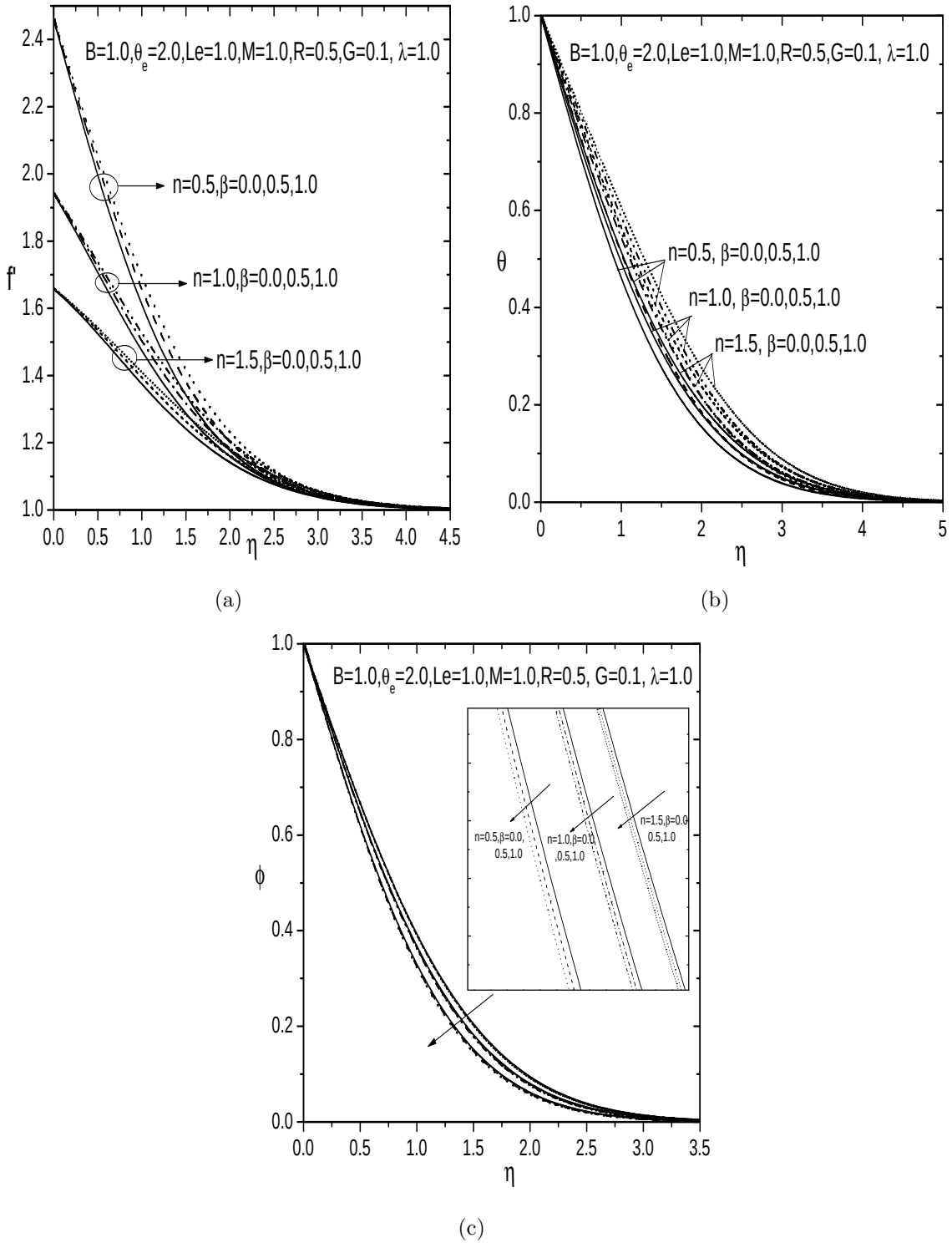

Figure 8.2: (a) velocity profile (b) temperature profile and (c) concentration profile for various value of β and n.

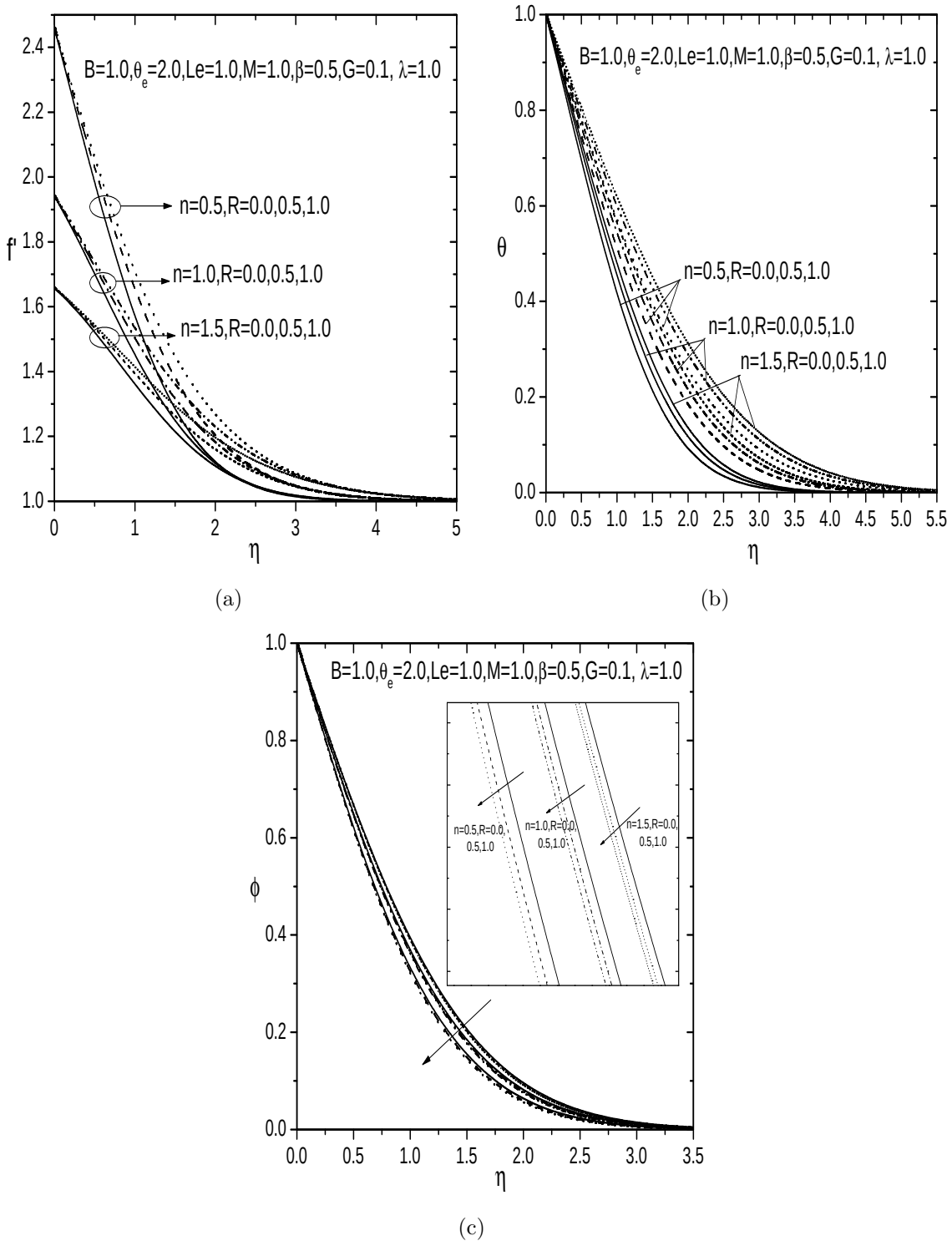

Figure 8.3: (a) velocity profile (b) temperature profile and (c) concentration profile for various value of R and n.

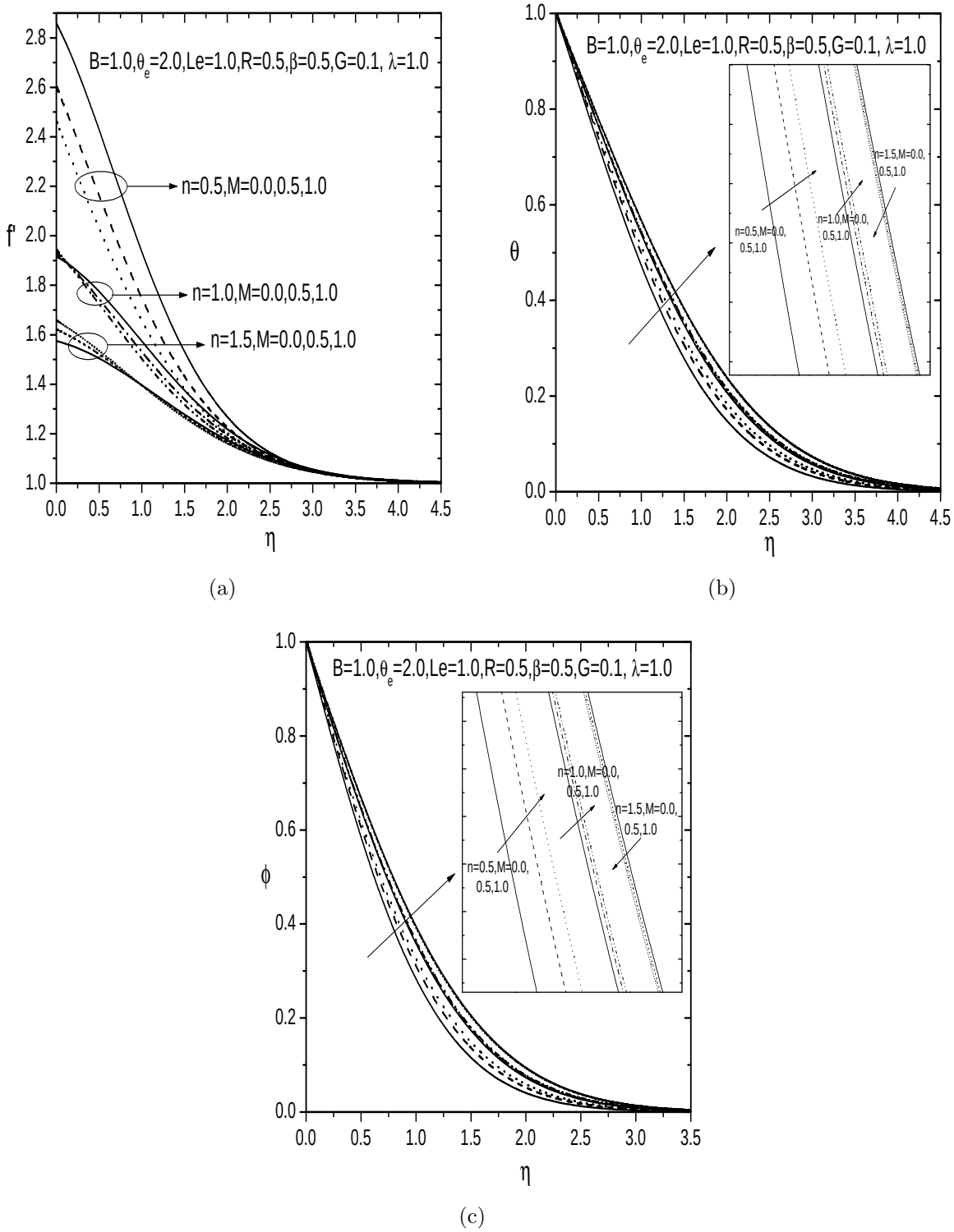

Figure 8.4: (a) velocity profile (b) temperature profile and (c) concentration profile for various value of M and n.

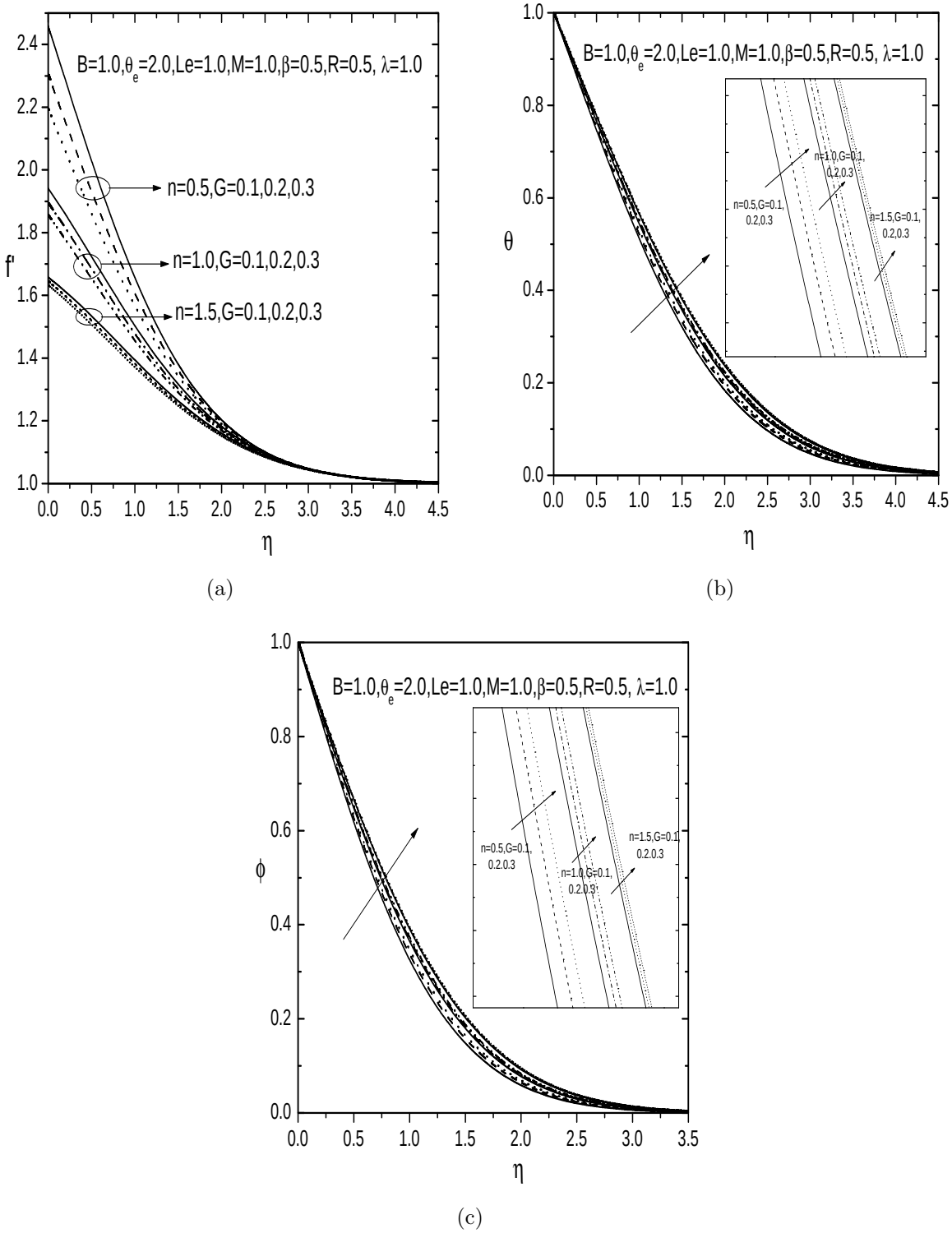

Figure 8.5: (a) velocity profile (b) temperature profile and (c) concentration profile for various value of G and n.

Table 8.1: *The heat and mass transfer coefficients for varying values of* n, θ_e, β, R, M *and* G.

n	θ_e	β	R	G	M	$-\left(1+\frac{4\mathrm{R}}{3}\right)\theta'(0)$	$-\phi'(0)$
0.5	2.0	0.5	0.5	1.0	0.1	0.838589	0.802625
1.0	2.0	0.5	0.5	1.0	0.1	0.773878	0.733599
1.5	2.0	0.5	0.5	1.0	0.1	0.733564	0.690834
0.5	1.0	0.5	0.5	1.0	0.1	0.963603	0.942952
0.5	1.5	0.5	0.5	1.0	0.1	0.863049	0.828684
0.5	2.5	0.5	0.5	1.0	0.1	0.827000	0.790533
0.5	2.0	0.0	0.5	1.0	0.1	0.999089	0.796610
0.5	2.0	1.0	0.5	1.0	0.1	0.733239	0.807343
0.5	2.0	1.5	0.5	1.0	0.1	0.657877	0.811142
0.5	2.0	0.5	0.0	1.0	0.1	0.598852	0.792743
0.5	2.0	0.5	1.0	1.0	0.1	1.029872	0.808876
0.5	2.0	0.5	1.5	1.0	0.1	1.192422	0.813286
0.5	2.0	0.5	0.5	0.0	0.1	0.915635	0.878206
0.5	2.0	0.5	0.5	1.0	0.1	0.864916	0.828747
0.5	2.0	0.5	0.5	1.5	0.1	0.822488	0.786514
0.5	2.0	0.5	0.5	1.0	0.0	0.868591	0.834579
0.5	2.0	0.5	0.5	1.0	0.2	0.818284	0.781197
0.5	2.0	0.5	0.5	1.0	0.3	0.803242	0.765404

8.4 Conclusions

The mixed convective transport over the vertical surface of a power-law fluid saturated with non-Darcy porous medium with thermal radiation, MHD and variable properties effects are, analyzed in this chapter.The main findings are summarized as follows:

- An enhancement in the variable viscosity decreases the velocity, heat and mass transfer but enhances temperature and concentration profiles.
- Increase in the thermal conductivity parameter leads to increase in the velocity, temperature and mass transfer but a decrease in the concentration profile.
- An increase in the values of the radiation parameter results an increase in the velocity, temperature, heat and mass transfer but decrease in the concentration profile.
- The temperature and concentration rises but the velocity, heat and mass transfer rates decreases with increasing values of magnetic field parameter.
- Increasing the non-Darcy parameter decreases the velocity, heat and mass transfer rates increases the temperature and concentration profiles.

Part IV

SUMMARY AND CONCLUSIONS

Chapter 9

Summary and Conclusions

In this thesis, an analysis of convective heat and mass transfer over a vertical plate in a power-law fluid saturated Darcy/non-Darcy porous medium and linear stability of the vertical throughflow in a horizontal porous layer saturated by a power-law fluid, is discussed.

The objective of this thesis is to study the effects of variable properties, double dispersion, Soret, thermophoresis, MHD and thermal radiation in a Darcy/non-Darcy porous medium saturated with power-law fluid on mixed convection flow. The Lie scaling group transformations are applied to get the similarity representation for the system of partial differential equations and then the resulting systems of equations are solved using shooting method. In addition, the linear stability analysis of the Darcy-Bénard convection of a power-law fluid with local thermal non-equilibrium is studied. The linearized disturbance equations are reduced to a eigenvalue problem by assuming a periodic train of convection cells. This eigenvalue problem is solved using finite differences and a matrix-based method. The important observations made from this study are listed below.

- Enhancement in the value of variable viscosity (θ_e) increases the velocity and decreases in temperature, concentration, heat and mass transfer rates in Darcy flow. Further, these results are opposite to the results of non-Darcy flow with respect to variable viscosity.

- An increase in the value of thermal conductivity (β) decreases the concentration, heat and mass transfer rates and increases the velocity and temperature in both Darcy and non-Darcy flows.

- The behaviour of the Darcy and non-Darcy flows: Higher values of the thermal dispersion parameter (Pe_γ) result in higher velocity, temperature and mass transfer distributions but lower concentration and heat transfer rate.

- Velocity, concentration and heat transfer rate increases with the increase in solutal dispersion parameter (Pe_ζ), whereas opposite results are reported for temperature and mass transfer rate. It is observed that these results are same in Darcy and non-Darcy porous medium.

- A rise in the value of thermophoresis parameter (τ) monotonically decreases the velocity, concentration gradients and heat transfer rate, but it increases the temperature and mass transfer rate. Here, the influence of thermophoresis is same in nature for both Darcy and non-Darcy flow cases.

- The effect of the radiation parameter (R) reduces the velocity and concentration profiles, but enhances the temperature, heat and mass transfer rates in both Darcy and non-Darcy flows.

- An increasing the value of Soret parameter (Sr) decreases the temperature and mass transfer rates, but increases the velocity, concentration and heat transfer rate.

- An increase in the values of the mixed convection parameter (λ) results in higher velocity, heat and mass transfer rates but lower temperature and concentration profiles.

- The influence of the non-Darcy parameter (G) enhances the temperature and concentration, but reduces the velocity, heat and mass transfer rates.

- The higher values of the magnetic field (M) result in lower velocity, heat and mass transfer rates, but higher temperature and concentration.

- The neutral stability curve is affected by both n and Pe, while it is unaffected by the sign of Pe. The effect of an increasing n for a given Pe is different for either smaller or larger values of Pe. Generally speaking, pseudo-plastic fluids $n < 1$ are more stable than dilatant fluids $n > 1$ when Pe is small, while they become more unstable if Pe is large.

- The effect of increasing Ω is to decrease the Ra_c and hence the effect of increasing Ω is to destabilize the system. The effect is more pronounced for very small Ω. The critical Rayleigh number is independent of Ω for very small H while for large H,it decreases with increasing Ω

- It is found that the critical Rayleigh number $\frac{Ra_c\Omega}{(1+\Omega)}$ based on the mean properties of the media vary monotonically with H and approaches a common limit as $H \to \infty$. It is also observed that the critical wave number k_c approaches a common limit as $H \to 0$ and $H \to \infty$ in the Darcy limit while it approaches two different limits, one as $H \to 0$ and another as $H \to \infty$ in the Brinkman regime.

Future Scope :

The work presented in the thesis can be extended to analyze the different effects considering viscosity variation with temperature, viscous dissipation, magnetic field, exothermic and endothermic reactions, and to different geometries using linear and non-linear stability analysis. Such an exhaustive study can be a rewarding experience though it is challenging as well as time consuming.

Bibliography

[1] A. A. Afify and N. S. Elgazey. Effect of double dispersion on non–Darcy mixed convective flow over vertical surface embedded in porous medium. *Applied Mathematics and Mechanics*, 34:1247–1262, 2013.

[2] A. A. Afify, M. J. Uddin, and M. Ferdows. Scaling group transformation for MHD boundary layer flow over permeable stretching sheet in presence of slip flow with newtonian heating effects. *Applied Mathematics and Mechanics*, 35(11):1375–1386, 2014.

[3] T. K. Aldoss, M. A. Al-Nimr, M. A. Jarrah, and B.J. Al-Shaér. Magnetohydrodynamic mixed convection from a vertical plate embedded in a porous medium. *Numerical Heat Transfer, Part A: Applications*, 28(5):635–645, 1995.

[4] L. S. B. Alves and A. Barletta. Convective instability of the Darcy-Bénard problem with through flow in a porous layer saturated by a power-law fluid. *International Journal of Heat and Mass Transfer*, 62:495–506, 2013.

[5] I. L. Animasaun. Effects of thermophoresis, variable viscosity and thermal conductivity on free convective heat and mass transfer of non-darcian MHD dissipative casson fluid flow with suction and nth order of chemical reaction. *Journal of the Nigerian Mathematical Society*, 34(1):11–31, 2015.

[6] N. Banu and D. A. S. Rees. Onset of Darcy-Bénard convection using a thermal non-equilibrium model. *International Journal of Heat and Mass Transfer*, 45(11):2221–2228, 2002.

[7] A. Barletta. Local energy balance, specific heats and the Oberbeck-Boussinesq approximation. *International Journal of Heat and Mass Transfer*, 52(21-22):5266–5270, 2009.

[8] A. Barletta and D. A. Nield. Linear instability of the horizontal throughflow in a plane porous layer saturated by a power-law fluid. *Physics of Fluids*, 23(1):013102.

[9] A. Barletta and L. Storesletten. Linear instability of the vertical throughflow in a horizontal porous layer saturated by a power-law fluid. *International Journal of Heat and Mass Transfer*, 99:293–302, 2016.

[10] H. Barrow and T. L. S. Rao. The effect of variable beta on free convection. *Brazilian Society of Chemical Engineering*, 16:704–709, 1971.

[11] G. K. Batchelor. *An Introduction to Fluid Dynamics*. Cambridge University Press, Cambridge, England, 2006.

[12] A. J. Benazir and R. Sivaraj. Influence of double dispersion on non-Darcy free convective magnetohydrodynamic flow of casson fluid. *Advances in Intelligent Systems and Computing*, 436:537–551, 2016.

[13] G. W. Bluman and S. C. Anco. *Symmetry and Integration Methods for Differential Equations*. Springer Verlag, 2009.

[14] H. C. Brinkman. A calculation of the viscous force exerted by a flowing fluid in a dense swarm of particles. *Applied Scientific Research*, 45:27–43, 1947.

[15] C. Chahtour, H. Ben Hamed, H. Beji, A. Guizani, and W. Alimi. Convective hydromagnetic instabilities of a power-law liquid saturating a porous medium: Flux conditions. *Physics of Fluids*, 30(1):013101, 2018.

[16] A. J. Chamkha, S. E. Ahmed, and A. S. Aloraier. Melting and radiation effects on mixed convection from a vertical surface embedded in a non–Newtonian fluid saturated non-darcy porous medium for aiding and opposing eternal flows. *International Journal of Physical Sciences*, 5(7):1212–1224, 2010.

[17] A. J. Chamkha and J. M. Al-Humoud. Mixed convection heat and mass transfer of non–Newtonian fluids from a permeable surface embedded in a porous medium. *International Journal of Numerical Methods for Heat & Fluid Flow*, 17(2):195–212, 2007.

[18] W. Chaoyang, T. Chuanjing, and Z. Xiaofen. Mixed convection of non–Newtonian fluids from a vertical plate embedded in a porous medium. *Acta Mechanica Sinica*, 6(3):214–220, 1990.

[19] C. H. Chen. Magneto-hydrodynamic mixed convection of a power-law fluid past a stretching surface in the presence of thermal radiation and internal heat generation/absorption. *International Journal of Non-Linear Mechanics*, 44(6):596–603, 2009.

[20] R. H. Christopher and S. Middleman. Power-law flow through a packed tube. *Industrial & Engineering Chemistry Fundamentals*, 4:422–426, 1965.

[21] R. Cortell. Suction, viscous dissipation and thermal radiation effects on the flow and heat transfer of a power-law fluid past an infinite porous plate. *Chemical Engineering Research and Design*, 89(1):85–93, 2011.

[22] G Dagan. Some aspects of heat and mass transfer in porous media. *Fundamentals of Transport Phenomena in Porous Media*, pages 55–64, 1972.

[23] H. P. G. Darcy. MLes Fontaines Publiques De La Ville De Dijon. *Victor Dalmont*, 1856.

[24] R. V. Dharmadhikari and D. D. Kale. Flow of non-newtonian fluids through porous media. *Chemical Engineering Science*, 40(3):527–528, 1985.

[25] Z. Dursunkaya and W. M. Worek. Diffusion-thermo and thermal-diffusion effects in transient and steady natural convection from a vertical surface. *International Journal of heat and mass transfer*, 35(8):2060–2065, 1992.

[26] E. R. G. Eckert and R. M. Drake. *Analysis of Heat and Mass Transfer*. McGraw Hill, New York, 1972.

[27] N. T. Eldabe, S. N. Sallam, and M. Y. Abou-zeid. Numerical study of viscous dissipation effect on free convection heat and mass transfer of MHD non–Newtonian fluid flow through a porous medium. *Journal of the Egyptian Mathematical Society*, 20(2):139–151, 2012.

[28] A. I. Fagbade, B. O. Falodun, and C. U. Boneze. Influence of magnetic field, viscous dissipation and thermophoresis on Darcy-Forcheimer mixed convection flow in fluid saturated porous media. *American Journal of Computational Mathematics*, 5:18–40.

[29] M. Ferdows, M. J. Uddin, and A. A. Afify. Scaling group transformation for MHD boundary layer free convective heat and mass transfer flow past a convectively heated nonlinear radiating stretching sheet. *International Journal of Heat and Mass Transfer*, 56(1-2):181–187, 2013.

[30] P. Forccheimer. Wasserbewegung durch borden. *Zeitschrift des Vereines Deutscher Ingenieure*, 45:1736–1788, 1901.

[31] T. Grosan and I. Pop. A note on the effect of radiation on free convection over a vertical flat plate embedded in a non-newtonian fluid saturated porous medium. *International Journal of Applied Mechanics and Engineering*, 11(3):715–722, 2006.

[32] M. A. A. Hamad, M. J. Uddin, and A. M. Ismail. Radiation effects on heat and mass transfer in MHD stagnation-point flow over a permeable flat plate with thermal convective surface boundary condition, temperature dependent viscosity and thermal conductivity. *Nuclear Engineering and Design*, 242:194–200, 2012.

[33] I. A. Hassanien and M. A. A. Hamad. Group theoretic method for unsteady free convection flow of a micropolar fluid along a vertical plate in a thermally stratified medium. *Applied Mathematical Modelling*, 32(6):1099–1114, 2008.

[34] Mustafa M. Hayat, T. and S. Obaidat. Simultaneous effects of MHD and thermal radiation on the mixed convection stagnation-point flow of a power-law fluid. *Chinese Physics Letters*, 28(7):074702, 2011.

[35] M. M. Helal and M. A. Saif. Free convection heat and mass transfer in a power law fluid past an inclined surface with thermophoresis. *Journal of the Egyptian Mathematical Society*, 21(3):224–232, 2013.

[36] C. W. Horton and F. T. Rogers. Convection currents in a porous medium. *Journal of Applied Physics*, 16(6):367–370, 1945.

[37] Khanafer K. Hossain, M. A. and K. Vafai. The effect of radiation on free convection flow of fluid with variable viscosity from a porous vertical plate. *International Journal of Thermal Sciences*, 40(2):115–124, 2001.

[38] M. A. Hossain and H.S. Takhar. Radiation effect on mixed convection along a vertical plate with uniform surface temperature. *Heat and Mass Transfer*, 31(4):243–248, 1996.

[39] C. J. Huang. Effects of internal heat generation and Soret/Dufour on natural convection of non–Newtonian fluids over a vertical permeable cone in a porous medium. *Journal of King Saud University-Science*, 30(1):106–111, 2018.

[40] D. B. Ingham and I. Pop. *Transport Phenomena in Porous Media: Vol-II*. Elsevier, Oxford, 2005.

[41] S. Jayanthi and M. Kumari. Effect of variable viscosity on non-darcy free or mixed convection flow on a vertical surface in a non-newtonian fluid saturated porous medium. *Applied mathematics and computation*, 186(2):1643–1659, 2007.

[42] N. G. Kafoussias and N. G. Williams. Thermal-diffusion and diffusion-thermo effects on mixed free-forced convective and mass transfer boundary layer flow with temperature dependent viscosity. *Int. J. Engng. Sci.*, 33:1369–1384, 1995.

[43] R. R. Kairi and P. V. S. N. Murthy. Effect of double dispersion on mixed convection heat and mass transfer in a non-Newtonian fluid-saturated non-darcy porous medium. *Journal of Porous Media*, 13(8):749–757, 2010.

[44] P. K. Kameswaran and P. Sibanda. Thermal dispersion effects on convective heat and mass transfer in an Ostwald de waele nanofluid flow in porous media. *Boundary Value Problems*, 243(1), 2013.

[45] R. Kandasamy, K. Gunasekaran, and S. B. H. Hasan. Scaling group transformation on fluid flow with variable stream conditions. *International Journal of Non-Linear Mechanics*, 46(7):976–985, 2011.

[46] R. Kandasamy, I. Muhaimin, and H. B. Saim. Lie group analysis for the effect of temperature-dependent fluid viscosity with thermophoresis and chemical reaction on MHD free convective heat and mass transfer over a porous stretching surface in the presence of heat source/sink. *Communications in Nonlinear Science and Numerical Simulation*, 15(8):2109–2123, 2010.

[47] A. A. Khidir. Viscous dissipation, ohmic heating and radiation effects on MHD flow past a rotating disk embedded in a porous medium with variable properties. *Arabian Journal of Mathematics*, 2(3):263–277, 2013.

[48] A. A. Khidir, M. Narayana, P. Sibanda, and P. V. S. N. Murthy. Natural convection from a vertical plate immersed in a power-law fluid saturated non-darcy porous medium with viscous dissipation and soret effects. *Afrika Matematika*, 26(7-8):1495–1518, 2015.

[49] B. R. Kumar and R. Sivaraj. MHD viscoelastic fluid non–Darcy flow over a vertical cone and a flat plate. *International Communications in Heat and Mass Transfer*, 40:1–6, 2013.

[50] S. Kumari and P. V. S. N. Murthy. Convective stability of vertical throughflow of a non-newtonian fluid in a porous channel with soret effect. *Transport in Porous Media*, 122(1):125–143, 2018.

[51] F. C. Lai and F. A. Kulacki. The effect of variable viscosity on convective heat transfer along a vertical surface in a saturated porous medium. *International Journal of Heat and Mass Transfer*, 33(5):1028–1031, 1990.

[52] E. R. Lapwood. Convection of a fluid in a porous medium. *In Mathematical Proceedings of the Cambridge Philosophical Society*, 44(4):508–521, 1948.

[53] J. X. Ling and A. Dybbs. The effect of variable viscosity on forced convection over a flat plate submersed in a porous medium. *Journal of Heat Transfer*, 114(4):1063–1065, 1992.

[54] N. C. Mahanti and P. Gaur. Effects of varying viscosity and thermal conductivity on steady free convective flow and heat transfer along an isothermal vertical plate in the presence of heat sink. *Journal of Applied Fluid Mechanics*, 2(1):23–28, 2009.

[55] A. Mahdy and F. M. Hady. Effect of thermophoretic particle deposition in non-newtonian free convection flow over a vertical plate with magnetic field effect. *Journal of Non-Newtonian Fluid Mechanics*, 161(1-3):37–41, 2009.

[56] M. A. Mahmoud. Thermal radiation effect on unsteady MHD free convection flow past a vertical plate with temperature-dependent viscosity. *The Canadian Journal of Chemical Engineering*, 87(1):47–52, 2009.

[57] O. D. Makinde and A. Aziz. Mhd mixed convection from a vertical plate embedded in a porous medium with a convective boundary condition. *International Journal of Thermal Sciences*, 49(9):1813–1820, 2010.

[58] M. A. Mansour and N. A. El-Shaer. Effect of magnetic field on non–Darcy axisymmetric free convection in a power-law fluid saturated porous medium with variable permeability. *Journal of Magnetism and Magnetic Materials*, 250:57–64, 2002.

[59] A. M. Megahed. Variable viscosity and slip velocity effects on the flow and heat transfer of a power-law fluid over a non-linearly stretching surface with heat flux and thermal radiation. *Rheol Acta*, 51:841–847, 2012.

[60] H. Mondal, D. Pal, S. Chatterjee, and P. Sibanda. Thermophoresis and Soret-Dufour on MHD mixed convection mass transfer over an inclined plate with non-uniform heat source/sink and chemical reaction. *Ain Shams Engineering Journal*, 2017.

[61] S. S. Motsa. A new spectral local linearization method for nonlinear boundary layer flow problems. *Journal of Applied Mathematics*, 2013:1–15, 2013.

[62] S. Mukhopadhyay and I. C. Mandal. Magnetohydrodynamic (MHD) mixed convection slip flow and heat transfer over a vertical porous plate. *Engineering Science and Technology, an International Journal*, 18(1):98–105, 20015.

[63] P. V. S. N. Murthy. Effect of double dispersion on mixed convection heat and mass transfer in non-darcy porous medium. *Journal of Heat Transfer*, 122:3, 2000.

[64] P. V. S. N. Murthy and P. Singh. Thermal dispersion effects on non–Darcy convection over a cone. *Computers & Mathematics with Applications*, 40(12):1433–1444, 2000.

[65] P. V. S. N. Murthy and P. Singh. Thermal dispersion effects on non-darcy convection over a cone. *Computers & Mathematics with applications*, 40(12):1433–1444, 2000.

[66] A. A. Mutlag, M. J. Uddin, M. A. A. Hamad, and A. I. M. Ismail. Heat transfer analysis for falkner-skan boundary layer flow past a stationary wedge with slip boundary conditions considering temperature-dependent thermal conductivity,. *Sains Malaysiana*, 42:855–862, 2013.

[67] P. A. L. Narayana and P. Sibanda. Influence of the soret effect and double dispersion on MHD mixed convection along a vertical flat plate in non-darcy porous medium. *International Journal of Nonlinear Science*, 12:352–364, 2011.

[68] P. L. Narayana, P. V. S. N. Murthy, and A. Postelnicu. Soret and dufour effects on free convection of non-newtonian power law fluids with yield stress from a vertical flat plate in saturated porous media. *Journal of Porous Media*, 12(10):967–981, 2009.

[69] D. A. Nield and A. Bejan. *Convection in Porous Media*. 4^{th} Ed., Springer-Verlag, New York, 2013.

[70] A. Noghrehabadi, M. Ghalambaz, and A. Ghanbarzadeh. Effects of variable viscosity and thermal conductivity on natural-convection of nanofluids past a vertical plate in porous media. *Journal of Mechanics*, 30(3):265–275, 2014.

[71] M Oberlack. Similarity in non-rotating and rotating turbulent pipe flows. *Journal of Fluid Mechanics*, 379:1–22, 1999.

[72] P. J. Olver. *Application of Lie Group to Differential Equations, Graduate Text in Mathematics*. Springer, New York, 1993.

[73] L. V. Ovsiannikov. *Group Analysis of Differential Equations*. Academic Press, New York, 1982.

[74] D. Pal and S. Chatterjee. Soret and Dufour effects on MHD convective heat and mass transfer of a power-law fluid over an inclined plate with variable thermal conductivity in a porous medium. *Applied Mathematics and Computation*, 219(14):7556–7574, 2013.

[75] M. K. Partha. Nonlinear convection in a non–Darcy porous medium. *Applied Mathematics and Mechanics*, 31(5):565–574, 2010.

[76] J. S. R. Prasad, K. Hemalatha, and B. D. C. N. Prasad. Mixed convection flow from vertical plate embedded in non–Newtonian fluid saturated non- darcy porous medium with thermal dispersion-radiation and melting effects. *Journal of Applied Fluid Mechanics*, 7(3):385–394, 2014.

[77] K. V. Prasad, K. Vajravelu, and R. A. van Gorder. Non–Darcian flow and heat transfer along a permeable vertical surface with nonlinear density temperature variation. *Acta Mechanica*, 220(1-4):139–154, 2011.

[78] M. Prats. The effect of horizontal fluid flow on thermally induced convection currents in porous mediums. *Journal of Geophysical Research*, 71(20):4835–4838, 1967.

[79] Ch. RamReddy, T. Pradeepa, and D. Srinivasacharya. Similarity solution for free convection flow of a micropolar fluid under convective boundary condition via lie scaling group transformations. *Advances in High Energy Physics*, 2015:650813, 2015.

[80] P. S. Rao, B. Kumbhakar, and B. V. Kumar. Effect of thermal radiation on MHD flow with variable viscosity and thermal conductivity over a stretching sheet in porous media. *Journal of Nanofluids*, 6(2):292–299, 2017.

[81] A. M Rashad. Influence of radiation on MHD free convection from a vertical flat plate embedded in porous media with thermophoretic deposition of particles. *Communications in Nonlinear Science and Numerical Simulation*, 113:2213–2222, 2008.

[82] A. M. Rashad, B. Mallikarjuna, A. J. Chamkha, and S. Hariprasad Raju. Thermophoresis effect on heat and mass transfer from a rotating cone in a porous medium with thermal radiation. *Afrika Matematika*, 27(7-8):1409–1424, 2016.

[83] L. Rayleigh. Lix. on convection currents in a horizontal layer of fluid, when the higher temperature is on the under side. *The London, Edinburgh, and Dublin Philosophical Magazine and Journal of Science*, 32(192):529–546, 1916.

[84] D. A. S. Rees. Microscopic modelling of the two-temperature model for conduction in heterogeneous media. *Journal of Porous Media*, 13(2):125–143.

[85] D. A. S. Rees. Microscopic modelling of the two-temperature model for conduction in heterogeneous media: three-dimensional media. *In Proceedings of the 4th International Conference on Applications of Porous Media*, page 15.

[86] D. A. S. Rees and I. Pop. Local thermal non-equilibrium in porous medium convection. *Transport phenomena in porous media III*, pages 147–173, 2005.

[87] C. H. Russell. *Fluid Mechanics*. Second Edition, Pearson, 2015.

[88] T. E. Schumann. Heat transfer: a liquid flowing through a porous prism. *Journal of the Franklin Institute*, 208(3):405–416, 1929.

[89] M. A. Seddeek, M. Y. Akl, and A. M. Al-Hanaya. Thermal radiation effects on mixed convection and mass transfer flow on vertical porous plate with heat generation and chemical reaction by using scaling group. *J. Natural Sciences and Mathematics*, 4:41–60, 2010.

[90] A. Selim, M.A. Hossain, and D. A. S. Rees. The effect of surface mass transfer on mixed convection flow past a heated vertical flat permeable plate with thermophoresis. *International Journal of Thermal Sciences*, 42(10):973–982, 2003.

[91] A. V. Shenoy. Non-Newtonian fluid heat transfer in porous media. *Advances in Heat transfer*, 24:102–191, 1994.

[92] J. C. Slattery. *Momentum, Energy, and Mass Transfer in Continua*. McGraw-Hill chemical engineering series, New York, 1972.

[93] E. M. Sparrow. *Radiation heat transfer*. Routledge, 2018.

[94] D. Srinivasacharya, B. Mallikarjuna, and R. Bhuvanavijaya. Radiation effect on mixed convection over a vertical wavy surface in Darcy porous medium with variable properties. *Journal of Applied Science and Engineering*, 18(3):265–274, 2015.

[95] D. Srinivasacharya, J. Pranitha, and Ch. Ramreddy. Magnetic effect on free convection in a non-darcy porous medium saturated with doubly stratified power-law fluid. *Journal of the Brazilian Society of Mechanical Sciences and Engineering*, 33(1):8–14, 2011.

[96] D. Srinivasacharya, J. Pranitha, and Ch. Ramreddy. Magnetic and double dispersion effects on free convection in a non–Darcy porous medium saturated with power-law fluid. *International Journal for Computational Methods in Engineering Science and Mechanics*, 13(3):210–218, 2012.

[97] F. M. Sutton. Onset of convection in a porous channel with net through flow. *The Physics of Fluids*, 13(8):1931–1934, 1970.

[98] L. R. K. R. W. D. R. Talbot, R. K. Cheng, R. W. Schefer, and D. R. Willis. Thermophoresis of particles in a heated boundary layer. *Journal of Fluid Mechanics*, 101(4):737–758, 1980.

[99] T. Tapanidis, G. Tsagas, and H. P. Mazumdar. Application of scaling group of transformations to viscoelastic second-grade fluid flow. *Nonlinear Functional Analysis and Applications*, 8(3):345–350, 2003.

[100] R. S. Telles and O. V. Trevisan. Dispersion in heat and mass transfer natural convection along vertical boundaries in porous media. *International Journal of Heat and Mass Transfer*, 36(5):1357–1365, 1993.

[101] R Tsai. A simple approach for evaluating the effect of wall suction and thermophoresis on aerosol particle deposition from a laminar flow over a flat plate. *International Communications in Heat and Mass Transfer*, 26(2):249–257, 1999.

[102] M. J. Uddin, M. Ferdows, and O. A. Beg. Group analysis and numerical computation of magneto-convective non-Newtonian nanofluid slip flow from a permeable stretching sheet. *Applied Nanoscience*, 4(7):897–910, 2014.

[103] M. J. Uddin, M. N. Kabir, and Y. M. Alginahi. Lie group analysis and numerical solution of magnetohydrodynamic free convective slip flow of micropolar fluid over a moving plate with heat transfer. *Computers & Mathematics with Applications*, 70(5):846–856, 2015.

[104] M. Umamaheswar, M. C. Raju, S. V. K. Varma, and J. Gireeshkumar. Numerical investigation of MHD free convection flow of a non-newtonian fluid past an impulsively started vertical plate in the presence of thermal diffusion and radiation absorption. *Alexandria Engineering Journal*, 55(3):2005–2014, 2016.

[105] J. C. Umavathi. Combined effect of variable viscosity and variable thermal conductivity on double-diffusive convection flow of a permeable fluid in a vertical channel. *Transport in Porous Media*, 108(3):659–678, 2015.

[106] K. Vafai. *Handbook of Porous Media*. 3^{rd} Ed., CRC Press, Taylor and Francis Group, 2015.

[107] J. E. Weber. Convection in a porous medium with horizontal and vertical temperature gradients. *International Journal of Heat and Mass Transfer*, 17(2):241–248, 1974.

[108] R. A. Wooding. Rayleigh instability of a thermal boundary layer in flow through a porous medium. *Journal of Fluid Mechanics*, 9(2):183–192, 1960.

[109] C. K. Wu and R. Greif. Thermophoretic deposition including an application to the outside vapor deposition process. *International Journal of Heat and Mass Transfer*, 39(7):1429–1438, 1996.

[110] S. W. Yuan. *Foundation of Fluid Mechanics*. Prentice Hall of India Pvt. Ltd., New Delhi, 1969.

[111] A. M. Zubair, M. Ashraf, Farooq I. M., and K. Ali. Heat and mass transfer analysis of unsteady MHD nanofluid flow through a channel with moving porous walls and medium. *AIP Advances*, 6(4):045222, 2016.